

ECGS Workshop 2012

European Center for Geodynamics and Seismology



european center for geodynamics and seismology
centre européen de géodynamique et de séismologie

Earthquake source physics on various scales



View of Luxembourg's Old City taken from the city quarter Grund.
© Luxembourg City Tourist Office

Luxembourg, October 3-5, 2012
Alvisse Parc Hotel Luxembourg

Scientific Committee

R. Abercrombie Boston University, USA
R. Archuleta University of California at Santa Barbara, USA
G. Beroza Stanford University, USA
G. Di Toro University of Padua, Italy
W. Ellsworth United States Geological Survey, USA
R. Harrington Karlsruhe Institute of Technology, Germany
S. Ide University of Tokyo, Japan
N. Lapusta California Institute of Technology, USA

R. Madariaga
L. Malagnini
K. Mayeda

A. Oth
G. Prieto
L. Rivera
W. Walter

Ecole Normale Supérieure, France
Istituto Nazionale di Geofisica e Vulcanologia, Italy
University of California at Berkeley, USA
Weston Geophysical Corporation, USA
European Center for Geodynamics and Seismology, Luxembourg
Universidad de los Andes, Colombia
Université de Strasbourg, IPGS-EOST, France
Los Alamos National Laboratory, USA

With the Support of

 Fonds National de la
Recherche Luxembourg

 EUR-OPA
EUROPEAN MAJOR HAZARDS AGREEMENT
ACCORD EUROPÉEN RISQUES MAJEURS



Musée National
d'Histoire Naturelle, Luxembourg

 SSA
Seismological Society of America



IASPEI

Oral Program
Wednesday, 3 October 2012

KEYNOTE LECTURE:

Investigating Earthquake Scaling Using Spectral Ratios and Simple Earthquake Models

William R. Walter¹, Rengin Gok¹ and Kevin Mayeda²

¹ Lawrence Livermore National Laboratory, Livermore, CA

² Weston Geophysical Corporation, Lexington, MA

Earthquakes span many orders of magnitude in size, and quantifying how they scale can reveal insights in the nature of how they initiate, grow and stop. Earthquakes also exhibit large variations in their apparent stress levels and quantifying if and how these values correlate with size, depth, and geographic location is a key part of improving our understanding of earthquake physics. To study earthquake source characteristics it is necessary to first account for and remove other (e.g. path and site) effects. A straightforward and longstanding approach is to use a nearby small event as an empirical Green function (EGF) in the analysis of a larger earthquake. Traditionally the two events needed to be very similar in terms of epicenter and mechanism, but the development of the coda spectral ratio methodology (Mayeda et al. 2007) allows a much greater number of events to be used for EGF analysis while also providing a lower variance estimate of the amplitude ratio between events. In the frequency domain the EGF is simply a spectral ratio, which normally has a sigmoid shape with the low frequency level related to the ratio of the moments, the inflection points are at the corner frequencies of the large and small event and the high frequency level is function of both of their moments and corner frequencies.

For earthquakes we use a simple single-corner-frequency spectral model with self- and non-self-similar scaling to model many coda spectral ratios, individually and simultaneously, to map out the source parameters and their uncertainties. Having a source model allows a better understanding of the uncertainties for particular ratios in terms of bandwidth and data quality. For EGF ratio studies the model shows the best (or lowest uncertainty in scaling) results are achieved when there is sufficient bandwidth to resolve the high frequency asymptote and the larger event moment is constrained, for example through longer-period waveform modeling. We show the results do not depend strongly on the shape of the source spectra except in regard to the rate of high frequency falloff above the corner frequency.

**This research was performed under the auspices of the U.S. Department of Energy by the Lawrence Livermore National Laboratory under contract number DE-AC52-07NA27344.*

Is the ongoing earthquake scaling controversy simply a matter of different modeling approaches and underestimated uncertainties?

Rachel E. Abercrombie

Boston University

The controversy concerning earthquake self-similarity continues with some studies finding stress drop to decrease for smaller earthquakes, and others finding constant stress drop across the same magnitude range. It is not clear whether the different results are from studying different earthquakes, or using different methods. Also, the uncertainties are not well constrained. I apply a range of methods to the same earthquakes to determine how different choices in modelling approach affect the results. I find that both random and systematic differences between the stress drops calculated using different approaches are larger than the published uncertainties.

I analyse earthquakes from the Wells (Nevada, M6 2008) earthquake sequence (M4-6), and the 1994 Northridge (M6.7, California) earthquake sequence (M4-6.7), using both coda and direct wave spectral ratio methods. I develop quality criteria for accepting a corner frequency measurement. I find that both coda and direct wave approaches give similar results for the same earthquake pairs, but that there is a systematic bias depending on whether the earthquake of interest is the larger or smaller in the spectral ratio. Mayeda & Malagnini (2009, GRL) calculated coda wave spectral ratios of the Wells M6 mainshock to large (M4-5) aftershocks. They found that the large aftershocks have lower stress drops than the mainshock. Different approaches to fitting the coda spectral ratios, and analysis of direct wave spectral ratios of the same earthquake pairs show no systematic bias, but significant random variation. For each large aftershock I select a closely located, correlated M~3 earthquake as an EGF, and calculate direct S wave spectral ratios between the large aftershocks and the EGF events. I model the direct wave ratios and calculate source parameters and uncertainties following Viegas *et al.* (2010, JGR). The estimates of corner frequency and stress drop are systematically lower for the large aftershocks when they are in the denominator of the ratio. I compare coda and direct wave spectral ratio methods for the Northridge earthquake sequence with similar results. I also compare the results to published time domain measurements of stress drop and seismic energy (Mori *et al.*, 2003). The direct wave spectral measurements correlate well with the time domain P wave duration measurements, and the seismic energy determined from the coda waves is in good agreement with the Mori *et al.* values for the larger $M_0 > 3 \times 10^{15}$ Nm earthquakes

I then apply the direct wave spectral ratio approach to earthquakes from Christchurch New Zealand (M2-6), and Parkfield, California (M1-2.5) to investigate whether it is possible to resolve differences in stress drop with magnitude, or with tectonic setting, within uncertainties.

The Apparent Stress Controversy: Does Earthquake Self-Similarity Hold and Who Cares?

Kevin Mayeda^{1,2}, Luca Malagnini³ and Seung-Hoon Yoo^{1,2}

¹ Weston Geophysical Corp

² U.C. Berkeley Seismological Laboratory

³ INGV, Roma

A number of recent studies, both from seismic observations and state-of-the-art laboratory experiments, challenge the idea of self-similarity of earthquakes. Using a novel technique based on the stable properties of seismic coda (Mayeda et al., 2007; Mayeda and Malagnini, 2010) over 20 large magnitude seismic sequences from different faulting regimes and tectonic environments, show a gradual increase in apparent stress up to around Mw 5.5, then becomes self-similar at higher magnitudes. We validate some of our results by comparing ground motion predictions using our derived scaling values and compare against those that had self-similar assumptions. This magnitude range typically corresponds to fault slip up to a few tens of centimeters, and amazingly this amount of fault slip corresponds to recent laboratory experiments that show complete lubrication when slip exceeds a few tens of centimeters at seismic slip velocities ($V=1$ m/s) and normal stresses representative of crustal depths. The laboratory results strongly suggest that real faults will weaken considerably when seismic slip exceeds a few tens of centimeters, however the mechanism of slip weakening can vary greatly depending upon the rock type (Di Toro et al., 2011).

Source scaling relations of km- to cm-scale (M_w 4 to -6) earthquakes: Experiences from mining- and fluid-induced seismicity, volcanic-hybrid seismic events and laboratory experiments

Grzegorz Kwiatek¹, Georg Dresen¹, Marco Bohnhoff¹, Rebecca Harrington², Elli-Maria Charalampidou¹, Fatih Bulut¹, Thomas Goebel³ and Beata Orlecka-Sikora⁴

¹ Helmholtz Centre Potsdam, GFZ German Research Centre for Geosciences, Section 3.2: Geomechanics and Rheology, Telegrafenberg, D14473 Potsdam, Germany

² Karlsruhe Institute of Technology, Geophysical Institute, Hertzstraße 16, D76187 Karlsruhe, Germany

³ University of Southern California, Department of Earth Sciences, 3651 Trousdale Parkway, Los Angeles, CA 90089-0740, USA.

⁴ Institute of Geophysics, Polish Academy of Sciences, ul. Księcia Janusza 64, 01-452 Warszawa, Poland

A key question in seismology is whether large and small earthquakes are governed by the same physics. Currently a broad observational gap exists between fracture and friction experiments performed in laboratory tests and field observations (Prieto et al., 2004). It remains controversial to what extent dynamic rupture and faulting observed in laboratory tests may provide insights into the nucleation and fracture processes of tectonic earthquakes and rockbursts in mines (Gibowicz, 1990; Abercrombie and Rice, 2005). If scaling relations for static and dynamic parameters of small earthquakes are known, then an extrapolation of such values will help us to understand the rupture process of larger, more devastating events.

Studies of earthquake scaling relations involve comparison of static and dynamic source parameters. The relation between seismic moment M_0 and source radius r_0 , $M_0 \propto r^3$, is the most important static scaling relation (Kanamori and Rivera, 2004). It allows the estimation of static stress drop, $\Delta\sigma \propto M_0/r^3$, resulting from an earthquake. The scaling between radiated energy E_0 and M_0 , $M_0 \propto E_0$, is commonly expressed as $\sigma_a = \mu E_0/M_0$ (apparent stress), where μ is the rigidity coefficient. This dynamic scaling relation is also considered as characteristic for the source process.

Many authors have suggested that the stress drop is roughly independent of seismic moment and it is commonly assumed that constant stress-drop scaling continues down to at least M_w 0. It is still a matter of debate whether apparent stress is constant over the whole magnitude range. Constant apparent stress values suggest that similar physical processes govern large and small earthquakes. A breakdown of self-similar scaling of seismic events may occur at a minimum source dimension or due to other physical processes. However, it may likewise also be of an artificial origin. This is especially important for source parameters of very small earthquakes, as they are strongly sensitive to quality of seismic data acquisition, data selection and data processing.

In this study we summarize results from recent scaling relations studies for seismicity covering a magnitude range between M_w -6 and M_w 4 representing source radii between a \sim 1cm and \sim 1km. We considered seismic recordings from various environments including mining-induced nano- and picoseismicity from Mponeng deep gold mine/South Africa; mining-induced microseismicity recorded in Rudna copper mine, Poland; fluid-induced microseismicity from the Berlín Geothermal Field, El Salvador; volcanic-hybrid microearthquakes recorded during 2006 crisis at Mt. St. Helens, USA, and acoustic emission data obtained by laboratory studies on

rock samples including stick-slip, shear band and compaction band experiments. In all studies we focused on accurate and reliable assessment of static and dynamic source parameters in order to investigate the self-similarity of earthquake rupture process. Inaccurate knowledge on attenuation and scattering of seismic waves as well as velocity mismodelling are found to be the main source of bias refraining from the reliable estimation of source characteristics. We suppressed unknown medium effects introduced into the waveforms using spectral ratio-based techniques. The application of spectral ratio technique also strongly simplified the analysis of data coming from experiments where acoustic emission sensors were used (laboratory experiments, JAGUARS project) to record the extremely small seismic events, as the local site effects and undefined transfer function were suppressed as well. The obtained results show that inappropriately corrected path effects as well as wrong selection of input data introduce an apparent breakdown in both static and dynamic scaling relations whereas spectral-ratio refined data confirm the self-similarity of earthquakes rupture process from small earthquakes down to at least $M_W -4.1$.

References

- Abercrombie, R., and J. Rice (2005). Can observations of earthquake scaling constrain slip weakening? *Geophys. J. Int.* 162, 406–424, doi: 10.1111/j.1365-246X.2005.02579.x.
- Gibowicz, S. (1990). The mechanism of seismic events induced by mining. In: *Rockbursts and Seismicity in Mines*, Fairhurst, C. (Editor), Balkema, Rotterdam, 1–27.
- Kanamori, H., and L. Rivera (2004). Static and dynamic scaling relations for earthquakes and their implications for rupture speed and stress drop, *Bull. Seismol. Soc. Am.* 94, 314–319, doi: 10.1785/0120030159.
- Prieto, G.A., P.M. Shearer, F.L. Vernon, and D. Kilb (2004). Earthquake source scaling and self-similarity estimation from stacking P and S spectra, *J. Geophys. Res.* 109, B08310, 13, doi: 10.1029/2004JB003084.

Volcanic seismic earthquakes at Mount St. Helens exhibit a constant seismically radiated energy per unit size

Rebecca M. Harrington¹, Grzegorz Kwiatek² and Seth C. Moran³

¹ Geophysical Institute, Karlsruhe Institute of Technology

² GFZ German Research Centre for Geosciences

³ US Geological Survey, Cascades Volcano Observatory

Given the attenuating properties of volcanic edifices, inferring the source properties of volcanic seismic events from waveforms is a challenging task. Here we exploit the short source-receiver distances of a temporary broadband seismometer deployment in September 2006 at Mount St. Helens to estimate the size-duration scaling of the earthquakes associated with the 2004-2008 eruption. We cross-correlate waveforms recorded on 11 broadband stations located less than 2 km from the crater and classify roughly 500 events into 8 families. We find that the size-duration scaling resembles that of similarly sized tectonic earthquakes observed in other shallow fault zones, namely constant-stress-drop scaling. The observed size-duration scaling also suggests that the amount of seismically radiated energy per unit seismic moment (scaled energy) is constant within event families, as well as between 6 of 8 event families. Cases where constant scaled energy values vary between families may result from a lack of resolution in the velocity model.

Investigations of laboratory-simulated volcanic seismic events generated during rock deformation experiments under both wet and dry conditions in a test chamber indicate that constant-stress-drop scaling occurs under dry conditions. In addition, size-duration scaling changes when fluids are present, suggesting that constant-stress-drop scaling occurs when faulting conditions are similar to those of tectonic earthquakes. The similarity of the size-duration scaling of the Mount St. Helens events with that of both laboratory-simulated and tectonically-generated earthquakes suggests that the mechanical failure processes are consistent with brittle-failure, or stick-slip, behavior. However, lower-than-expected corner frequency values relative to event size indicate that the rupture velocities may be low compared to that of tectonic earthquakes ($< 2.5\text{-}3$ km/s). The low corner frequencies likely result from low shear wave velocities in the volcanic edifice (assuming that the rupture velocity is $0.9 \times$ shear-wave velocity), rather than from low static stress drop values.

KEYNOTE LECTURE:

Earthquake source physics at various depths, energy budget and scaling

Germán A. Prieto¹, Sarah A. Barrett² and Gregory C. Beroza²

¹ Universidad de los Andes, Colombia

² Geophysics Department, Stanford University, USA

The behavior of rupture as a function of earthquake size has been under debate over many years now. The fundamental earthquake source parameters (magnitude, duration, radiated energy, etc.) follow relationships over many orders of magnitude and resolving this scaling laws is key in our understanding of the physics of earthquakes and the ground motions associated with them.

One unresolved question is the behavior of rupture as a function of depth. Recent observations of frequency dependent radiation of mega-thrust earthquakes, or very different scaling of non-volcanic tremor sources compared to “normal” earthquakes, suggest that the earthquake rupture mechanism may vary as a function of depth. In particular the physical mechanism of intermediate-depth earthquakes is not well constrained. In contrast to conditions in the crust and shallow lithosphere, at temperatures and pressures corresponding to depths >50 km one would expect rocks to yield by creep or flow and not by brittle failure, so there has to be a physical mechanism that allows for brittle or brittle-like failure for intermediate-depth earthquakes.

I will present recent results of earthquake source, both static and dynamic, parameters that may help in deciphering the mechanism of intermediate-depth earthquakes. I will compare results from the Bucaramanga seismic nest with other results in the literature and observations of crustal earthquakes. Compared to shallower earthquakes, rupture areas are more limited and seismic data suggests that seismic efficiency is very low. The scaling law of these intermediate-depth earthquakes does not follow a self-similar model and may rather be controlled by patches of constant size that slip regularly.

Radiated Energy of Recent Great Earthquakes

Annemarie S. Baltay¹, Satoshi Ide² and Gregory C. Beroza¹

¹Department of Geophysics, Stanford University

²Department of Earth and Planetary Science, University of Tokyo

We investigate the radiated seismic energy of recent great ($M_w > 8$) earthquakes that are well recorded by the Global Seismographic Network, including 2011 M_w 9.0 Tohoku, 2010 M_w 8.8 Maule, 2005 M_w 8.7 Nias, 2007 M_w 8.5 Bengkulu, and the recent 2012 M_w 8.6 Off-Sumatra earthquakes. We use a teleseismic eGf deconvolution approach to estimate radiated seismic energy, expanding on the method of *Ide et al.* [2011]. Both P - and S - wave broadband displacement coda records (from 90 s prior to 270 s after the direct arrival) from GSN stations at distances of 30° to 90° from the epicenter are analyzed. Smaller events ranging in size from M_w 6.5 to M_w 7.4 and located within ~ 50 km of the mainshock are used as eGf events. We assume a standard corner frequency and Brune ω^{-2} spectrum for each eGf and correct the main event spectrum accordingly to remove wave propagation effects. We estimate radiated energy from the area under the squared velocity source spectrum. We use several different eGf events to analyze each of these great earthquakes, and average the radiated energy from all eGf events and all three components (P -wave vertical, S -wave radial and transverse). Using P -wave vertical, and S - wave radial and transverse components yields consistent source spectra and radiated energy estimates, indicating that the eGf deconvolution results in stable and reliable results.

The radiated energy, E_s , of each of the great earthquakes analyzed is fairly consistent with individual estimates of *Convers and Newman* [2011], and other studies. We find the scaled energy, E_s/M_o , of the five great thrust earthquakes to be very similar, between 1 - and 2×10^{-5} , corresponding to apparent stresses of 0.4 to 0.8 MPa, while the 2012 Off-Sumatra strike slip event has a much higher scaled energy of 8×10^{-5} , an apparent stress of 3 MPa (Figure 1). This discrimination of higher apparent stress for strike slip earthquakes has been observed previously [*Choy and Boatwright*, 1995; *Perez-Campos and Beroza*, 2001] but this is perhaps the first time the energy of such a large strike slip event has been measured. Overall, the scaled energy for each of these events is in the same range of scaled energy that is observed for earthquakes over a wide range of sizes, from M 1.0 to M 9.0. This corroborates the hypothesis that scaled energy and apparent stress are constant globally, with variation, and not dependent on earthquake magnitude.

We also study the azimuthal directivity of radiated seismic energy from these very large events. We find that some of the earthquakes, especially the Tohoku-Oki 2011, have strong directivity, while others, such as the Bengkulu 2007, show less clear patterns. In general, the energy shows directivity in the known direction of rupture, as emphasized with forward modeling by *Favrea and Archuletta* [2001]. When coupled with the time-dependent source inversion of *Ide et al.* [2011], we show that the trench-ward directivity of energy from the Tohoku-Oki 2011 event can be explained by the dual nature of that event. The lack of energy towards the trench may explain tsunami generation, and we see a similar pattern in the other great earthquakes considered here. We model each rupture with simple Haskell line sources, and are able to fit the observations very well with these simple rupture models. In the case of the Off-Sumatra 2012 event, a observed lack of directivity in the teleseismic energy

estimates supports rupture on several conjugate, orthogonal fault planes. We find at least a factor of two, and up to an order of magnitude, difference in energy from maximum to minimum, implying that directivity effects should be considered when estimating energy teleseismically.

Events as small as M_w 6.5 have adequate signal-to-noise at teleseismic distances, and thus can be used as eGfs, implying that mainshocks as small as $\sim M$ 8 can be analyzed with this method. We test this with the M_w 7.8 Northern Sumatra earthquake of April 2010 to show that we can estimate energy consistent with that of *Convers and Newman* [2011]. This analysis also supports that a typical eGf-mainshock magnitude difference of 1.5 units yields stable results. Lastly, we propose that a database of eGf events could be used to calculate radiated energy and apparent stress of great, hazardous events in near real time. Potential eGf events can be pre-processed and the analysis run when a new great earthquake occurs. Since so little is still known about the great, hazardous events, any information learned quickly after the occurrence of the event has the potential to aid in risk mitigation and for seismic or tsunami hazard warning.

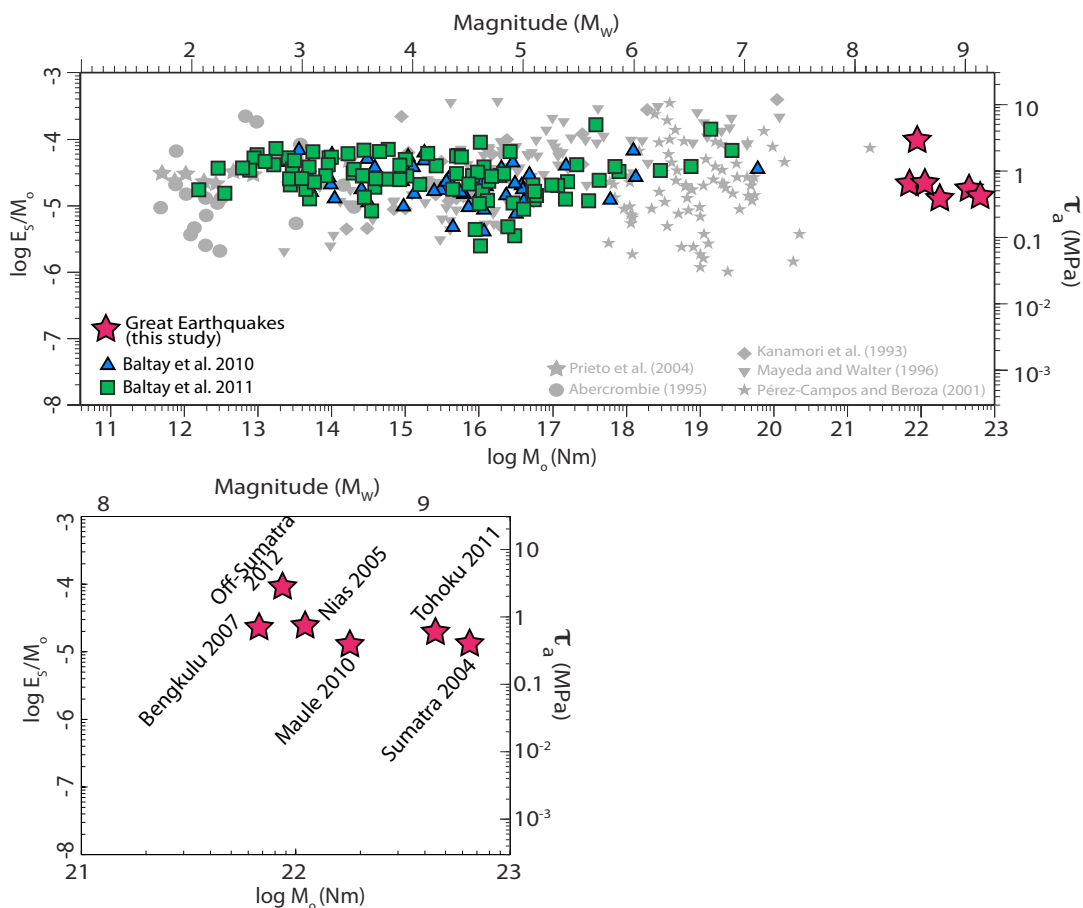


Figure 1. (Top) Scaled energy and apparent stress of the five great earthquakes (red stars) overlain on *Ide and Beroza* [2001] figure compiling many other studies. Also shown are the scaled energy results from *Baltay et al.* [2010] from the western US, and *Baltay et al.* [2011] from Honshu, Japan. Energy of the great earthquakes is consistent with that of other earthquakes, from $\sim M$ 2 to M 7. (Bottom) Close up of scaled energy and apparent stress of great earthquakes. Apparent stress is similar and between 0.4 and 0.8 MPa for the five thrust events, and higher for the 2012 Off-Sumatra strike slip event.

Very Long Period Source Characteristics and Radiated Energy of Large Earthquakes

L. Rivera¹ and H. Kanamori²

¹ IPGS-EOST, Université de Strasbourg, France

² California Institute of Technology, USA

During more than two decades (~ 1970-2000) significant efforts have been made to seek similarity and scaling laws of earthquakes. More recently, thanks to a significant improvement of our observational capability (GSN, GPS, InSAR, FNET, etc.) the pendulum is now on the opposite side and we now recognize a great diversity of seismic source parameters (rupture velocity, stress drop, etc.). Breakdown of similarity is particularly clear for large earthquakes and each one of them brings new knowledge on earthquake mechanics.

The aim of this work is to explore the very long-period characteristics of large earthquakes ($T > 400$ s). Although theoretically the seismic moment is defined at zero frequency, it is in practice estimated at quite diverse frequencies depending on the event size, the kind of data at hand, and the long period noise level. With the implicit assumption that the source spectrum is already flat at these frequencies it is then assumed that the observed value represents a good estimation of the static value. Very complex events like the 2009 Samoa-Tonga earthquake most likely present abnormal spectral behavior at long period. It was in fact through detailed analysis of very long period (800s) waves that the anomalous character of the Samoa-Tonga event became evident (Lay, et al., 2010). Since this kind of analysis is not made systematically we do not know if this is a unique case, or if other "special" events have been overlooked. On the other hand, there are some recent suggestions (Tanimoto and Ji, 2010) that some events had an enhanced spectral amplitude at long period. (e.g., 2004 Sumatra and 2010 Chile) and that their published seismic moment values are underestimated. In this work, we systematically study the long period ($400 \text{ s} < T < 2000 \text{ s}$) characteristics of the worldwide large events since 1990 for the purpose of detecting possible anomalous spectral behavior at long period and possible biases in the published seismic moment values. We focus on earthquakes having M_w (gCMT) ≥ 7.9 (28 events). These events have enough signal strength to clearly overcome the background noise at periods longer than 500 s. For these events we use three components of the data holdings at IRIS-FDSN for epicentral distances between 5 and 90 degrees sampled at 1 sps.

By using the W phase source inversion algorithm (Kanamori and Rivera, 2008) as a basic tool, we analyze each event using the following three-stage procedure:

- (S1) We perform 'standard' W phase inversion using the three component ground motion and the frequency band [1-5 mHz]. This is the frequency band we usually choose for such large events.
- (S2) We perform 'constrained' inversion by using only the vertical component data. By 'constrained' we mean that the focal mechanism is fixed at that obtained in (S1) and a linear inversion is performed to find the value of the seismic moment, M_0 , which best explains the data in a least square sense.

(S3) Now, instead of the original frequency band, we shift to increasingly longer periods: A) [1.0-2.50 mHz]; B) [1.0-1.25 mHz] and C) [0.8-1.00 mHz]. For each one of these, we perform a 'constrained' inversion (using only the vertical component and the focal mechanism as obtained in (S1)). Each one of these inversions yields a value of the seismic moment.

By comparing the values obtained in stage (S3) with the one obtained in (S2) we study the stability of the seismic moment estimates with increasing period. We also investigated the energy spectrum for many of these events. The results will be discussed in relation to other properties of rupture: location, depth, rupture velocity, stress drop, etc.

The 2012 Sumatra great earthquake sequence

Zacharie Duputel¹, Hiroo Kanamori¹, Victor C. Tsai¹, Luis Rivera²,
Lingsen Meng¹, Jean-Paul Ampuero¹ and Joann M. Stock¹.

¹ Seismological Laboratory, California Institute of Technology, 1200E. California Blvd., Pasadena, California 91125, USA

² IPGS-EOST, CNRS/Université de Strasbourg, UMR 7516, 5 rue René Descartes, 67084 Strasbourg Cedex, France

On 11 April 2012, the Cocos Basin region of the Indo-Australian plate was hit by a $M_w=8.6$ earthquake, followed two hours later by another $M_w=8.2$ event. These two earthquakes are the largest strike-slip events ever recorded and also among the largest intraplate earthquakes instrumentally recorded. A complex source process for the $M_w=8.6$ mainshock was detected early on by preliminary source analyses based on broadband seismological observations. Our analysis of surface-wave directivity and moment rate functions corroborates this complexity and suggests partition of the rupture into at least two distinct subevents. To further resolve the rupture process, we developed a procedure to invert very long period seismic data for multiple-point-source parameters. The current optimum source model at long period consists of two parallel WNW-ESE striking faults separated by ~ 150 km. Short-period P wave back-projection results suggest an additional intermediate faulting on an orthogonal NNE-SSW fault. A detailed analysis of surface wave amplitudes indicates a centroid depth below the Moho between 20km and 40km. This major earthquake sequence thus involved substantial deep lithospheric deformation that may eventually lead to a localized plate boundary, and brings a new dimension to the seismotectonics of the Indo-Australian diffuse plate boundary.

Oral Program
Thursday, 4 October 2012

KEYNOTE LECTURE: Incorporating Earthquake Source Physics into Ground Motion Models for Seismic Hazard Studies

Norman Abrahamson

UC Berkeley, Pacific Gas & Electric

The development of modern ground motion prediction equations (GMPE) is not just a statistical fitting of observed ground motions, but also relies on seismological and geotechnical models to constrain the GMPEs as they are extrapolated to conditions (short distances large magnitudes, and rupture geometries) not well represented in the available empirical data. Other examples include breaks in the magnitude scaling (key for large subduction earthquakes), depth dependence of stress-drops, effects of rupture geometries such as fault bends and splay faults, and effects of fault dip. Numerical simulations based on kinematic finite-fault methods is one approach for constraining GMPEs. A key issue for finite-fault simulations of ground motions is the method for generating the source parameters for future earthquakes, such as rupture dimensions, slip model, hypocenter location, slip-time function. Previous numerical simulation exercises using simulation methods that were validated against past data but with alternative methods for the simulating source properties for future earthquakes has led to large differences in the median ground motions of up to a factor of 3 even for magnitude-distance ranges that are reasonably well constrained by the empirical data. While seismic hazard studies should capture the epistemic uncertainty associated with defining the distribution of source properties, the lack of consistent results between different simulation procedures is a main reason that finite-fault numerical simulations are not widely used in seismic hazard analyses in California. Earthquake source physics studies can be used to improve and constrain the available models for generating representative suites of rupture sources for use in hazard analysis. The ground motion field is clearly moving to finite-fault simulations that will augment the empirical data sets, but the engineering applications will favor empirical models until consistent descriptions of the ruptures for use in finite-fault simulations are available.

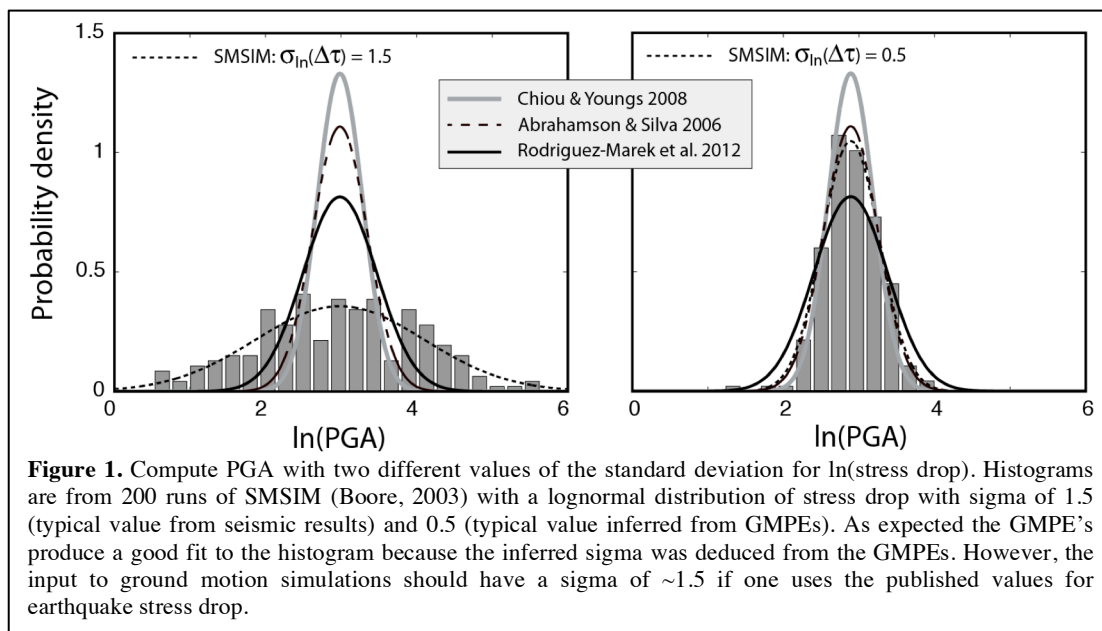
KEYNOTE LECTURE: Stress Drop Variability

R.J. Archuleta¹, F. Cotton², M. Causse² and J. Crempien¹

¹ Department of Earth Science, University of California, Santa Barbara, California;

² Institut des Sciences de la Terre, Université Joseph Fourier, Grenoble

Since the seminal work of Aki (1967) the average stress drop has been assumed to be constant — allowing for scaling of earthquakes of different magnitudes. Though some studies show stress drop increasing with earthquake magnitude, an issue for the conference, overall the average stress drop has remained in the range of 1-4 MPa for the last four decades. The average stress drop can vary depending on the tectonics of the region. What has also been true is that the variability of the stress drop has always about a factor of 10-30 around the mean. The standard deviation (sigma) of seismically determined stress drops is about 3-4 times larger than the sigma of the inferred stress drop based on ground motion prediction equations (GMPEs) (Figure 1). This inconsistency does not make sense. Is the seismically derived variability real, or is it a consequence of the method for determining the stress drop?



The prediction of ground motion from simulation methods will depend on the distribution of the stress drop, either directly or indirectly. Thus it is critical to get the correct standard deviation from seismic observations. (Using a sigma from the GMPE's is a circular argument.) The crux of the problem is that stress drop is generally derived from $M_0 f_c^3$ where M_0 is seismic moment and f_c is corner frequency. Thus uncertainty in stress drop is driven by uncertainty in f_c . We propose to compute stress drop from the root-mean-square acceleration (Hanks, 1979; McGuire and Hanks, 1980): $\Delta\tau \propto a_{rms} \sqrt{f_c}$ which has a much weaker dependence on f_c and directly related to a ground motion parameter root-mean-square acceleration relevant to simulations.

Understanding Earthquake Scaling in the Context of Complex Fault Systems and Crustal Geophysics

Egill Hauksson¹ and Lucile M. Jones²

¹ California Institute of Technology, Seismological Laboratory, Pasadena, CA 91125, USA

² US Geological Survey, Pasadena, CA 91106, USA

We analyze the waveform relocated (1981 to 2011) catalog of more than 500,000 earthquakes recorded along the Pacific North-America plate boundary in southern California. This seismicity, with five mainshocks of $M > 6.5$, reflects regional plate-boundary tectonics and other crustal deformation processes in the crust as well as the physical properties of the crust. The plate boundary is expressed as a system of late Quaternary faults or principal slip zones (PSZs) that accommodate major earthquakes. There are numerous smaller slip surfaces adjacent to the PSZs, which accommodate background seismicity as well as in some cases aftershocks. The plate tectonic strain loading dominates the dynamic process and causes the largest earthquakes along the PSZs, moderate-sized events in their immediate vicinity, and small earthquakes across the whole region.

To analyze earthquake scaling in the context of this fault system, we measure the Euclidian distance from every hypocenter to the nearest PSZs. In addition, we assign crustal geophysical parameters such as heat flow value and shear or dilatation strain rates to each epicenter. Stress drop values are available for a subset of ~60,000 events. We extend our catalog by adding these parameters to the standard earthquake parameters of each event such as date, location, depth, magnitude, seismic moment, and error estimates.

We use this extended catalog to investigate seismogenic thickness and fault zone width as well as earthquake scaling. We find that the seismicity rate is a function of location, with the rate dying off exponentially with distance from the PSZ. The decay per kilometer is similar as the decay per kilometer of depth in the rate of earthquakes below 5 km. About 80% of the small earthquakes are located within 5 km of a PSZ. For small earthquakes, stress drops increase in size with distance away from the PSZs. The magnitude distribution near the PSZs suggests that large earthquakes are more common close to the PSZs, and they are more likely to occur at greater depth than small earthquakes. In contrast, small quakes can occur at any geographical location but tend to cluster at the top and bottom of the seismogenic zone.

What determines the magnitude frequency distribution for earthquakes has been vigorously debated. These data suggest that the probability that an earthquake rupture will grow into a large earthquake may be influenced by the presence of a through-going fault structure. A small initiation with a certain amount of slip could stop quickly far from a fault and become a high stress drop earthquake. A small initiation with the same amount of initial slip near a PSZ can propagate more easily on the existing fault and grows into a larger event with a smaller stress drop.

An optimal combination of heat flow and strain rate is required to accommodate the crustal deformation processes that cause about 80% of the seismicity, which we refer to as the goldilocks seismicity. The available elasticity in the rock matrix or the thickness of the seismogenic zone, controlled by crustal temperature, needs to be in

the right range to store sufficient strain energy, and the strain-loading rate needs to be adequate to bring the rock matrix to failure. Four out of five largest earthquakes ($M > 6.5$) that have occurred over the last 30 years prefer average heat flow and average shear strain rate. These earthquake sequences occurred on faults adjacent to the fastest moving main plate boundary fault, the San Andreas fault. In some cases, their aftershocks extend over a range of heat flow and strain rate values because the mainshock fault rupture extends for a long distance, although the seismicity did not exhibit significant subsequent spatial or temporal migrations to particular values of heat flow or shear strain rates. Non-plate tectonic processes such as gravitational collapse of the high Sierra Nevada or geothermal activity explain seismicity occurring at extreme values of heat flow and shear strain rates.

Stress drop and scaling variations in Japan: what is the driving mechanism?

Adrien Oth

European Center for Geodynamics and Seismology, Luxembourg, adrien.oth@ecgs.lu

A fundamental controversy still exists upon the scaling characteristics of seismic source parameters such as stress drop and radiated energy. Over the past two decades, a significant number of studies provided persuasive evidence for an increase of the latter with seismic moment respectively magnitude, while other researchers casted doubt on these findings, arguing for constancy of stress drop and seismic energy-to-moment ratio and thus similarity of the rupture process between small and large earthquakes.

Recently, a countrywide study in Japan carried out by Oth et al. (2010) showed no evidence of any clear scaling break between small and large magnitude earthquakes. On the other hand, the continuation of this countrywide study, analyzing individual earthquake sequences as well as separating the catalogue of used events into different mechanisms, provided indications that these individual sequences can show significant deviations from self-similarity, and that these deviations are closely related to the dominant faulting mechanism of the sequence.

The study presented at the meeting extends these results to a significantly enlarged dataset (including aftershocks of the giant Tohoku earthquake) and to the discussion of lateral stress drop variations and their causes. In particular, the lateral stress drop variations will be discussed in conjunction with the variations observed in several other geophysical parameters of interest in earthquake source physics, such as faulting style, heat flow and shear strain rate. Of these parameters, heat flow shows the clearest relationship with the observed stress drop variations, indicating that above other factors, the thermally controlled shear strength of the crust is the key parameter in controlling the stress drop of crustal earthquakes.

Flat acceleration source spectrum is an ordinary property of stochastic self-similar earthquake fault with propagating slip pulse

A. A. Gusev

Institute of Volcanology and Seismology, Petropavlovsk-Kamchatsky. e-mail: gusev@emsd.ru

The classical "*omega-square*" model of earthquake source spectrum has a strong empirical support; but its adequate theoretical foundation is lacking. It will be shown how one can explain this spectral behavior by combining three concepts regarding earthquake source: (1) the theoretical description of the failure of fault asperity, after Das&Kostrov [1983, 1986]; (2) the concept, originated by Andrews [1981] and generally supported by inverted slip distributions [Tsai 1997; Somerville et al. 1999], that the field of the stress drop over an earthquake fault is stochastically self-similar (fractal) function with 2D amplitude spectrum of $1/k$ type; and (3) the idea that in an earthquake fault, a running dislocation strip [Haskell 1964] or slip pulse [Heaton 1990] is formed, that sweeps the fault area. To unite these concepts, it is assumed that the limiting distance of propagation of Rayleigh waves generated by a failing spot on a fault is determined by the width of the running slipping strip.

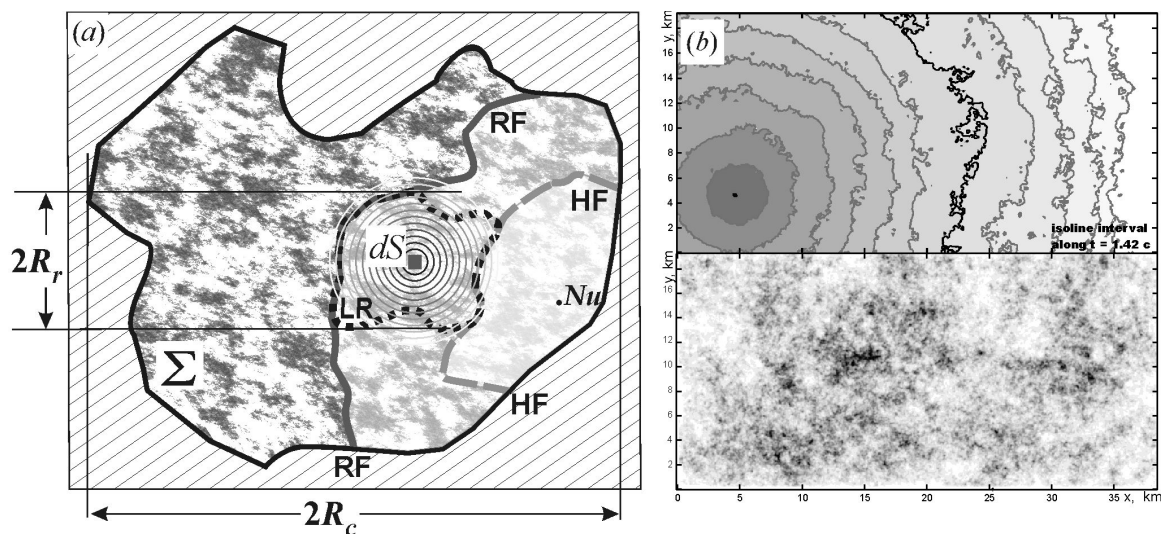


Figure 1. (a) A cartoon depicting an earthquake source S of size $2R_c$. Nu is the nucleation point/hypocenter. The dotted contour LR of size $2R_r$ depicts limits for propagation of Rayleigh waves from a particular elementary radiator dS . Lines RF (for rupture front) and HF (for healing front) indicate generalized positions of these fronts. These lines are not defined strictly, and merely outline the boundaries of a strip where the tortuous and fragmented fractal rupture front is localized at a certain time instant. (b, top) - rupture front propagation over an example simulated source. Wiggling isolines show positions of the fractal front each 1.42 s. Shades of gray represent time: the later, the lighter. The bold isoline gives a particular example position of the front. (b, bottom) - similar map of stress drop. Shades of gray reflect amplitude; maxima are darker.

It is also hypothesized that over its width, the slipping strip is formed by a tortuous, multiply connected rupture front with geometry of a random fractal line. Such geometry provides source incoherency at high k , that leads to low directivity of high-frequency radiation.

The theory of Kostrov&Das [1986] was developed for failure of small strong asperity on a big low-cohesion fault patch. It is applied as an approximation for the case of small elementary failing fault patch surrounded by larger low-cohesion area formed during propagation of a slip pulse. Seismic waves are simulated by kinematic numerical procedure that realizes the described approach. Simulated acceleration source spectra are flat at high frequency. Typically they are two-cornered, in agreement with observations. At a fixed seismic moment and fault size, the main parameter that defines high-frequency acceleration spectral level seems to be the relative width of the slip pulse (R_r/R_c).

To conclude, a technique for simplified kinematic simulation of seismic waves radiated by an earthquake source in a broad frequency band is successfully created; this technique is internally consistent and theoretically well founded. It provides explanation of many properties of broad-band strong ground motion and can be used for its simulation.

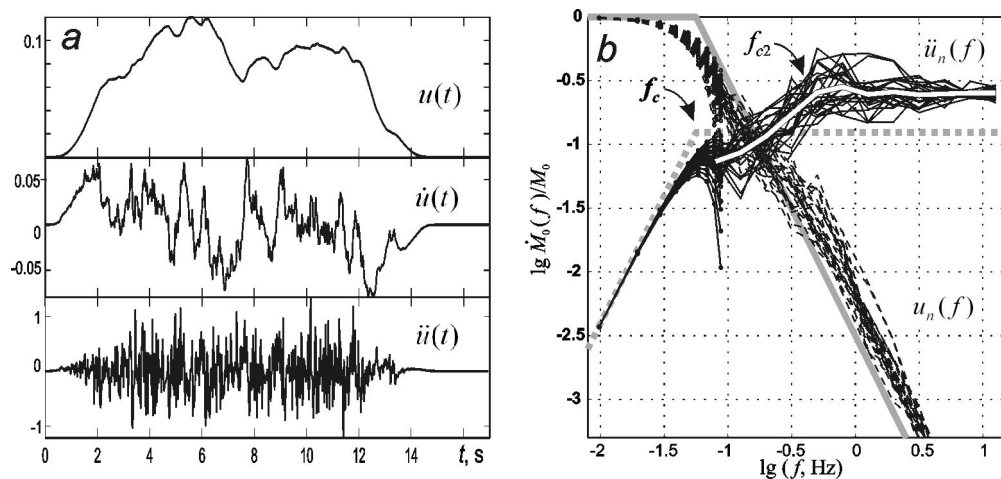


Figure 2. Typical results of simulation. (a) - example body wave time histories $u(t)$, $\dot{u}(t)$ and $\ddot{u}(t)$ at a far-field receiver on the ray normal to the fault. $R_r/R_c=0.06$; fault size 38×19 km. (b) 25 realizations of reduced acceleration amplitude spectra, original (on the left) and smoothed over bins of log-equal size of $1/3$ -octave width (on the right), depicted as a bunch of thin solid lines. All spectra are reduced to unit seismic moment. Similar displacement spectra are shown as dashed lines. Average acceleration spectrum is shown as the white line. Flat mean acceleration spectrum and two spectral corners f_c and f_{c2} are clearly seen. The main corner-frequency f_c is set as $1/2\pi T_{rms}$, where T_{rms}^2 is the second normalized central power moment for $u(t)$. Gray lines - stylized displacement (solid) and acceleration (dashes) spectra for the single-corner variant of ω^{-2} model.

Stress drop variability and dynamic fault weakening for extended earthquake sources

M. Cocco and E. Tinti

Istituto Nazionale Geofisica e Vulcanologia

Earthquake science has made extraordinary progress in the last years promoted by high-quality data, high-precision observations, improved computational facilities and laboratory experiments. Despite these advances and an improved understanding of physical processes, the grand challenge is nowadays to reconcile seismological measurements, geological observations and the key findings of laboratory experiments.

Several different observations on natural and experimental faults indicate that many different processes control dynamic fault weakening. These processes act at different spatial and temporal scales and they depend on geometrical and mechanical properties of fault zones. In this framework, asserting self-similarity of earthquake ruptures implies that we have established a hierarchy among length-scale or time-scale parameters characterizing each process and that a single process or a single length-scale dominates the others. This demonstration has never been achieved so far, because we don't know all the constitutive laws governing the dynamics of these processes. Therefore, we rely on physical intuitions for interpreting observations in terms of self-similarity.

Laboratory experiments might represent the future solution to identify the constitutive laws governing each process and to pinpoint the distinct length- and time-scale parameters. Moreover, bridging the gap between laboratory experiments and seismological observations should require that the physical processes governing experimental faults are the same operating in natural faults. These questions are still open and demand for answers to promote new discoveries.

In absence of such solutions, seismologists adopt a phenomenological approach and measure several macroscopic parameters on virtual mathematical planes of zero thickness. These phenomenological variables at macroscopic scale characterize our dynamic rupture models.

Seismologists provide estimates of several parameters characterizing the earthquake energy budget and the source processes on extended faults (such as radiated energy, stress drop, coseismic slip, rupture history, slip duration etc...). Most of these estimates are model dependent and they do not allow us to distinguish the processes controlling dynamic fault weakening.

In this study we focus on the frictional work, defined as irreversible work against frictional stresses, the different stress drop parameters and the seismological fracture energy. We use kinematic models inferred from geophysical data inversion and dynamic models from 3D simulations to investigate the variability of these parameters for extended faults. We conclude that, even in a scale-invariant world, the heterogeneity of rupture history on extended faults yields a variability of macroscopic phenomenological parameters that can bias commonly used, model-dependent, scaling laws.

Earthquake scaling relationships estimated from a 20 year catalog of source models derived from InSAR data

Gareth J. Funning¹, Jennifer Weston², Ana M. G. Ferreira², John R. Elliott³ and Barry E. Parsons³

¹ University of California, Riverside, USA

² University of East Anglia, Norwich, UK

³ University of Oxford, UK

The question of how moment release in earthquakes scales to other source parameters, such as fault length and average slip, is a long-standing controversy in earthquake science. The question has wide practical implications (e.g. in estimating seismic hazard due to known unruptured fault segments) and also theoretical implications (e.g. in the debate about self-similarity of earthquakes across all magnitudes). Here we use a catalog of earthquake source parameters derived from published InSAR earthquake studies to address this question. InSAR data may be considered preferable for this purpose over traditional sources such as aftershock data and seismic inversion models, as several key source parameters – in particular, the fault length – can in many cases be measured directly from the data. In a previous study (Weston et al., 2011), we found no systematic bias in seismic moment overall between InSAR-derived models and Global Centroid Moment Tensor solutions, suggesting that the InSAR-derived moment estimates are suitable for use in this way.

We have compiled fault length, width, average slip and seismic moment estimates from published studies of over 70 individual earthquakes, with $5 < M_w \leq 8.5$. Using grid searches, we find the best-fitting one- and two-trend scaling relationships between length and moment, treating all events together and also separately by mechanism type (strike-slip, thrust and normal). We additionally consider the relationship between fault average slip and fault length.

We find:

1) The best-fitting single scaling relationship (Figure 1) between moment and length has a slope of 1.81 in log-log space (i.e. $M_0 \propto L^{1.81}$). This is more consistent with ‘L model’ scaling (e.g. Scholz, 1982) which predicts a slope of 2. Indeed, thrust events, when considered separately, show a slope approximately equal to 2; strike-slip events show a slope of ~ 1.6 ; there are insufficient normal events at high magnitudes.

2) The data do not require a change of scaling regime around $M7.2$ as suggested previously (e.g. from a slope of 3 at low magnitudes to a slope of 1 at high magnitudes; Romanowicz, 1992; Figure 1).

3) Ratios of average slip to length fall broadly into two fields (Figure 2) – high slip-to-length events ($1-3 \times 10^{-4}$) and low slip-to-length events ($0.4-4 \times 10^{-5}$). The low slip-to-length category includes subduction earthquakes and events occurring on strike-slip faults with fast slip rates (> 2 mm/yr); the high slip-to-length category includes several blind faulting earthquakes, typically occurring on faults with low slip rates (< 2 mm/yr).

These data, being completely independent of the data used in other scaling studies may provide a means to adjudicate between existing competing models of earthquake scaling.

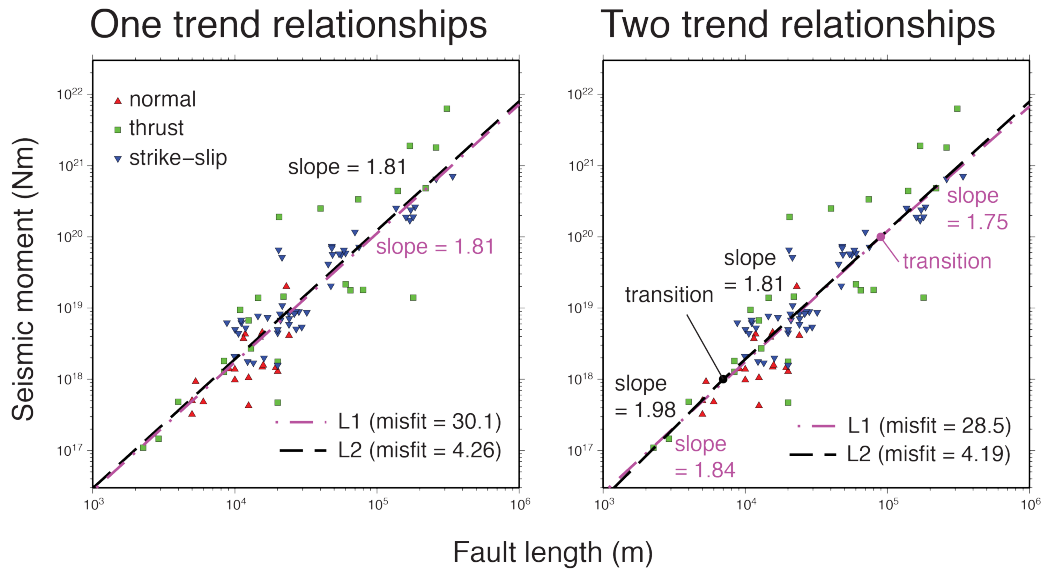


Figure 1. Moment-length scaling. *Left:* The best-fitting single trend has a slope of 1.81, minimising either the L1 or L2 norm. *Right:* The best-fitting two-trend scaling relationship deviates little from a straight line in log-log space, with the two slopes being very similar in value for both solutions. Given the doubling in numbers of free parameters for the two trend case, the <5% improvement in misfit is not significant.

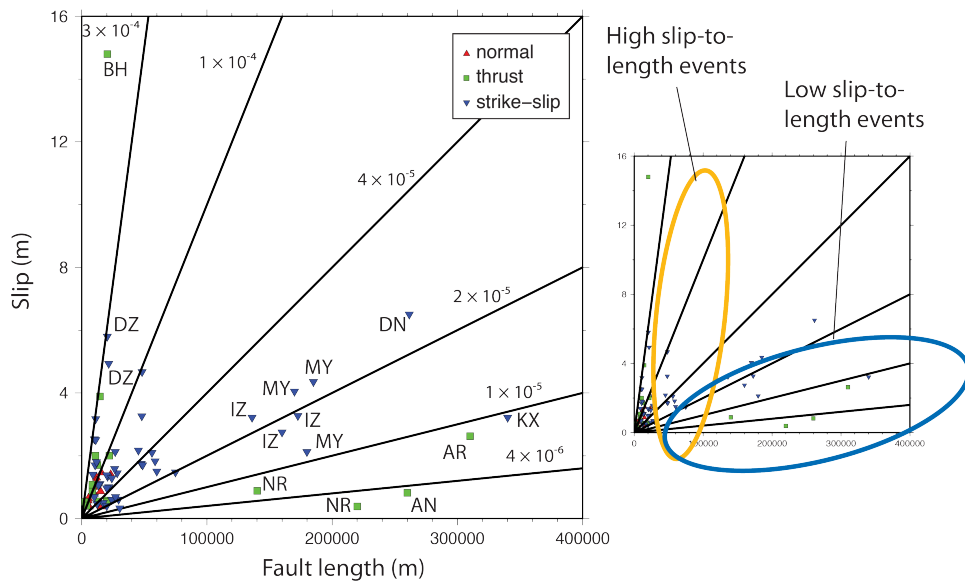


Figure 2. Slip-length scaling. Low slip-to-length events (ratios $0.4\text{--}4 \times 10^{-5}$) include all of the large strike-slip and subduction megathrust earthquakes from high-slip-rate plate boundary faults. High slip-to-length events (ratios $1\text{--}5 \times 10^{-4}$) tend to be from faults with low slip rates (< 2 mm/yr). This may reflect differences in the length of recurrence time (and therefore fault healing) between the two types of events, consistent with ‘age-law’ formulations of rate-and-state friction. [Event names: BH – Bhuji, (2000) DZ – Duzce (1999), IZ – Izmit (1999), MY – Manyi (1997), DN – Denali (2002), NR – Nazca Ridge (1997), AN – Antofagasta (1995), AR – Arequipa (2001), KX – Kokoxilli (2001)]

Uncertainty Quantification in Earthquake Source Studies: The SIV Initiative and its Implications for Source Parameter Estimation

P. Martin Mai

Division of Physical Sciences & Engineering King Abdullah University of Science & Technology

Earthquake source inversions are applied almost routinely nowadays to estimate the spatio-temporal rupture evolution on one or more fault planes using seismic and/or geodetic data. However, the uncertainties in the resulting rupture models are hardly ever quantified and disseminated, although the (often rapidly online) published inversion solution are interpreted as an accurate kinematic representation of the earthquake rupture process. Because reliable earthquake source studies are mandatory (i) to investigate earthquake mechanics, (ii) to develop spontaneous dynamic rupture models, and (iii) to build models for generating rupture realizations for ground-motion simulations, adequate uncertainty quantification for finite-fault rupture models is urgently needed. It is important to recognize also that earthquake source inversions constitute an inherently ill-posed inverse problem to which many a priori assumptions and uncertain observations are applied which are often not clearly reported.

The Source Inversion Validation (SIV) project is a collaborative effort to understand the variability between rupture models for a single earthquake (as manifested in the finite-source rupture model database) and to develop robust uncertainty quantification for earthquake source inversions. The SIV project proposes an open-access online testing platform to examine the current state-of-the-art in earthquake source inversion, and to develop and test novel source inversion approaches.

In this presentation I will review the current status of the SIV project, and summarize the findings and conclusions of the most recent benchmarks: a forward-modeling test on Green's function calculations, and an inversion for synthetic data from spontaneous dynamic crack-like strike-slip earthquake on steeply dipping fault. Additionally, I will discuss how common source parameter estimation (and subsequent interpretations) are affected by intra-event variability of finite-fault rupture models.

The Scale Dependence of Rupture Barriers

Jeffrey J. McGuire¹, John A. Collins¹, Pierre Gou ard², Emily Roland³, Dan Lizarralde¹, Margaret S. Boettcher⁴, Mark D. Behn¹, Yajing Liu⁵ and Robert D. van der Hilst²

¹ Woods Hole Oceanographic Institution

² Massachusetts Institute of Technology

³ U.S.G.S. Anchorage

⁴ University of New Hampshire

⁵ McGill University, Montreal

Mid-Ocean Ridge Transform faults (RTFs) are better at stopping large ruptures than any other type of tectonic fault system. The largest earthquakes on RTFs rupture only a small portion of the available fault area and, the rupture area does not scale linearly with the total area of the seismogenic zone [Boettcher and Jordan 2004]. This scaling indicates that significant portions of the oceanic lower crust and uppermost mantle within RTF fault-zones have physical properties that have been altered (relative to normal oceanic lithosphere) to prevent the propagation of large ruptures. The relatively short seismic cycles, ~5-15 years, of some RTFs have demonstrated that the rupture barriers are stationary in space from one earthquake cycle to the next [Boettcher and McGuire 2009]. However, in at least the best constrained cases these barriers do not appear to result from large geometrical discontinuities of the fault-surface. Despite these RTF rupture barrier zones being the most efficient rupture-stopping fault segments that we know of, local observations have recently revealed that they are also the most seismogenically active portions of plate boundaries with rates exceeding 1000 earthquakes per day ($M > \sim 0$) in very localized (~10km) regions. Thus, rupture barrier regions of RTFs show a clear scale dependence in that they are velocity weakening for small slip (earthquakes smaller than magnitude ~4) but velocity strengthening for large ($M 5-6$) ruptures over multiple seismic cycles.

Recently a deployment of ocean bottom seismometers captured a $M 6$ earthquake on the Gofar Transform fault on the East Pacific Rise and gives us our first high-resolution view of these rupture barriers [McGuire et al., 2012; Roland et al., 2012]. The September 18, 2008 $M 6.0$ Gofar earthquake was preceded by a swarm of ~20,000 foreshocks that lasted about one week and was confined to a 10-km-long rupture barrier. The foreshock sequence coincided with a ~3% decrease in the average shear-wave speed in the high-porosity fault zone. Active source seismic images constrain the porosity of the rupture barrier fault-zone to be a few percent all the way through the seismogenic zone, which is in strong contrast to results from other EPR RTFs that generate large earthquakes [Roland et al. 2012]. Our observations suggest that the material properties of fault segments capable of rupturing in large earthquakes and those of rupture barrier regions differ, possibly as a result of enhanced fluid circulation within the latter. Moreover, the seismicity-rate in the rupture barrier regions appears to vary strongly with time during the seismic cycle (Figure 1). It is at least an order of magnitude higher during the last 10% of the seismic cycle than it is during the first 10% of the seismic cycle. This may be a demonstration of the importance of absolute stress levels, not purely stressing-rate, on controlling seismicity-rate.

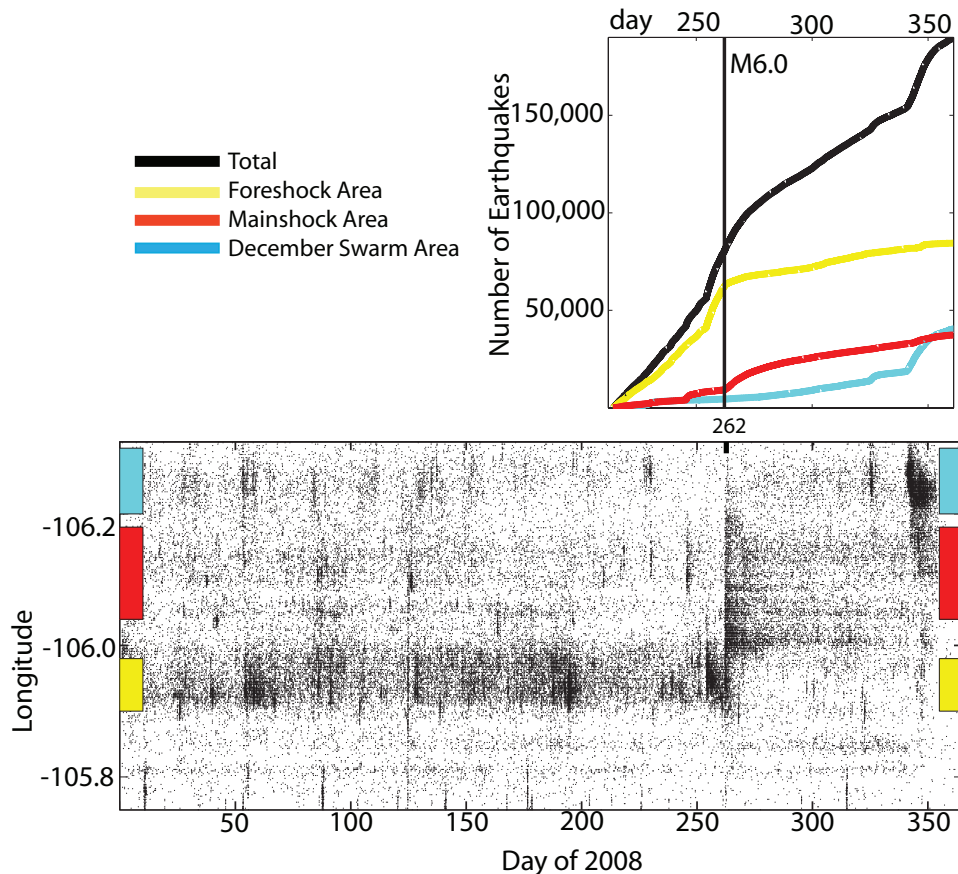


Figure 1. From McGuire et al., 2012. The temporal distribution of earthquakes on the western portion of the Gofar Transform fault during 2008 from McGuire et al., 2012. Top) Cumulative number of earthquakes in the waveform-detection earthquake catalog (black line). The yellow, red, and cyan curves show cumulative earthquakes in the foreshock zone (105.9° – 105.98° W), mainshock rupture zone (106.04° – 106.18° W), and the December swarm zone (106.2° – 106.3° W) respectively. The M6.0 mainshock occurred on day-of-year 262 or Sept. 18 (vertical black line). Bottom) Locations and times of all of the earthquakes in the STA/LTA catalog covering the entire year of 2008. The solid yellow, red, and cyan rectangles denote the same sections of the fault as the colored curves in the upper panel.

References

- Boettcher, M. S. & Jordan, T. H. Earthquake scaling relations for mid-ocean ridge transform faults. *J. Geophys. Res.-Solid Earth* **109**, 21, 2004jb003110 (2004).
- Boettcher, M. S. and J. J. McGuire, Scaling Relations for Seismic Cycles on Mid-Ocean Ridge Transform Faults, *Geophys. Res. Lett.*, 36, L21301, doi:10.1029/2009GL040115 2009.
- McGuire, J.J., J. A. Collins, P. Gouedard, E. Roland, D. Lizarralde, M. S. Boettcher, M. D. Behn, R. D. van der Hilst, Capturing the End of a Seismic Cycle on the Gofar Transform Fault, *Nature Geoscience*, DOI:10.1038/NGEO1454, 2012.
- Roland, E., Lizarralde, D., J. A. Collins, and J. J. McGuire, Constraints on the material properties that control earthquake behavior from seismic velocity structure at the Quebrada-Discovery-Gofar transform faults, East Pacific Rise, *J. Geophys. Res.*, submitted 2012.

Modeling scale-invariant heterogeneity of earthquakes

Satoshi Ide

Earth and Planetary Science, University of Tokyo

Earthquake sources are characterized by several scaling relations between macroscopic source parameters, such as fault size, slip amount, duration, stress drop, seismic moment, and radiated seismic energy. These macroscopic scaling relations suggest the self-similarity of seismic sources, at least as a first degree approximation. In addition to these relations, several studies suggested that the heterogeneity of seismic sources is also scale invariant: namely a small earthquake is simply a self-similar miniature of a large event, though further studies are necessary to confirm this hypothesis.

To realize the properties of statistically self-similar complex rupture, Ide and Aochi (2005) modeled an earthquake using a hierarchical patch model, in which heterogeneity of fault plane is represented by numerous circular patches whose size-frequency statistics obeys a power law. Each patch has its own slip-weakening law and the most important assumption is that the slip-weakening distance and fracture energy of each patch is proportional to the patch radius. By solving the elastodynamic equation using BIEM, Ide and Aochi (2005) demonstrated that this model can simulate various features observed in real earthquakes, such as multiple subevents, overall subshear rupture propagation with occasional supershear propagation, irregular rupture onsets like initial phases, and spontaneous termination.

This model can be applied to real earthquakes. The March 11, 2011, Tohoku-Oki earthquake (Mw 9.0) is one of the best studied earthquakes and its very complex rupture propagation was revealed consistently by many research groups (e.g., Ide et al., 2011). A unique feature is that the rupture occurred repeatedly between shallow and deep parts of the plate interface. The delay of the largest slip near the trench that is responsible to the disastrous tsunamis is also strange. These features are naturally explained by a cascading rupture of circular patches distributed mainly based on the historical seismicity in the Tohoku-Oki region (Ide and Aochi, submitted).

Gutenberg-Richter breakdown and the smallest earthquakes at the San Andreas Fault Observatory at Depth

William L. Ellsworth¹ and Kazutoshi Imanishi²

¹ U.S. Geological Survey, Menlo Park, CA, USA

² Geological Survey of Japan/AIST, Tsukuba, Ibaraki-ken, Japan

According to Rate and State theory the minimum radius of a nucleation zone that will initiate an earthquake is given by

$$h^* = G d_c / (B-A) \sigma$$

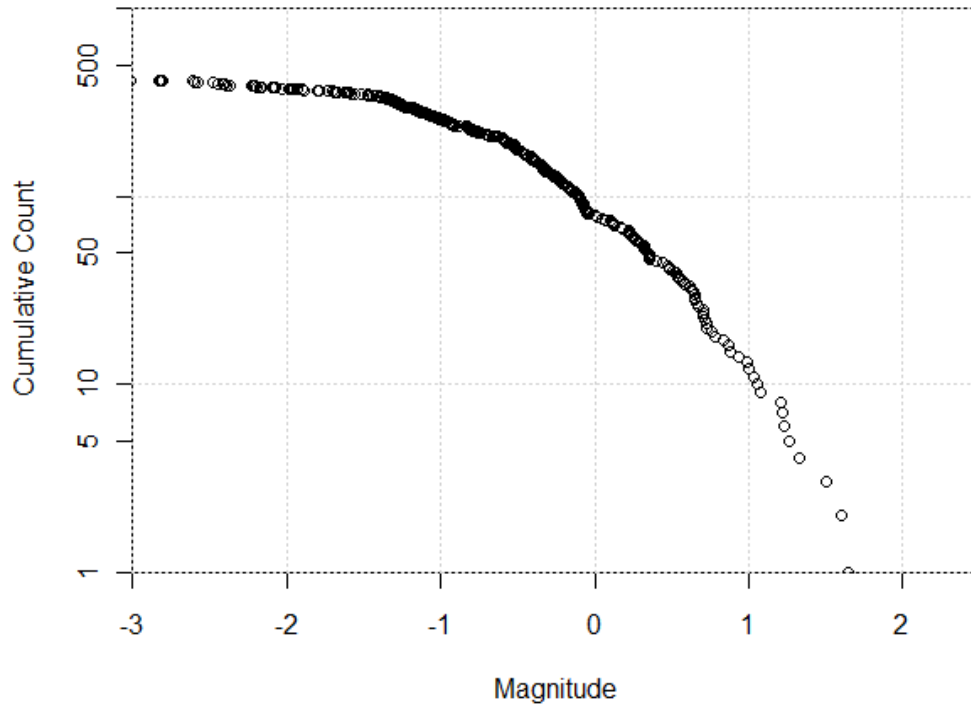
where G is the shear modulus, d_c is the sliding distance over which friction evolves, $B-A$ is the velocity weakening parameter and σ is the effective normal stress. Laboratory derived values for d_c and $B-A$ suggest that the minimum earthquake should have a magnitude well below $M_w = 0$, assuming that the range of stress-drops observed at larger magnitude continues to apply. Indeed, earthquakes with $M_w < -3$ have been observed in the SAFOD borehole and events with $M_w < -4$ have been observed in deep mines in South Africa. It remains an open question, however, how to connect the minimum source dimension for nucleation, h^* , to either the magnitude of the minimum earthquake or earthquake population statistics for the smallest earthquakes.

To explore this problem, the frequency-magnitude distribution of earthquakes occurring within a 1.5 km radius of the SAFOD borehole was studied. At SAFOD the fault is creeping almost everywhere, except for a few isolated patches that produce repeating earthquakes (Zoback et al., 2011, doi:10.2204/iodp.sd.11.02.2011). Between May 2009 and May 2012 over 400 earthquakes were detected by a high-gain 15 Hz seismometer installed in the SAFOD main hole at a depth of 2550 m below the land surface. These earthquakes exhibit a linear Gutenberg-Richter frequency-magnitude relation with $b = 0.7$ for $M_w \geq -0.5$. Below $M_w -0.5$, however, the G-R relation breaks down and $b = 0.3$ or smaller. The breakdown is not believed to be an artifact of incomplete detection of events, but rather reflects a change in earthquake population statistics. The breakdown begins for earthquakes with source dimensions of $O(3$ m) and mean slip of $O(100$ microns) according to measurements made using the Multi-Window Spectral Ratio method of Imanishi and Ellsworth (2006, doi: 10.1029/170GM10).

We consider the implications of rate-and-state friction of a minimum size for h^* for the breakdown in the G-R relation. We assume that on this creeping fault the distribution of velocity weakening patch sizes and their earthquake cycle times sum to produce a G-R distribution with constant b -value at all scales. Those with radii $\gg h^*$ always produce earthquakes while those with radii $\ll h^*$ do not. The question is what happens as the radius approaches h^* ? Chen and Nadia Lapusta (2009, doi: 10.1029/2008JB005749) conducted numerical simulations of the behavior of a velocity weakening patch embedded in a velocity strengthening (creeping) fault as an analog to the San Andreas Fault at SAFOD. They found that as the radius of the patch passed through the transition radius between always stable and fully seismic rupture it produced earthquake events with dimensions smaller than h^* . This

mechanism provides a good match to the observations when the transition to a fully-coupled patch occurs at $M_w=0$.

Earthquakes within 1.5 km of SAFOD Main Hole Seismometer



Oral Program
Friday, 5 October 2012

KEYNOTE LECTURE:

Long-term behavior of fault models with enhanced co-seismic weakening: Importance of earthquake nucleation

Nadia Lapusta

California Institute of Technology, USA

Until relatively recently, rock experiments on low-velocity friction and in situ measurements had indicated that earthquake faults have shear strength of the order of 100 MPa at typical seismogenic depths, which is large compared to typical earthquake stress drops of 1-10 MPa. Yet numerous lines of evidence indicate that large, mature faults operate under substantially lower levels of shear stress, including low heat outflow, significant changes in stress state following large events as indicated by microseismicity, and geometry of thrust-belt wedges. Theories and recent lab observations of substantial co-seismic weakening provide a potential explanation to the heat outflow observations, yet the dramatic change from high static to low dynamic strength during seismic events may be considered as a contradiction to the relatively low inferred values for static stress drops.

We will discuss fault models of long-term fault slip that reconcile high static strength and low co-seismic strength with typical stress drops (2D models by Lapusta, Noda, and Rice; work in progress on 3D models by Jiang and Lapusta). The models incorporate fault heterogeneity through places susceptible to earthquake nucleation; the presence of such locations on natural faults is supported by multiple lines of observations. Earthquakes start at the nucleation sites while the fault stress is still far, on average, from its static strength, and propagate due to wave-mediated stress concentrations coupled with substantial shear-heating-induced weakening. Hence the fault operates at the levels of shear stress that are much lower than its average static strength, with the resulting stress drops in the typical range of 1-10 MPa.

Since most of the slip is accumulated at the low dynamic strength, the model results in low heat outflow, consistently with observations. The seismic events have short durations of local slip, resulting in the so-called pulse-like propagation, as inferred for natural faults. The model should be applicable to large, mature faults that have achieved, through millions of years of relative sliding, sufficient shear localization for the shear-heating dynamic weakening mechanisms used in the model to apply.

The nucleation-prone locations are crucial to producing such fault behavior. Two types of such locations are examined in the model: places of stress concentration between stably creeping and locked segments and “weaker” patches that have smaller friction coefficients. Our findings emphasize the importance of earthquake nucleation sources and their properties, and their potential control over the entire dynamics of mature faults.

KEYNOTE LECTURE:

Friction during earthquakes from rock deformation experiments

Giulio Di Toro^{*1,2}, Stefan Nielsen², Elena Spagnuolo², Steven Smith² and Marie Violay²

¹ Dipartimento di Geoscienze, Università di Padova, Via Gradenigo 6, Padova, Italy

² Istituto Nazionale di Geofisica e Vulcanologia, Via di Vigna Murata 605, Roma, Italy

* Presenting author's e-mail address: giulio.ditoro@unipd.it

Friction is the basic parameter that controls fault slip during an earthquake. However, at seismic slip rates little is known about how the dynamic friction coefficient (μ) varies with rock composition, normal stress, displacement, ambient temperature and fluid conditions. Insights arise from experiments performed with dedicated apparatus that reproduce some of the deformation conditions achieved during earthquakes (up to 50 m of slip for the Tohoku 2011 M 9.0 earthquake; slip rates of 0.1-10 m/s, accelerations $> 10 \text{ m s}^{-2}$, and normal stress $> 50 \text{ MPa}$).

In this contribution we will review and discuss the results of experiments performed under coseismic deformation conditions, including those from a Slow to High Velocity Apparatus (SHIVA) recently installed at INGV, Rome. SHIVA uses two brushless engines (max power 300 kW, max torque 930 Nm) in a rotary shear configuration to slide hollow rock cylinders (30/50 mm int./ext. diameter) at slip rates ranging from 0.01 mm s^{-1} up to 6.5 m s^{-1} , accelerations up to 80 m s^{-2} and normal stresses up to 50 MPa. SHIVA is equipped with a sample chamber to carry out experiments in the presence of fluids (up to 15 MPa fluid pressure), a gouge sample holder (tested up to 27 MPa in normal stress), and an environmental/vacuum chamber connected to a mass spectrometer to measure gas release during frictional sliding. In particular we will show that:

- 1) faults are lubricated ($\mu < 0.1$) during earthquakes, independent of the rock type and weakening mechanisms involved (flash weakening, melt and gel lubrication, thermal pressurization, etc.);
- 2) fault lubrication is achieved after a power-law strength decay from a peak value at the initiation of sliding to a steady state value achieved over a weakening distance D_w ;
- 3) D_w decreases linearly (independently of rock type) with normal stress and the square root of the slip rate;
- 4) friction has a strong dependence with slip rate and fault healing is almost instantaneous once slip rate decreases;
- 5) in silica-bearing rocks, the shear stress dependence on normal stress at steady-state is highly non-linear;
- 6) different weakening mechanisms are activated at increasing mechanical work rates per unit fault surface: for instance, gel lubrication and flash weakening are more efficient than melt lubrication at low work rates ($< 1 \text{ MW m}^{-2}$);
- 7) in experiments performed with the pressure vessel in the presence of pore fluids (un-drained conditions), thermal pressurization is less efficient than other weakening mechanism (flash heating and weakening, powder lubrication, etc.);

8) when the shear stress on the sample (rather than the slip rate) is progressively increased, spontaneous creep episodes (lasting a few mm to a few cm in slip) are triggered and they precede the large stress drops typical of earthquake instabilities;

9) importantly, microstructural and geochemical investigation of post-mortem samples evidence strong similarity with natural products from exhumed faults, suggesting that the physico-chemical coseismic processes triggered in the laboratory are activated in nature.

The above experimental data, in some cases supported by geological and geophysical observations, have implications which are not trivial to relate to seismological observations and standard source scaling relations. For example, we will discuss comparisons of experimental measurements and seismological estimates of energy dissipation and coseismic stress drops on faults in the companion contribution at this meeting (Nielsen et al.).

An attempt to reconcile friction experimental measurements with seismological observations

Stefan Nielsen¹, Elena Spagnuolo¹, Steven Smith¹, Marie Violay¹ and Giulio Di Toro^{1,2}

¹ Istituto Nazionale di Geofisica e Vulcanologia, Roma, Italy

² Dipartimento di Geoscienze, Università di Padova, Padova, Italy

Experiments performed on rocks at deformation conditions typical of seismic slip, reviewed in the companion presentation at this meeting (Di Toro et al.), show an extremely low friction coefficient, the activation of lubrication processes and a power-law strength decay from a peak value to a residual, steady-state value. In this presentation we discuss the implications that such experimental results would have on seismogenic faults and whether they are compatible with seismological estimates. In particular, we discuss coseismic stress drop and the scaling of fracture energy G .

1) Comparison of fracture energy G measured in the laboratory and G' estimated from seismological data. Here we refer to friction σ_f as the shear stress resisting sliding (not to be confused with the dimensionless friction coefficient). Dynamic friction measured in the experiments under high stress and slip rate shows wide variations in both steady-state value and weakening rate. However, when the experimental procedure is accurate enough to allow good signal-to-noise ratios and a high degree of repeatability in the results, one consistent feature appears throughout a wide variety of experimental conditions and lithologies: weakening follows a power-law in the form $\sigma_f = (u+u_0)^{-\alpha} + \sigma_{SS}$ where σ_{SS} is a residual friction at steady-state, u is slip and u_0 a small constant. The best-fitting exponent α for a large number of experiments is $\alpha \approx 0.34$.

The resulting experimental fracture energy (defined, for a given slip amount u , as the integral between the frictional curve and the minimum frictional level reached $\sigma_f(u)$) scales as $G \propto u^{1-\alpha}$, a power-law in some aspects in agreement with the seismological estimates of $G' \propto u^{1.28}$ proposed by Abercrombie and Rice (2005) or $G \propto u^2$ proposed by Tinti et al (2005). The values of G and G' are comparable for slips of about $u=1\text{cm}$ (G approx 10^4 J/m^2). Both gradually increase with slip up to about 10^6 J/m^2 , however, it appears that fracture energy G' is perceptibly larger than G in the range of slip $0.1 < u < 10$ and also that G' increases more rapidly with slip because the exponent in G is lower than in G' (i.e. 0.66 vs. 1.28 or 2). We next discuss the possible causes of such discrepancy.

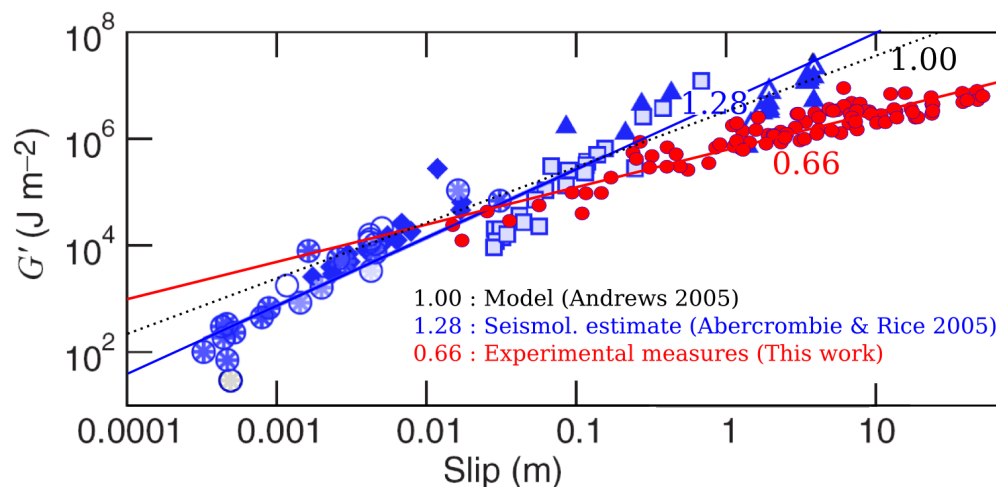
As discussed in Shipton et al., 2006, the effective G' observed at the seismological scale should implicitly incorporate energy sinks other than frictional dissipation alone.

On a planar fault, the stress level off-fault is sufficiently high to induce anelastic damage on a thickness increasing with length propagation, as initially proposed by Poliakov et al (2002). In a model by Andrews (2005) the dissipation due to plastic strain results in G scaling with slip so that $G \propto u^1$, an exponent value intermediate between that due to frictional decay and that estimated from seismological data.

However natural fault surfaces are rough at many different scales and the slipping zone is often made of non-cohesive rock (gouge). Instead, experiments are

performed on smooth, machined surfaces (wavelength $< 10^{-3}$ m) and often on cohesive rocks. During coseismic slip, the non-planarity of natural faults results in asperity removal (especially at a wavelengths > 0.1 m) and off-fault damage which will introduce energy sink in addition to that of friction on the sliding surface itself. Moreover, in the presence of fault gouge (non-cohesive rock), typical at depths $< 6-7$ km, a relevant portion of energy may be dissipated during the slip-localizing process. Since G' is obtained by estimating the amount of dissipation with respect to strain energy and radiated energy, it will implicitly incorporate the sum of all dissipative processes due to rupture propagation and fault slip, necessarily larger or equal to the laboratory, friction-only related measurements.

With increasing fault slip, the size of the topographical asperities which are removed, the wavelength of fault bends which are involved and the thickness of the damage zone increases, so that the effective G' may, on the one hand, be larger than the experimentally measured G , but on the other hand, it may also increase faster (e.g with a larger exponent). The fault surface topography can be described by a distribution with power spectrum $P(k)=k^{-1-2H}$ where k is wavenumber and H is the Hurst (or Hausdorff) exponent. Assuming that different scales can be decoupled we may integrate the elastic work due each wavenumber interval when fault undergoes a given offset u . If a fraction of the elastic strain work is dissipated while the asperities are cyclically strained, such process yields a power-law in $G' \propto u^{2H-1}$. A value $H \approx 1.15-1.5$ would yield a scaling in agreement with seismological estimates, however, measures of H for natural faults usually fall in the range $0.5 < H < 1$ for which this model under-predicts the exponent estimated from seismological observations.



2) Low friction does not necessarily imply large stress drops. For rupture to propagate, well-known energy considerations show that fracture energy G , rupture length L and stress drop $(\sigma_0 - \sigma_f)$ should scale so that $(\sigma_0 - \sigma_f)^2 > 2\mu G/L$, where σ_0 is initial stress and σ_f is dynamic sliding stress. Lowering both σ_0 and σ_f by an equal amount will not restrain rupture propagation and will leave the stress drop unchanged; seismic radiation will remain unaltered too. As a consequence stress drop can match the relatively moderate seismological estimates under a low sliding friction, even for a virtually total dynamic stress drop, provided that a relatively low prestress is assumed.

On the other hand, these observations have the following implications: (1) a low dynamic stress implies a low amount of heat produced during sliding, in agreement with the absence of a significant heat flow on seismic faults; (2) a low

initial stress is in agreement with some down-hole measurements close to major active faults, though punctual stress measurements are not necessarily representative of average values; (3) the radiation efficiency $\eta = 2 E_S / (\sigma_0 + \sigma_1)$, may be higher than in classical high-stress models because the average stress $\frac{1}{2}(\sigma_0 + \sigma_1)$ will be lower while stress drop and radiated energy E_S may remain the same.

Earthquake nucleation: stressing rate affects foreshock occurrence and minimum earthquake size

Gregory C. McLaskey, Brian D. Kilgore, Nicholas M. Beeler and David A. Lockner

U.S. Geological Survey, Menlo Park, California, USA

We have conducted laboratory experiments on the large-scale biaxial apparatus in Menlo Park, CA that shed light on earthquake nucleation processes and foreshock occurrence. We studied a set of 13 consecutive stick-slip cycles performed at 5 MPa constant normal stress and 0.001 MPa/s shear loading rate. The 2 m long fault cut diagonally in the 0.419 m thick granite sample is instrumented with an array of slip and strain sensors that are used to measure stress redistribution and premonitory slip during the nucleation phase as well as stress drop, slip velocity, and rupture speed during dynamic rupture. In all cases studied, nucleation is characterized by a sequence of gradually accelerating aseismic slip events (and associated stress redistribution) in the center of the fault while the ends of the fault remain locked. Most event-to-event differences in nucleation are due to variations in the timing of this sequence. For the fastest nucleation sequences observed, aseismic slip and stress redistribution begins 10 seconds prior to the stick-slip instability, and slip localizes to a zone in the center of the fault in the final 20 ms before instability. This slipping zone expands at a rate of ~ 20 m/s before it accelerates to seismic speeds close to 2000 m/s. The slowest nucleation sequences observed begin 30 seconds prior to the stick-slip instability, localization occurs 400 ms before instability, and the slipping zone expands at ~ 1 m/s.

Many stick-slip events are accompanied by impulsive, high frequency foreshocks 5-50 ms prior to the dynamic rupture of the entire fault. These foreshocks are detected with an array of piezoelectric sensors that measure high frequency (100 Hz – 1 MHz) surface displacements. Foreshock hypocenters are determined with 10 mm accuracy along strike and depth based on the arrival times of P- and S-waves that are clearly identifiable in the recorded signals. The focal mechanism, source time history, and absolute size of the foreshocks are quantified by comparing recorded signals to synthetic seismograms. Elastodynamic Green's functions are computed with a generalized ray theory code and verified with 3D finite element models. Instrument response functions for the piezoelectric sensors are quantified *in situ* using ball impact calibration sources. Recorded ground displacements from individual foreshocks have pulse-shaped farfield P- and S-waves. The duration of the body wave pulse is typically 3-10 μ s, which constrains the source radius to less than 7-22 mm. Typical foreshocks have peak moment rates of 250-750 kNm/s, and scalar seismic moments of 0.07-4 Nm ($M_w = -6.8$ to -5.5). The foreshock focal mechanisms are consistent with a shear dislocation on the fault.

A distinct sequence of these high frequency foreshocks is often detected during the nucleation phase. The foreshock locations migrate along strike and roughly track the expansion of the slipping region during nucleation. The locations of individual foreshocks persistently cluster on localized patches within the interior of the fault. These patches collectively comprise only a small fraction ($\sim 1\%$) of the fault region that is inferred to be slipping during this stage of the nucleation process. By studying the relative timing of stress changes and seismicity, we conclude that the foreshock patches are loaded by aseismic slip of the surrounding region during the nucleation of the larger stick-slip instability. Based on measurements of local shear strain, we

estimate that this type of loading causes local stressing rates to exceed the 0.001 MPa/s externally applied shear stressing rate by at least three orders of magnitude. Additionally, we find that those fault patches that persistently produce high-frequency foreshocks during rapidly nucleating stick-slip events will not produce foreshocks and instead slip aseismically when nucleation proceeds at a slower rate.

While the meter-sized nucleation region of the stick-slip instability is generally consistent with previous theoretical estimates of earthquake nucleation length (Okubo and Dieterich, 1984; Ampuero and Rubin, 2008), the foreshocks we record are significantly smaller than the theoretical minimum length scale over which an earthquake can nucleate under quasi-static loading conditions and homogeneous fault properties. This work shows that these tiny earthquakes (M_w -6) only occur when the local fault stressing rate is high. This conclusion is supported by numerical modeling (Kaneko and Lapusta, 2008; Fang et al. 2010) that indicates that earthquake nucleation size will shrink when the stressing rate is increased. A stressing rate dependence on the nucleation properties of earthquakes may help explain the existence of extremely small earthquakes recorded in active gold mines, and tiny aftershocks recorded at SAFOD, California.

References

- Ampuero, J. P., and A. M. Rubin (2008), Earthquake nucleation on rate and state faults aging and slip laws, *J. Geophys. Res.*, 113, B01302.
- Fang, Z., J. H. Dieterich, and G. Xu (2010), Effect of initial conditions and loading path on earthquake nucleation, *J. Geophys. Res.*, 115, B06313,
- Kaneko, Y., and N. Lapusta (2008), Variability of earthquake nucleation in continuum models of rate-and-state faults and implications for aftershock rates, *J. Geophys. Res.*, 113, B12312.
- Okubo, P. G., and J. H. Dieterich (1984), Effects of physical fault properties on frictional instabilities produced on simulated faults, *J. Geophys. Res.*, 89(B7), 5817–5827.

Friction on faults and scaling laws: hypotheses, dynamic models, and comparisons against lab experiments

Luca Malagnini¹, Irene Munafo¹, Massimo Cocco¹, Stefan Nielsen¹,
Elena Spagnuolo¹, and Kevin Mayeda²

¹ Istituto Nazionale di Geofisica e Vulcanologia, Sezione di Sismologia e Tettonofisica

² University of California, Berkeley

Seismic spectra may be described using small sets of parameters whose uncertainties have been, until recently, too large to be used for the definition of clear scaling relationships. For example, the Brune stress drop may be given in terms of seismic moment and corner frequency through a functional form in which the cube of f_c appears. Consequently, the error bars associated to the Brune stress drops get easily very high and, possibly, may completely hide possible variations of this parameter for increasing moment magnitudes.

We recently developed a spectral ratio technique that allows spectral measurements with very little error bars, like those of corner frequency and apparent stress, that may be used to obtain acceptable error bars for the estimates of Brune stress drop and radiated seismic energy.

We assume the following: i) the Brune spectral model accurately describes seismic spectra; ii) no overshoot or undershoot are allowed; iii) the yield stress equals the critical pre-stress; iv) Anderson theory of faulting holds. Based on these assumptions, shear stress of critically stressed faults is calculated at the time of failure, together with “dynamic” friction coefficients that provide evidence for a progressive frictional weakening of faults for increasing seismic slip (and moment magnitude). A scaling law is provided to describe the seismological observations.

The functional form obtained for the inferred frictional weakening is compared with lab observations collected on SHIVA, a state-of-the-art high-pressure high-velocity frictional apparatus. The interpretation of the scaling law is given in terms of a dynamic model.

Using a constitutive friction law to constrain co-seismic slip: the 2004 Parkfield example

Alon Ziv

Department of Geophysics and Planetary Sciences, Tel-Aviv University, Tel Aviv, Israel

I describe a new approach for co-seismic slip inversion, whereby both GPS displacements and first day aftershock rate changes are used jointly to constrain the solution. The joint inversion incorporates Dieterich's aftershock model, which adopts a constitutive friction law that depends logarithmically on the sliding rate. The method is applied to the 2004 Parkfield earthquake. By successfully fitting both the GPS and the aftershocks datasets, I show compatibility with the adopted aftershock model. Yet while typical laboratory values for the friction dependence on the logarithm of sliding speed are in the range of 0.005 to 0.015, satisfactory fit to both aftershocks and GPS datasets can only be obtained for a constitutive friction parameter that is more than an order of magnitude lower than the laboratory values. While the resolving power of GPS-only inversions using 300 uniform cells drops quickly with distance from the GPS stations, such that the slip distribution below about 4 kilometers and near the fault ends cannot be resolved, the resolution of the joint inversion using 1200 non-uniform cells is high both near the surface and in areas of aftershock activity at depths inaccessible to GPS-only inversions. Thus, despite the threefold increase in the number of model parameters, the resolution of the joint inversion is much better than that of the GPS-only inversion. A consequence of the adopted aftershock model and the irregular aftershock distribution is that the slip distribution is extremely non-smooth, with the aftershock zones acting as barriers.

Frictional properties of Zuccale Fault rocks from room temperature to in-situ conditions: the effect of temperature and fluid pressure on slip stability

André Niemeijer^{1,*}, Cristiano Collettini², Steven A.F. Smith³ and Chris Spiers¹

¹ Utrecht University, Faculty of Geosciences, HPT Laboratory, The Netherlands

² Dipartimento di Scienze della Terra Università degli Studi di Perugia, Italy

³ Istituto Nazionale di Geofisica e Vulcanologia, Rome, Italy

* Corresponding author, email: niemeijer@geo.uu.nl

The Zuccale fault is a regionally-important, low-angle normal fault, exposed on the Isle of Elba in Central Italy, that accommodated a total shear displacement of 6-8 km. The fault zone structure and fault rocks formed at less than 8 km crustal depth. The present-day fault structure is the final product of several deformation processes superposed during the fault history. Here, we focus on a series of highly foliated and phyllosilicate-rich fault rocks that represent the basal horizon of the detachment. Previous experimental work on foliated, intact samples, sheared in their in-situ microstructural (foliated) condition, demonstrated a markedly lower friction coefficient compared to homogeneously mixed powdered samples of the same material. In this study, we report results from a series of rotary shear experiments performed on 1 mm thick powdered gouges made from several fault rock types obtained from the Zuccale Fault. The tests were done under conditions ranging from room temperature to in-situ conditions (i.e. at temperatures up to 300 °C, applied normal stresses up to 200 MPa and fluid-saturated.) The ratio of fluid pressure to effective normal stress was held constant at either $\lambda=0.4$ or $\lambda=0.8$ to simulate an over-pressurized fault. The samples were sheared at a constant sliding velocity of 10 $\mu\text{m/s}$ for at least 5 mm, after which a velocity-stepping sequence from 1 to 300 $\mu\text{m/s}$ was started to determine the velocity dependence of friction. This can be represented by the rate-and-state parameter (a-b), which was determined by an inversion of the data to the rate-and-state equations.

Friction of the various fault rocks is between 0.3 and 0.7, similar to values obtained in a previous study, and decreases with increasing phyllosilicate content. Friction decreases mildly with temperature whereas normal stress and fluid pressure do not affect friction values systematically. All samples exhibited velocity-strengthening, inherently stable behavior under room temperature conditions and (a-b) increases with increasing sliding velocity (Figure 1). In contrast, velocity-weakening, accompanied by stick-slips, is observed for the strongest samples at 300 °C and sliding velocities below 10 $\mu\text{m/s}$. An increase in fluid pressure under these conditions leads to a further reduction in (a-b) for all samples (Figure 2), so that they exhibit unstable, stick-slip behavior at low sliding velocity.

The results suggest that phyllosilicate-bearing fault rocks can deform by stable, aseismic creep at low resolved shear stress and low shear rate conditions. An increase in fluid pressure or loading of stronger portions could lead to a runaway instability. However, this instability could be limited in size and velocity due to the observed strengthening at higher sliding velocities. This has important implications for potential rupture dimensions in this geometrically complex fault zone.

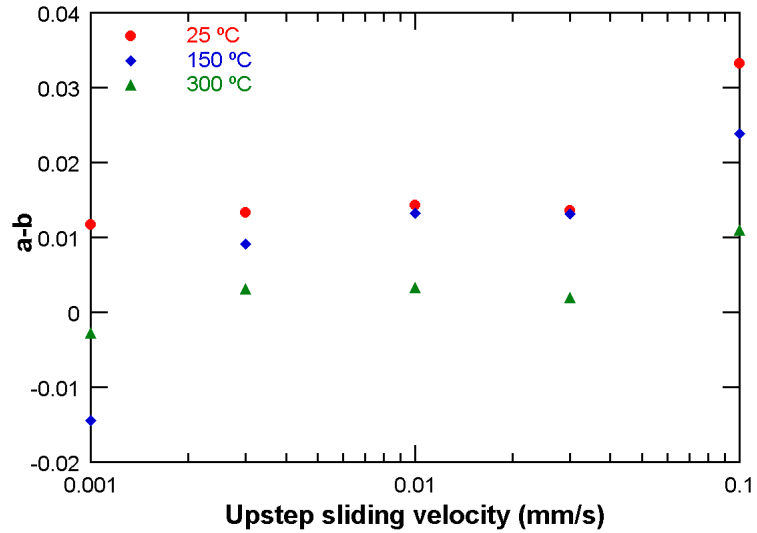


Figure 1. The rate- and state parameter ($a-b$) as a function of upstep sliding velocity for Zuccale Fault rock, sample ZF05 (non-foliated composed of dolomite, calcite plus minor talc) for three different temperatures. The applied effective normal stress was 120 MPa and fluid pressure was 80 MPa ($\lambda=0.4$) in all cases

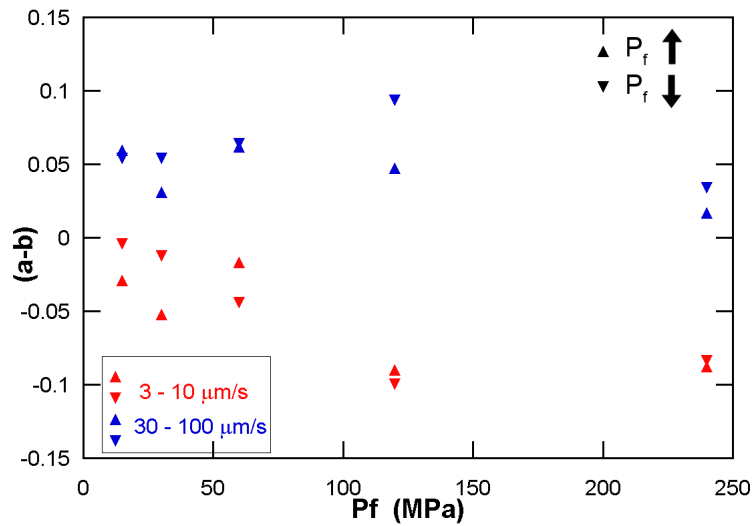


Figure 2. The rate- and state parameter ($a-b$) as a function of fluid pressure for Zuccale Fault rock, sample ZF02 (foliated, composed of tremolite, calcite, talc and clays) for two different velocity steps and two experiments in which fluid pressure was increased and decreased with strain. The applied effective stress was 60 MPa and the temperature was 300 °C.

Failure Mechanisms and Instabilities Associated with Slow Slip Events

Wen-lu Zhu and Audrey Ougier-Simonin

Department of Geology, University of Maryland, College Park MD 20742, USA

Before the discovery of seismic tremor and other slow slip events [e.g., Obara, 2002; Rogers and Dragert, 2003], movements along faults were regarded as bi-modal, either through continuous aseismic sliding, or through sudden rupture of locked sections that generates earthquakes. Slow slip events augment the importance of the transitional slip behavior, which creates new challenges to our understanding of the mechanics of faulting and earthquakes.

Recent studies indicate that slow slip events, including low to very low frequency earthquakes and seismic tremor arise from shear slip [e.g., Shelly et al., 2006, 2007]. The moment rate spectra of these slow slip events appear to be markedly different from those of regular earthquakes [e.g., Ide et al., 2007]. It is generally accepted that high pore pressure is the cause for triggering slow slip events. The basic premise is that increasing fluid pressure leads to reduction of the effective normal stress and thus enables slip along an otherwise aseismic fault. However, the failure mechanisms associated with slow slip are unknown. It is also unclear whether high pore pressure leads to different scaling relations of energy release during slip.

In this study, we conducted deformation experiments on porous sedimentary rocks to investigate effects of high pore pressure on failure mechanisms and slip instabilities. Our data show that the presence of high pore pressure enables unstable slip at the otherwise stable (i.e., velocity strengthening) conditions. This high pore pressure induced slip exhibits a typical transitional behavior--- compared to slip instability in the velocity weakening regime, the stress drop associated with the high pore pressure induced slip is smaller, and the fracture energy release rate is much slower. Interestingly, the scaling relation between the fracture energy release and slip duration resembles the moment rate spectra of the slow slip events, markedly different from that during slip at the velocity weakening conditions.

The prevalence of the slow slip events indicates that this slip instability is not limited to specific rock types or specific tectonic environments. While the deformation mechanisms responsible for the brittle-ductile transition at different tectonic settings vary considerably, our study demonstrates that instabilities enabled by high pore pressure in the transitional regime exhibit different slip characteristics. Our data support the idea that tremor and slow slip events are results of instabilities at the transitional regime between velocity weakening and velocity strengthening [e.g., Liu and Rice, 2005; Perfettini and Ampuero, 2008].

Rupture nucleation and onset of dynamic propagation: new clues from the 2009 L'Aquila earthquake

L. Chiaraluca, L. Valoroso, R. Di Stefano, D. Piccinini, L. Scognamiglio, E. Tinti and M. Cocco

Istituto Nazionale Geofisica e Vulcanologia

The 2009 L'Aquila main shock (6th of April, M_w 6.1) is an important study-case for earthquake science for many different reasons: (i) it is one of the best recorded normal faulting earthquake with a distinctive foreshock-aftershock sequence; (ii) it allowed the collection of an excellent multi-disciplinary near-source data set; (iii) despite its moderate magnitude, it revealed a surprising complexity of source processes, including an unusual rupture directivity; (iv) its impact on society and seismologists is unique.

In this study we mainly focus on the nucleation volume of this event. We have analysed the seismograms recorded by the permanent national seismic network managed by the Istituto Nazionale di Geofisica e Vulcanologia as well as those recorded by a temporary dense local network installed immediately after the main shock. We applied cross-correlation and double-difference techniques both for identifying and to locate seismic events and repeaters. We have analysed the near-source strong motion waveforms to investigate the early stages of the rupture initiation and dynamic rupture propagation. Therefore, we compare the main-shock rupture history with the foreshocks and aftershocks distribution.

The rupture onset is characterized by an initial emergent phase (EP) with small seismic moment release followed by an impulsive phase (IP) characterised by both larger moment release and high rupture speed. The rupture speed is large enough to exclude a slow initiation also during the initial stage (time lapse between EP and IP).

Seismicity clusters around the nucleation patch, where numerous repeaters have located both during the foreshock and aftershock sequences. The whole foreshock sequence clustered within the nucleation volume activating the deepest portion of the main-shock fault plane plus a secondary off fault segment. Foreshocks' repeaters are mainly located on the fault plane, very close to the rupture initiation.

Aftershock distribution is anti-correlated with coseismic slip distribution. Zooming within the nucleation area, we observe that seismicity is noticeably absent in the zone separating the EP and the IP phases, which is a low slip fault area. It is worth noting that the EP phase is located in a very high V_p and relatively low Poisson ratio (σ) region while the IP is located outside the low σ volume.

We have also computed the stress drop values of foreshocks and aftershocks to investigate the spatial-temporal pattern of fault zone heterogeneities.

We will discuss this complex nucleation and rupture process together with the inferred heterogeneous distribution of the material/mechanical rock properties, seismicity pattern and coseismic slip, showing how different competing mechanisms control the initial stage of rupture and the dynamic rupture propagation.

Dynamic inversion of intermediate depth earthquakes and Brune's model

S. Ruiz and R. Madariaga

Laboratoire de Géologie, Ecole Normale Supérieure, 75231 Paris Cedex 05, France

Almost 45 years ago Aki and Brune proposed that far field spectra had universal properties. It is not known whether an equivalent model exists for near field records. One way to solve this problem is to model near field records with dynamic source models that are simple and robust. For this purpose, we have developed a method to do dynamic inversion of well recorded intermediate depth earthquake in the magnitude range from 6.5 to 7.2. The data are strong motion records from instruments located near the epicentre of the earthquake. The accelerograms are integrated to ground velocity or ground displacement and filtered with causal Butterworth filters in a frequency band that removes high frequency components above 1 Hz and low frequency components that may be affected by instrument rotation and other non-linear effects. For the moment, the source is described by an elliptical sub-fault approximation where the initial stress and rupture resistance are specified by a few elliptical patches. As is well known since the late 70s dynamic inversion is not unique: two extreme models may be inverted from any set of observed seismograms. One of them is a barrier model where earthquake resistance (friction) resists rupture propagation or an asperity model where initial stress concentration controls rupture propagation. For elliptical sub-fault approximations it is very simple to convert a barrier into an asperity model of the source.

Among the earthquake we have inverted we chose three examples: an event in Northern Chile on 16 December 2007 recorded by the IPOC network of GFZ and IPG in Paris. The other is the Iwate intermediate depth earthquake of 24 July 2008 (see Figure 1) and, finally, in collaboration with Mexican colleagues V. Cruz-Atienza, Diaz-Mojica and S.K. Singh we inverted the Zumpago intermediate depth earthquake of 11 December 2011.

The dynamic inversion problem is non-linear. In our inversions we use either the Neighbourhood Algorithm (NA) of Sambridge or a Genetic Algorithm developed by Cruz-Atienza. We use an L2 norm to compare the observed and synthetic seismograms. Both algorithms converge very rapidly when the number of parameters that describe the dynamic source model is small, less than 12 parameters, say. Once the best model has been found, a region in parameter space around the optimal solution is searched for well fitting solutions using a Monte Carlo (MC) sampling technique, Figure 2. We adopt a very simple friction law based on Ida's linear slip-weakening model. It turns out that the peak stress (T_u) and slip weakening distance (D_c) are not independent so that we have to renormalize the solution space using the energy release rate ($G_c = \frac{1}{2} T_u D_c$). In the new coordinates the Monte Carlo method produces a well defined compact area where good solutions of the inversion of the dynamic inversion problem live.

We will show results of kinematic and dynamic inversion of the 24 July 2008 ($M_w=6.8$) Northern Iwate intermediate depth earthquake in Japan using strong motion records from the K NET and Kik-Net networks. The rupture of this moderate magnitude earthquake is modelled with a single elliptical patch. The geometry of the

rupture, rupture velocity and slip distribution are estimated first by kinematic inversion. The results of kinematic inversion are highly non-unique, especially concerning rupture velocity. We use them to define the parameter space in which we search for dynamic models. The rupture geometry, stress and friction parameters are then obtained by dynamic inversion using both asperity and barrier models. Both approaches converge to very similar source models with semi-minor axes of 4 km, maximum slip of about 4 m and large stress drops in the 30-45 MPa range. Rupture duration was less than 3 s because of very high sub Rayleigh rupture propagation speeds. Energy release rate for the best models was in the range 23-36 MJ/m², a rather large value for events of this size. For both kinematic and dynamic inversions we found families of solutions that fit the strong motions data within a certain error, confirming the strong trade-off among inverted parameters.

Comparing the spectra of observed and modelled spectra we find the central part of the synthetic spectra reproduce very well the observed ones with many characteristics that recall Brune's spectra. Corner frequency varies from station to station with a numerical coefficient that depends on the ratio of available to fracture energy (κ). Actually, dynamic inversion solutions are controlled by the dynamic similarity parameter κ and by seismic moment M_0 . These two parameters define a region of model space where dynamically similar models fit the observations with approximately the same misfit.

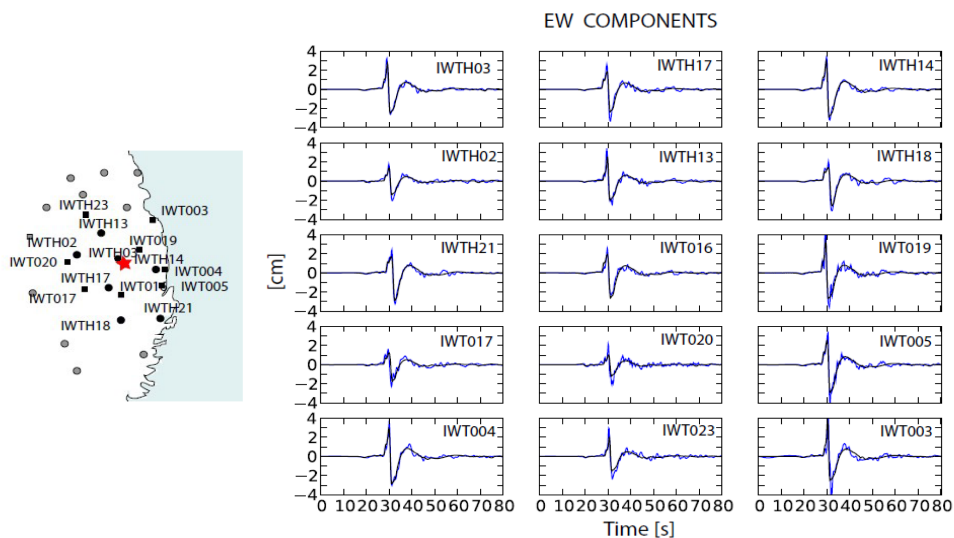


Figure 1. Fit of ground velocities for EW components at 14 K-net and Kik-net stations in Japan. The fit is excellent meaning that our simple model has captured the main features of this event

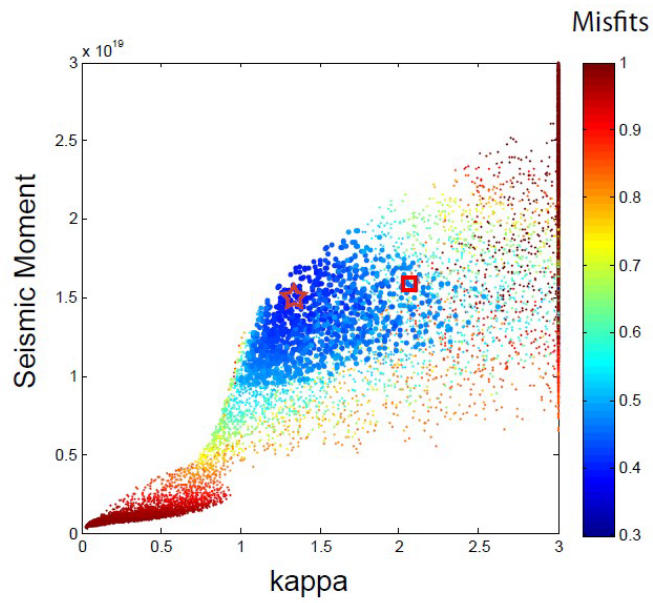


Figure 2. MC study of the vicinity of the best model in parameter space. Well fitting models fill a well defined region of parameter space. The Red star is the best model found by NA. The small red diamond is a super-shear event. Dark blue models fit the data within 20 % of the best residual.

Insights on earthquake dynamics enabled by high-frequency source imaging with dense seismic arrays

Jean-Paul Ampuero

California Institute of Technology, Seismological Laboratory, USA

Earthquake dynamic rupture is controlled by fault weakening processes with spatio-temporal scales that are shorter than the resolution of most earthquake source studies. Finite source inversions based on strong motion data with limited frequency band can typically resolve source features at scales larger than a few km, coarser than estimates of the size of rupture front process zone, assuming critical slip distances shorter than 1 m. Moreover, the severe non-uniqueness of the source inverse problem imposes regularization assumptions that restrict the range of admissible rupture kinematics and might exclude physically possible rupture patterns. For instance, few finite source inversion schemes allow for multiple rupture pulses, a phenomenon found in dynamic models of self-similar pulse-like rupture.

In order to reveal the real nature of rupture complexity we need to break the high frequency barrier and develop non-parametric source imaging. This presentation is a synthesis of the contribution of array seismology to this endeavor, taking as examples the 2011 Tohoku-Oki and 2012 off-Sumatra earthquakes, and including an outlook on new applications and array instrumentation needs.

In the last decade, very large earthquakes have been recorded by dense and large seismic arrays at teleseismic distance, such as the USArray, the Japanese and the European networks. Array processing of high-frequency waves and back-projection to the source region have provided some of the finest images of earthquake ruptures. The basic technique is now applied routinely and high-resolution techniques have emerged that provide reliable images of spatio-temporal details of large earthquake ruptures.

During the 2011 M9 Tohoku-Oki earthquake, array back-projection was instrumental in revealing that high and low frequency slip were not located at the same depth on the megathrust. Moreover, the down-dip portion of the rupture was quite slow while at the same time radiating high frequency bursts. This behavior was reproduced by simulations of dynamic rupture on a heterogeneous fault made of asperities surrounded by regions of low stress drop. Such models are consistent with a view of the bottom rheological transition region of subduction faults that previously emerged from observations of slow slip and tremor phenomena.

During the 2012 M8.6 off-Sumatra earthquake, back-projection source imaging revealed extremely intriguing rupture patterns. This oceanic intraplate earthquake broke several large segments on a system of orthogonal strike-slip faults. Moreover, in two occasions the rupture branched preferentially into the compressional branch. The rupture speed was remarkably steady and relatively slow. These observations indicate a pressure-insensitive strength and provide insights on the rheology of the uppermost mantle. Dynamic rupture simulations can indeed reproduce such branching pattern provided the “effective” friction coefficient (i.e., the slope of the yield envelope in shear/normal stress space) is near zero.

Synthetic tests constructed with computed or empirical Green’s functions indicate that the timing and position of high frequency radiation is reliably determined

by teleseismic back-projection. However, developments are still needed to obtain robust constraints on slip power as function of frequency, including the effect of source coherency. Such developments could allow constraining rise time, currently one of the most elusive source parameters. Better integration with the more traditional, lower frequency source inversion approaches is also desired, although the complementarity of high and low frequency slip might be a fundamental obstacle. The fusion of information between multiple arrays is also a topic of ongoing developments.

Array back-projection provides rapid estimates of rupture size, directivity and location of high-frequency radiation. This information could be integrated with situational awareness tools to allow damage estimation soon after large events. The back-projection technique can be adapted to arrays at regional and local distances. A new generation earthquake observation system could be based on multiple strong motion small-aperture arrays. If implemented in real time, back-projection could feed estimates of rupture size into earthquake early warning systems, solving a shortcoming of current systems based on algorithms designed for point sources. Moreover, initiatives are emerging to develop a global system of broad band arrays, which could be specifically designed for source imaging applications.

One of the challenges in array design for source imaging is site selection. The key required characteristic, coherency as a function of inter-station distance and frequency, is not easily predictable and can be measured only with medium term deployments. Techniques are being developed to extract statistical properties of the propagation medium from short term noise measurements, which can then be used to build a proxy for wavefield coherency.

A Dynamic Rupture Model with Slip Reactivation for the 2011 Mw 9.0 Tohoku earthquake

L. A. Dalguer and P. Galvez

Swiss Seismological Service, ETH-Zurich, Switzerland

The giant megathrust 2011 Mw 9.0 Tohoku earthquake was exceptional well recorded with thousands of sensors located all over Japan that provides a great opportunity for seismologist and engineers to investigate in detail the rupture process and the underlying physics of this type of mega-thrust events. Kinematic source models inverted from seismological, geodetic and tsunami observations, including source images from back-projection, indicate that the earthquake featured complex rupture patterns, with multiple rupture fronts and rupture styles. The compilation of these studies reveals fundamentally three main feature: 1) spectacular large slip over 50m, 2) the existence of slip reactivation and 3) distinct regions of low and high frequency radiation: the regions of large slip in the shallower part of the fault dominates the low frequency radiation and the bottom part dominates the high frequency radiation.

Earthquakes with extremely high slip can result from fault melting, pressurization, lubrication or other thermal weakening mechanisms that reduces further the frictional strength to lower levels. Kanamori and Heaton (2000) proposed a friction model in which frictional strength drops initially to certain value, but then at large slips there is a second drop in frictional strength.

We introduce Kanamori and Heaton's friction model to investigate the features mentioned above in a simple spontaneous dynamic rupture asperity model governed by slip weakening friction. The model is composed of large asperity patches of radius between 30 to 50 km in the intermediate and shallower part, and small patches of asperities at the bottom of the fault to account for the strong high frequency radiation. The very shallow part of the fault is considered as a stable zone that operates during rupture with an enhanced energy absorption mechanism. We model this zone by assuming negative stress drop and large critical slip distance.

With this model we reproduce the main features of this earthquake described above. Rupture initiates propagating toward the east and north. After around 40 sec of rupture initiation, the second drop of the frictional strength in the main asperity produces strong slip reactivation capable to break the free-surface with high slip. This slip reactivation also excites the small asperity patches producing burst of high frequency radiation, which in turn produces a third rupture of an asperity propagating southward. In addition, the synthetic ground motion pattern along the Japanese coast of the Tohoku event is consistent with the observed ones. Within the framework of our frictional model, the slip reactivation plays a fundamental role to produce multi type of ruptures, to break the free-surface and to reach a magnitude Mw9.0. Without this ingredient, the earthquake is inhibited to a magnitude Mw8.2.

Constrains on fault properties from integration of observations and dynamic rupture models of the Tohoku-Oki Earthquake

Yihe Huang and Jean-Paul Ampuero

Division of Geological and Planetary Sciences, California Institute of Technology,
Pasadena, CA 91125, USA

As the most devastating earthquake in Japan history, Tohoku-Oki Earthquake has triggered a number of studies, facilitated by the best instrumentation in the area. Regardless of different details, there is consistency in certain observational results. The large and low-frequency slip is generated in the shallower region as indicated by finite fault inversions. In contrast, teleseismic back-projection studies indicate that the high-frequency energy around 1 Hz originates from the deeper part of the rupture. Huang et al. (2012) presented a 2D dynamic rupture model that reproduces these first-order observations of the along-dip rupture process during the initial 100 s (Fig. 1). The model is based on minimalistic assumptions, e.g. linear slip-weakening friction, the presence of deep asperities and depth-dependent initial stresses. The model also explains the quantitative constraints on the ratio of shallow versus deep radiation from teleseismic back-projection source imaging. Our results indicate that the stress state is very different between the shallower and deeper regions. Though the stress drop is small near trench, the reflected waves inside the front wedge always induce high transient stress drop and amplify the final slip. In the deeper region, the stress drop is negative between the small asperities. These regions conceptually represent the places where overshoot occurred in the previous earthquakes.

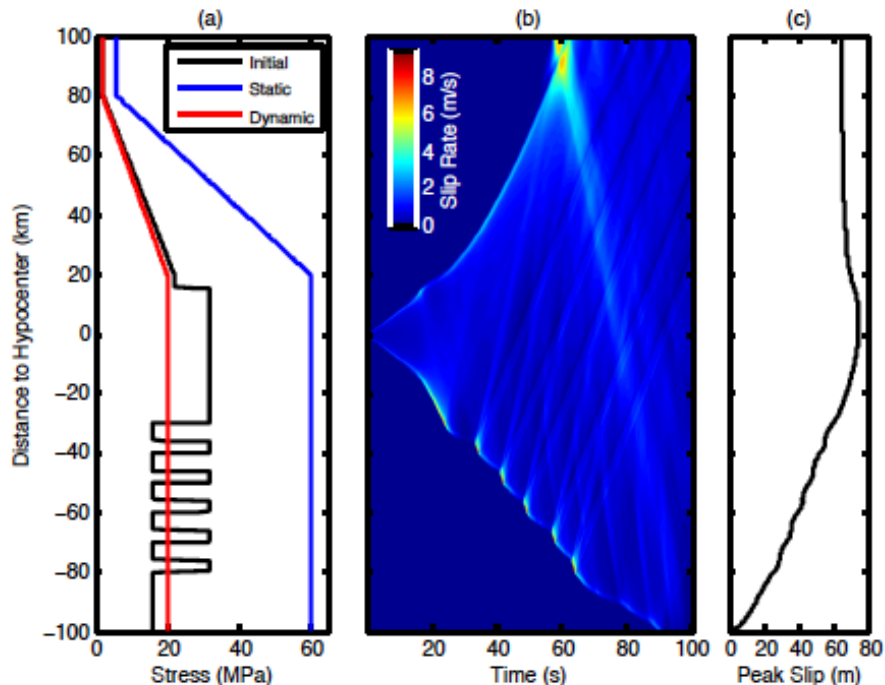


Figure 1. (a) Initial shear stress, static strength and dynamic strength in the numerical model setup as a function of distance to the hypocenter. (b) Spatiotemporal distribution of slip rate. (c) Peak slip as a function of distance to the hypocenter.

Our current efforts aim at developing a more complete dynamic model for the Tohoku earthquake, to hopefully provide tighter constraints on mechanical properties

of the megathrust, by determining the full range of models that explain the available data. For instance, one intriguing question is how the initial stress and frictional parameters affect the final slip distribution. The slip inversion results show different along-dip profiles (Fig.2). Our simulations can define the range of stress distributions consistent with those slip profiles.

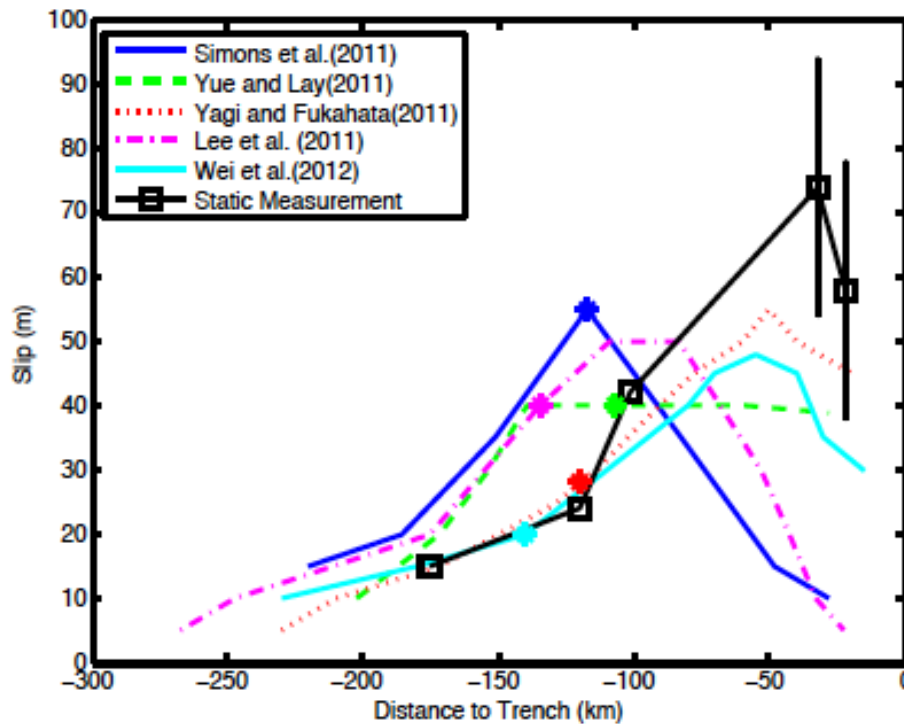


Figure 2. Approximate along-dip slip profiles for slip inversion results of different groups. The star denotes the hypocenter used by each group. The static measurement includes data points from Sato et al. (2011), Ito et al. (2011) and Hino et al. (Tohoku University).

Another goal of our simulations is to compare crack-like and pulse-like models. In our previous model, we assumed linear slip-weakening friction, which minimizes the possibility of pulse-like rupture. However, after healing is allowed in the model, the rupture naturally has a depth-dependent rise time. Quantitative and systematic comparison of the seismograms generated by the numerical models to the real recordings will ultimately constrain the range of admissible models.

Our simulations also address the question of the energy partition during the Tohoku-Oki earthquake. More specifically, they provide constraints on the fracture energy and estimates of the heat generated that can be compared to the forthcoming drilling hole data. Since we have some constraints of the total energy and radiated energy, answering these questions is a crucial step to see the whole picture of the Tohoku-Oki earthquake.

Source Properties and Complexity of Dynamic Ruptures in Elastic and Plastic Media

Alice-Agnes Gabriel¹, Jean-Paul Ampuero², Luis A. Dalguer¹ and P. Martin Mai³

¹ ETH Zurich, Switzerland

² Caltech, California, USA

³ KAUST, Saudi Arabia

Although kinematic earthquake source inversions show dominantly pulse-like subshear rupture behavior, seismological observations, laboratory experiments and theoretical models indicate that earthquakes can operate with different rupture styles: either as pulses or cracks, that propagate at subshear or supershear speeds. In Gabriel et al. (2012, JGR) we conducted 2D in-plane dynamic rupture simulations with a spectral element method to study rupture styles on faults governed by velocity-and-state-dependent friction with dramatic velocity-weakening at high slip rate. We observed a diversity of rupture styles, which we classified based on their stability (decaying, steady or growing), rupture speed (subshear or supershear), healing properties (cracks or pulses) and complexity (simple or multiple fronts). Rupture styles and their transitions depend on the state of stress and strength of the fault, which may help constrain these parameters on active fault zones. We define specific source signatures which may be resolvable in near-field seismograms and source spectra. For instance, growing pulses lead to re-activation of slip due to gradual stress build-up near the hypocenter (Fig.1(a)), as inferred in some source studies of the 2011 Tohoku-Oki earthquake (Fig.1(b)). We subsequently investigated the effects of off-fault non-elastic response on rupture properties. High stress concentrations at earthquake rupture fronts may generate an inelastic off-fault response at the rupture tip, leading to increased energy absorption in the damage zone. Macroscopic source properties from different rupture styles are significantly affected by off-fault plasticity. For pulse-like ruptures the contribution of plastic strain to the seismic moment is significant. We observe saturation of peak slip rate to values increasing with increasing initial stress and decreasing angle of maximum compressive stress to the fault strike. Plasticity limits rupture and healing front speeds, leading overall to shorter rise times. Investigating in detail self-similar pulse-like ruptures, we are able to define quantitative relations between off-fault energy dissipation and macroscopic source properties. We find that a non-linear relation between peak slip velocity and rupture speed that is well explained by classical fracture mechanics arguments (Fig. 2). We furthermore find that the closeness to failure (CF) parameter introduced by Templeton and Rice (2008) is an adequate predictor of rupture speed for slow ruptures (Fig.2, inset): Rupture speeds smaller than ~60% of S-wave speeds are captured by a simple, direct dependence on CF; Rupture speeds larger than ~80% S-wave speed are dominated by the S-parameter. These findings contribute to calibrate the "velocity-toughening" equivalent proposed by Andrews (2005), and to build a self-consistent theoretical framework for the study of the earthquake energy balance based on observable earthquake source parameters.

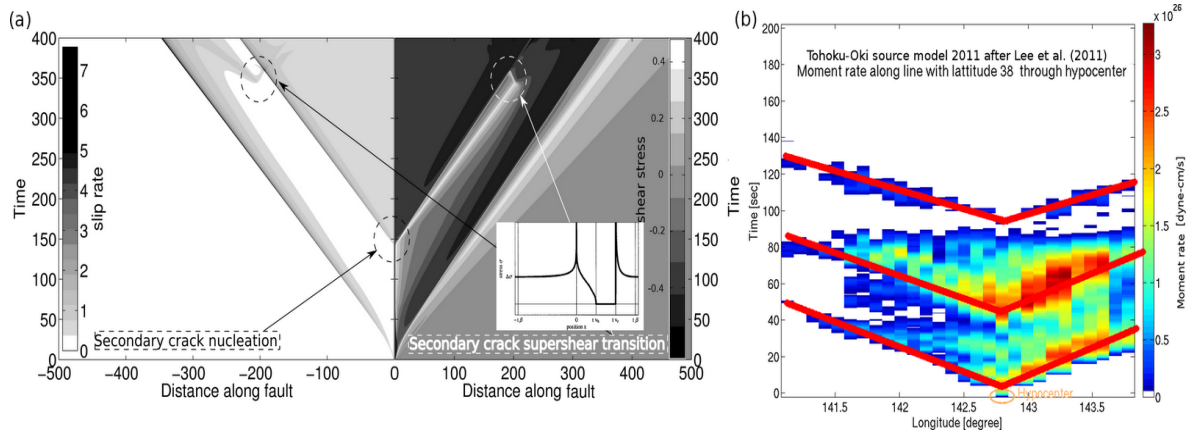


Figure 1. Re-activation of slip. (a) 2D spectral element spontaneous in-plane dynamic rupture simulation. Spatio-temporal evolution of slip rate (left) and shear stress change (right). A growing pulse triggers a subshear crack, which in turn nucleates a supershear crack. (b) Re-activation of slip inferred for the Tohoku-Oki (Japan) 2011 earthquake: spatio-temporal distribution of moment rate at the hypocentral latitude (38 deg.) from the source inversion model by Lee et al. (2011).

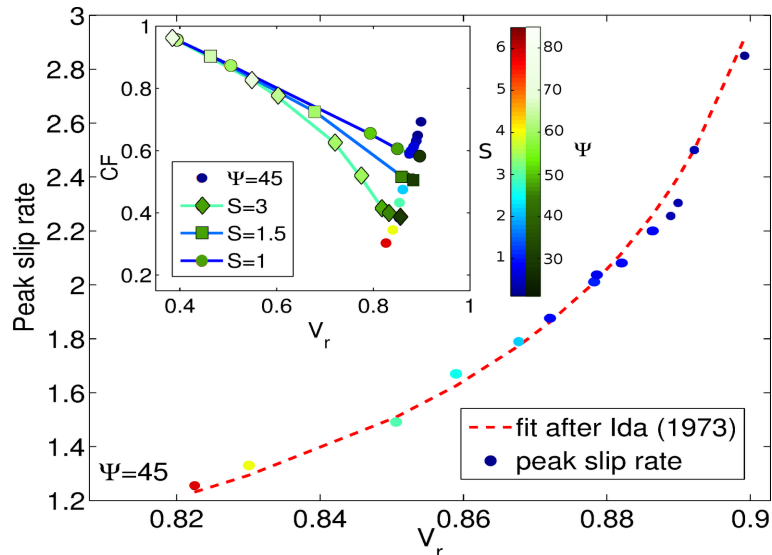


Figure 2. Relations between rupture velocity V_r , closeness to failure CF (Templeton and Rice, 2008) and peak slip rate, as a function of relative strength parameter S and orientation of principal background stress Ψ . The dashed line is a relation predicted from fracture mechanics arguments.

References:

- Andrews, D. J. (2005), Rupture dynamics with energy loss outside the slip zone, *J. Geophys. Res.*, 110, B01,307, doi:10.1029/2004JB003191.
- Gabriel, A.-A., J.-P. Ampuero, L. A. Dalguer, and P. M. Mai (2012), The transition of dynamic rupture modes in elastic media, submitted to *J. Geophys. Res.*
- Ida, Y. (1973), The maximum acceleration of seismic ground motion, *Bulletin of the Seismological Society of America*, 63 (3), 959–968.
- Lee, S.-J., B.-S. Huang, M. Ando, H.-C. Chiu, and J.-H. Wang (2011), Evidence of large scale repeating slip during the 2011 Tohoku-Oki earthquake, *Geophys. Res. Lett.*, 38, L19306, doi:10.1029/2011GL049580.
- Templeton, E. L., and J. R. Rice (2008), Off-fault plasticity and earthquake rupture dynamics: 1. Dry materials or neglect of fluid pressure changes, *J. Geophys. Res.*, 113, B09,306, doi:10.1029/2007JB005529.

Poster Program

Radiated energy of $3.0 \leq M \leq 5.0$ earthquakes in rupture patches and rupture barriers on Gofar Transform Fault, East Pacific Rise

Pamela Moyer¹, Margaret Boettcher¹, Jeffrey McGuire² and John Collins²

¹ University of New Hampshire

² Woods Hole Oceanographic Institution

While the largest earthquakes on mid-ocean ridge transform faults (RTFs) exhibit many of the most systematic behaviors known in seismology, little is known about the seismic characteristics of the $3.0 \leq M \leq 5.0$ events. Many of the largest RTF earthquakes occur by repeatedly re-rupturing the same portion of the fault on a relatively regular basis. For example, the $M \sim 6.0$ earthquakes on the fast slipping Gofar and Discovery transform faults on the EPR re-rupture every ~ 5 -6 years [McGuire, 2008], and the $M 6.2$ - 6.4 earthquakes on the longer, intermediate slipping Blanco transform fault of the Juan De Fuca Ridge repeat every ~ 14 years [Boettcher and McGuire, 2009]. During each of the last four seismic cycles on Gofar transform fault the largest earthquakes have ruptured only a single asperity (*rupture patch*), suggesting that the intervening fault segments (*rupture barriers*) stop the propagation. By determining the ratio of radiated energy to seismic moment for moderate size earthquakes recorded on Gofar transform fault during an ocean bottom seismometer (OBS) deployment that successfully captured a $M 6.0$ earthquake [McGuire et al., 2011], we investigate whether known variations in frictional behavior along strike affect rupture processes of $3.0 \leq M \leq 5.0$ earthquakes.

The 2008 OBS experiment on Gofar transform fault recorded an entire seismic cycle, including a foreshock sequence that was both extensive ($\sim 20,000$ earthquakes within the week prior to the mainshock) and localized (within a ~ 10 km region), as well as the $M 6.0$ mainshock and its aftershock sequence [McGuire et al., 2012]. The foreshocks occurred in the previously determined rupture barrier [McGuire, 2008; Boettcher and McGuire, 2009]. Using waveforms recorded with a sample rate of 50 Hz on Keck Foundation OBS accelerometers, we are investigating ratios of radiated energy to seismic moment for $M \geq 3.0$ earthquakes that occurred in both rupture barriers and rupture patches (Figure 1). To ensure sufficient bandwidth at high frequencies and eliminate the effects of coupling resonance, we calculate radiated energy using an omega-squared source model, where the corner frequency is derived from an empirical Green's function (EGF) method. We obtain seismic moment by fitting the omega-squared source model to the low frequency amplitude of individual event spectra and account for attenuation using a best-fit value of Q obtained from a velocity model through the foreshock zone [Roland, et al., 2012]. Our initial results for eight earthquakes in the foreshock and aftershock regions on Gofar transform fault have log of energy to moment ratios between -4.4 and -4.8 . This subset of events does not show systematic differences between the rupture process of moderate magnitude earthquakes on rupture patches and rupture barriers.

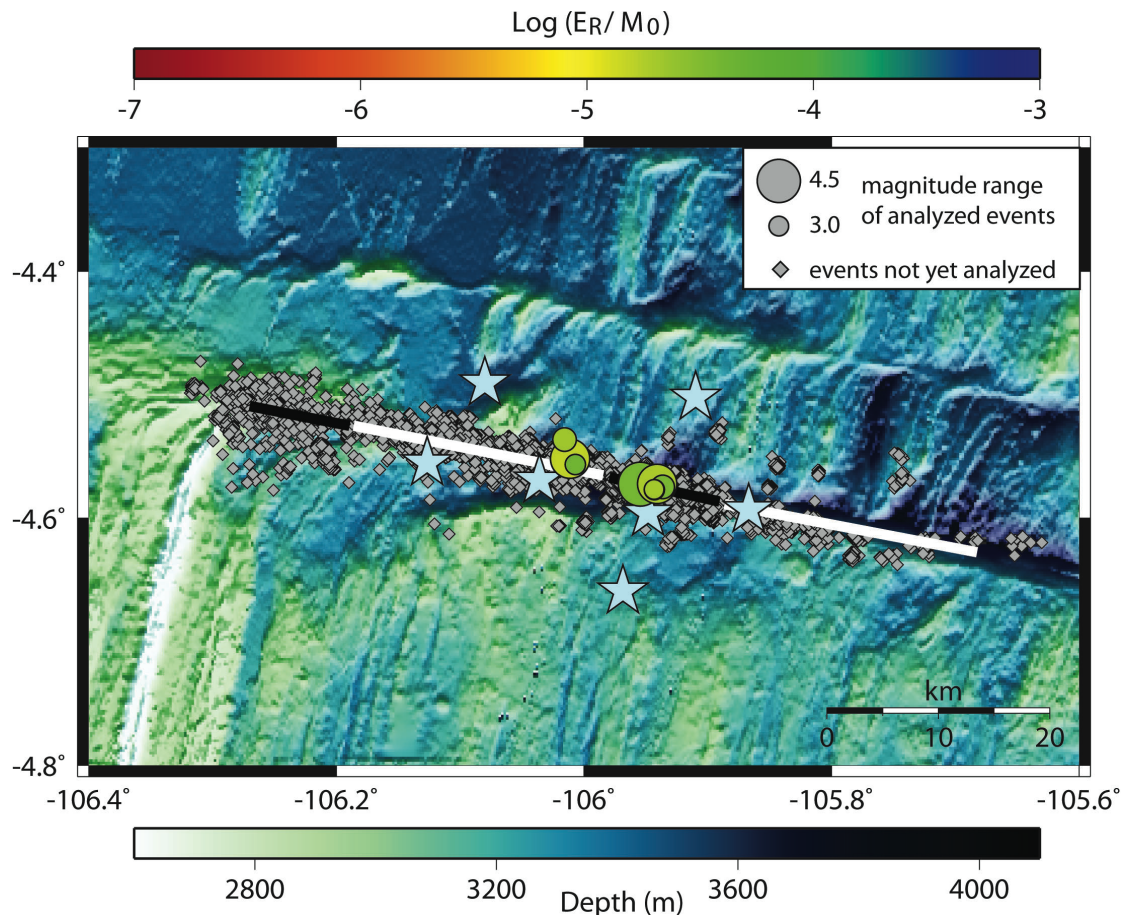


Figure 1. Initial radiated energy to moment ratio results for eight earthquakes on Gofar transform fault on the East Pacific Rise. The color of the circle indicates the energy to moment ratio on a scale that covers the observed range from previous studies. Stars mark the location of the seven OBS accelerometers. Gray circles are earthquakes that occurred from August–December on the western segment of Gofar transform Fault during the 2008 OBS experiment. White and black thick lines delineate rupture patches and rupture barriers respectively.

References

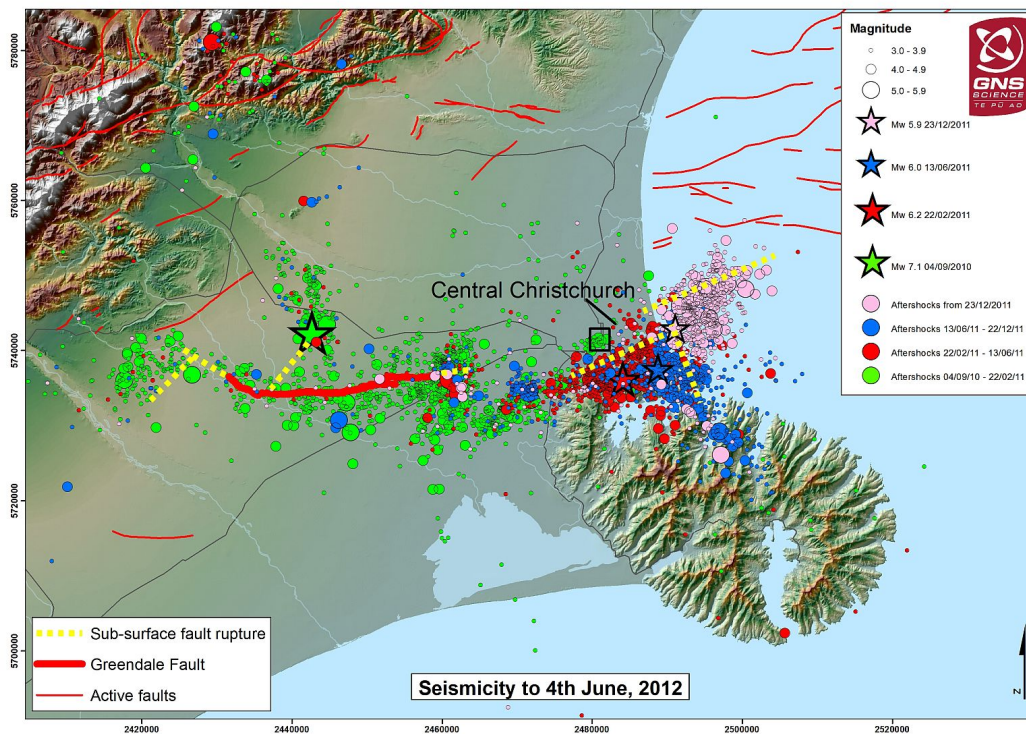
- Boettcher, M. S., and T. H. Jordan (2004), Earthquake Scaling Relations for Mid-Ocean Ridge Transform Faults, *J. Geophys. Res.*, *B12302*, doi:1029/2004JB003110.
- Boettcher, M. S., and J. J. McGuire (2009), Scaling relations for seismic cycles on mid-ocean ridge transform faults, *Geophys. Res. Lett.*, *36*, L21301, doi:21310.21029/22009GL040115.
- McGuire, J. J. (2008), Seismic Cycles and Earthquake Predictability on East Pacific Rise Transform Faults, *Bull. Seis. Soc. Am.*, *98*, 1067-1084, doi: 1010.1785/0120070154.
- Roland, E., Lizarralde, D., J. A. Collins, and J. J. McGuire, Constraints on the material properties that control earthquake behavior from seismic velocity structure at the Quebrada-Discover-Gofar transform faults, East Pacific Rise, *J. Geophys. Res.*, submitted 2012.

Source studies of the ongoing (2010-2011) sequence of recent large earthquakes in Canterbury

Caroline Holden

GNS Science, New Zealand

On September 4, 2010, a surface rupturing crustal earthquake (Mw7.1) struck the Canterbury Plain region in New Zealand's South Island (Gledhill et al., 2011). The Canterbury Plains is a region of relatively low seismicity, and the structure that ruptured was a previously unmapped fault. The earthquake has since been followed by more than 7000 catalogued aftershocks, of which two were of magnitude 6.3. On Tuesday 22 February 2011 a destructive Mw 6.3 aftershock with shallow depth struck approximately 10 km SE of downtown Christchurch, causing extensive damage and 180 fatalities in the central city and eastern suburbs of the city. This earthquake was very energetic, with recorded maximum vertical accelerations of 2.2 g near the epicentre. It caused much larger levels of building damage, landslides, rock falls and liquefaction than the initial Mw 7.1 Darfield mainshock. On June 13 2011 a further aftershock of magnitude (ML) 6.3 struck Christchurch. It was located only a few km south-east of the previous event, and again caused extensive damage, landslides, rock falls and liquefaction. Maximum accelerations of over 2g were also recorded. Unlike the Mw 7.1 event no surface rupture has been found for either of the two M6.3 aftershocks. The source process of all of these events have been well constrained by geodetic and seismological data. I will present an overview of the observations as well as kinematic source models of the earthquakes.



Spectral inversions of data from the Canterbury earthquake sequence, New Zealand, for source, path and site parameters

Anna Kaiser¹ and Adrien Oth²

¹ GNS Science, New Zealand

² European Center for Geodynamics and Seismology, Luxembourg

The Canterbury earthquake sequence beginning with the Mw 7.1 September 2010 Darfield earthquake comprises a rich aftershock sequence that includes several damaging events $> Mw 6$. These earthquakes are low-recurrence events, occurring in a low-strain-rate area ~ 140 km east of the major plate boundary Alpine Fault in the central South Island. The sequence represents one of the best recorded crustal earthquake sequences in a low-strain-rate region worldwide. The high apparent stress and high recorded ground accelerations (> 2 g) of the largest events, as well as the punctuated behaviour of the aftershock sequence (Gerstenberger et al. 2012), suggest that the region typically produces high stress events occurring on strong regional faults. Identifying the source characteristics, scaling relationships and particular controlling influences on ground motions for the Canterbury aftershock sequence as a whole is critical to understanding its behaviour and has implications for similar low-strain rate regions worldwide.

To separate and quantify source, path and site parameters specific to the Canterbury earthquake sequence, we have conducted preliminary inversions using the generalized linear inversion method of Oth et al. (2010) applied to aftershock acceleration spectra. Results were obtained using a small data subset of 166 earthquakes (Mw 3.6 – 6.2) and 1057 source-stations paths (Figure 1). The resulting source spectra are relatively well characterized by the omega-square model. The distribution of associated stress drops shows a preliminary median value of 2.8 MPa, somewhat higher than the average value for crustal events obtained using this method in Japan. Further inversions will be conducted using an expanded dataset from the Canterbury earthquake sequence to better quantify Canterbury source characteristics and any spatial and temporal variations.

References:

- Gerstenberger, M.C.; Fry, B.; Abercrombie, R.; Doser, D.; Ristau, J, 2012. On the relation of stresses to aftershock decay. *Seismological Research Letters* 83(2): 365.
- Oth, A.; Bindi, D.; Parolai, S.; Di Giacomo, D. 2010. Earthquake scaling characteristics and the scale-(in)dependence of seismic energy-to-moment ratio: Insights from KiK-net data in Japan. *Geophysical Research Letters* 37: L19304.

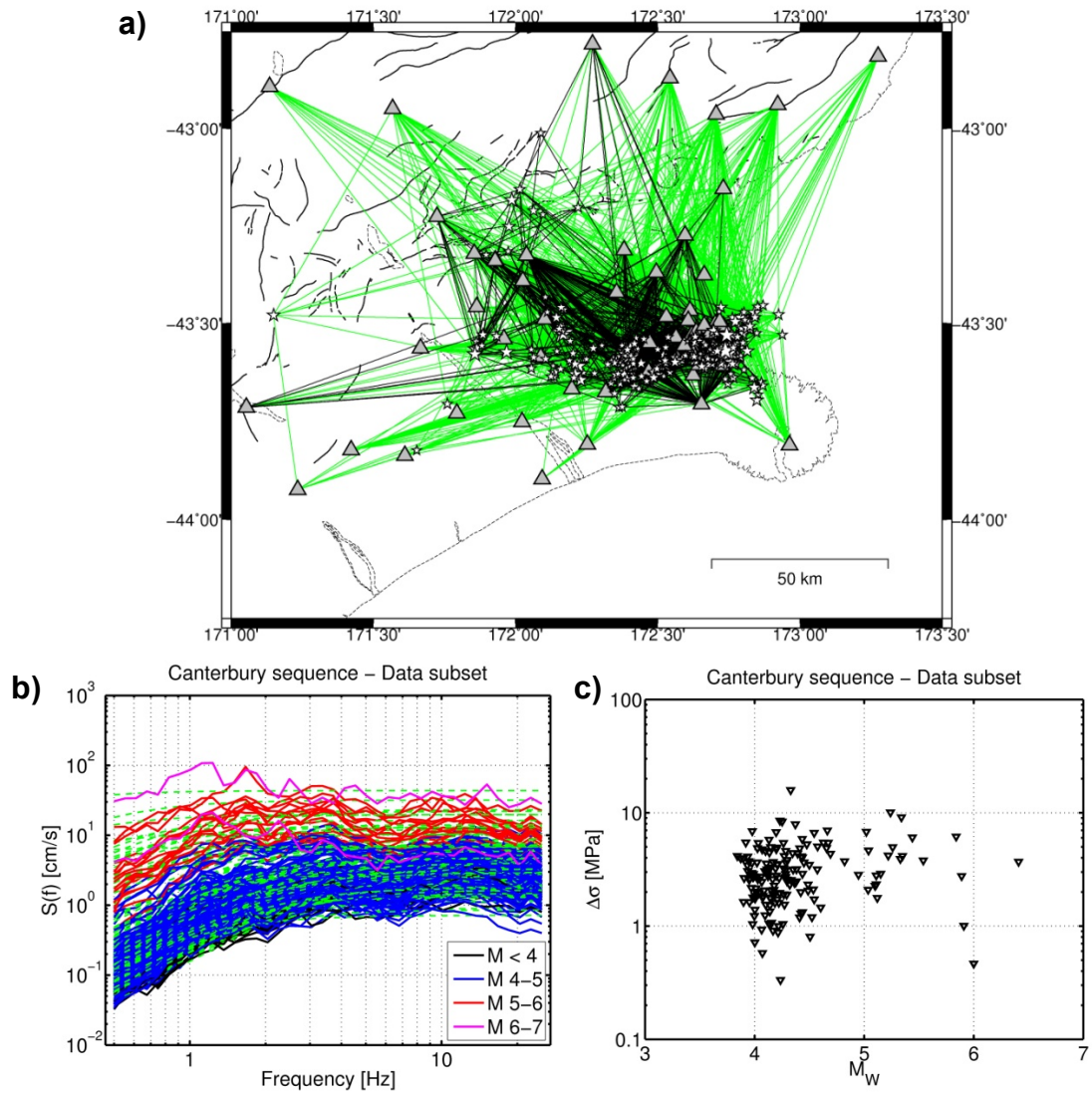


Figure 1. Preliminary spectral inversion results. (a) Source-station paths of available strong motion data from the Canterbury earthquake sequence up until end of April 2012 (green lines) and a preliminary data subset used in initial analyses (black lines). Sources and stations are shown as stars and triangles respectively. (b) Preliminary results for source spectra derived for the data subset shown in (a) compared to omega-squared models (green lines). (c) Stress drops derived from the source spectra in (b).

Understanding the NGA-West ground-motion prediction equations for PGA and PGV

Annemarie S. Baltay¹, Thomas C. Hanks² and Gregory C. Beroza¹

¹ Department of Geophysics, Stanford University

² United States Geological Survey, Menlo Park, CA

Next Generation of Attenuation (NGA) ground-motion prediction equations (GMPE) use as many as 19 parameters to empirically describe peak ground acceleration (PGA) as a function of magnitude and distance. These parameters are complexly related and may trade off in ways that are not intuitively understood; due to the empirical nature and historical precedent of the GMPEs, the relationships are not strictly based on earthquake source physics. We have adapted the simple, point-source models of *Hanks and McGuire* [1981], *Boore* [1983] and *McGarr et al.* [1981] to fit peak ground acceleration (PGA) and peak ground velocity (PGV) dependent on magnitude and source-site distance in the NGA-West data set, finding a least-squares best fit stress drop for all of the data.

Combining a finite fault model with the point-source representations predicts PGA recorded at 10 km to saturate at $M > 6.7$, assuming contributions to PGA from points on the fault farther than 15 km are negligible at those distances. We indeed find a constant PGA of $\sim 0.3g$ above this magnitude, albeit in the midst of considerable scatter. Between $M 4.5 - 8$, our theoretical relation for PGA matches the four most commonly used NGA-West 2008 GMPEs very well. Only knowledge of stress drop, f_{max} , and the material parameters density and shear wave velocity are necessary to model the theoretical relationship. The fit results in a stress drop of ~ 5 MPa for all events, consistent with stress drop studies in similar active regions; Class 1 events, analogous to mainshocks, in the NGA data set, however, have stress drops somewhat greater than that of the Class 2 events, on-fault aftershocks. Peak ground velocity (PGV) is modeled using both the Brune-derived point source model of *McGarr* [1981], and the stochastic model of *Boore* [1983]. We find that the PGV saturates at a slightly higher magnitude, $\sim M 7$, as compared to PGA, above which the median ground motion is ~ 35 cm/s. This might be expected given the more broadband nature of PGV as compared to the high-frequencies of PGA, which attenuates more over the same source-receiver distance. While our PGV model compares well to the NGA-West 2008 GMPEs for magnitudes less than $M 7$, our model shows more saturation in the larger magnitudes. Stress drop determined from the two PGV relations shows a weaker dependence on the Class 1/Class 2 distinction as compared to the PGA-determined stress drop.

The stress drop modeled in these relations is derived from a *Brune* [1970] omega-squared self-similar model, yet is estimated by an inherently different method, namely, derived from strong ground motion parameters, as compared to the oft-employed spectral method of estimating corner frequency. This stress drop is referred to as the stress parameter in stochastic ground motion modeling [ie. *Boore*, 1983] and hence understanding its behavior is interesting not only for source physics but also for strong ground-motion applications. By estimating the stress drop here through an intrinsically different method, we find that stress drop is not dependent on magnitude for large populations of earthquakes, but inter-event variability is inherent to earthquakes, and is not an artifact of the method or a data bias.

Comparing the NGA data set with PGA and PGV data from M 3 – 7 crustal earthquakes in Japan shows excellent agreement, extending the comparison of our models and the NGA GMPEs to smaller magnitude earthquakes. That these very simple constant stress-drop, point-source models, together with the finite-fault approximation at large magnitudes, match the NGA PGA and PGV data well suggest that considerable simplicity underlies the parametrically complex NGA-West GMPEs. Furthermore, it underscores the application of the self-similar, Brune derived, physical point source models to a broad range of data.

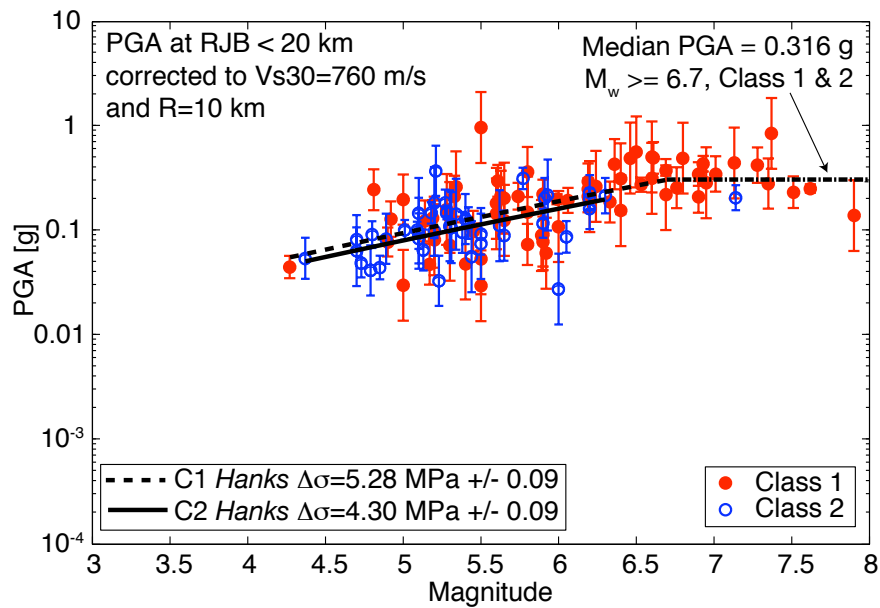


Figure 1. PGA data from the NGA-West 2008 data base, color coded by Class 1 (mainshocks) and Class 2 (on-fault aftershocks), with error bars showing the standard error from multiple recordings of the same earthquake. Best-fit stress drops using the *Hanks* [1979] PGA relationship are slightly higher for the Class 1 events as compared to the Class 2 events. Above the saturation point of M 6.7, the median ground motion is $\sim .3$ g. Overall, the hybrid model, considering smaller magnitudes as point sources and $M > 6.7$ as finite faults, describes the data well.

Validation of Source Scaling using Ground Motions from the 2008 Wells, Nevada Earthquake Sequence

Seung-Hoon Yoo¹ and Kevin Mayeda^{1,2}

¹Berkeley Seismological Laboratory, University of California Berkeley, Berkeley, CA, USA

²Weston Geophysical Corporation, Lexington, MA, USA

The behavior of earthquake source scaling has been the topic of significant debate in the earthquake source community over the past two decades and remains controversial. However, high quality records from a magnitude 6 earthquake, which was occurred near the Wells, Nevada on February 21, 2008, and its aftershocks provided an unprecedented opportunity to take an in-depth look at the source scaling and ground motion. For this earthquake sequence, conflicting scaling relations were reported in two previous studies (*Mayeda and Malagnini, 2010; Baltay et al., 2011*), which apply quite similar methods based on coda envelope measurements. And recent comparisons of the ground-motion prediction equations (GMPE's) with this data set have shown significant overestimated ground motions for the aftershocks, while being in agreement with the mainshock ground motions (*Petersen et al., 2011*). To evaluate the reported scaling relationships and better understand the observed discrepancy in the GMPE's, we revisit the Wells, NV earthquake sequence. We investigate the source parameters of the earthquakes using the coda spectral ratio method (*Mayeda et al., 2007*) and find the stress drops of the aftershocks are 2-5 times lower than that of the mainshock. We compute pseudo spectral acceleration (PSA) ratios using broadband records and compare with theoretical source ratios assuming the self-similar and non-self-similar scaling. We find that we can only match ratios between the mainshock and selected aftershocks if we use non-self-similar scaling. If we assume self-similar scaling, we cannot fit the observed data, especially at higher frequency, by a significant margin. Considering the differences in the stress drop between the small and large earthquakes might help to enhance the prediction capability of the ground motions for this region. By validating source scaling with PSA ratios, these results can be used as constraints in stress parameterization used in the GMPE's.

Is the ongoing earthquake scaling controversy simply a matter of different modeling approaches and underestimated uncertainties?

Rachel E. Abercrombie

Boston University

The controversy concerning earthquake self-similarity continues with some studies finding stress drop to decrease for smaller earthquakes, and others finding constant stress drop across the same magnitude range. It is not clear whether the different results are from studying different earthquakes, or using different methods. Also, the uncertainties are not well constrained. I apply a range of methods to the same earthquakes to determine how different choices in modelling approach affect the results. I find that both random and systematic differences between the stress drops calculated using different approaches are larger than the published uncertainties.

I analyse earthquakes from the Wells (Nevada, M6 2008) earthquake sequence (M4-6), and the 1994 Northridge (M6.7, California) earthquake sequence (M4-6.7), using both coda and direct wave spectral ratio methods. I develop quality criteria for accepting a corner frequency measurement. I find that both coda and direct wave approaches give similar results for the same earthquake pairs, but that there is a systematic bias depending on whether the earthquake of interest is the larger or smaller in the spectral ratio. Mayeda & Malagnini (2009, GRL) calculated coda wave spectral ratios of the Wells M6 mainshock to large (M4-5) aftershocks. They found that the large aftershocks have lower stress drops than the mainshock. Different approaches to fitting the coda spectral ratios, and analysis of direct wave spectral ratios of the same earthquake pairs show no systematic bias, but significant random variation. For each large aftershock I select a closely located, correlated M~3 earthquake as an EGF, and calculate direct S wave spectral ratios between the large aftershocks and the EGF events. I model the direct wave ratios and calculate source parameters and uncertainties following Viegas *et al.* (2010, JGR). The estimates of corner frequency and stress drop are systematically lower for the large aftershocks when they are in the denominator of the ratio. I compare coda and direct wave spectral ratio methods for the Northridge earthquake sequence with similar results. I also compare the results to published time domain measurements of stress drop and seismic energy (Mori *et al.*, 2003). The direct wave spectral measurements correlate well with the time domain P wave duration measurements, and the seismic energy determined from the coda waves is in good agreement with the Mori *et al.* values for the larger $M_0 > 3 \times 10^{15}$ Nm earthquakes

I then apply the direct wave spectral ratio approach to earthquakes from Christchurch New Zealand (M2-6), and Parkfield, California (M1-2.5) to investigate whether it is possible to resolve differences in stress drop with magnitude, or with tectonic setting, within uncertainties.

Static Source Parameters of the West Bohemia/Vogtland Earthquake Swarms

J. Michálek^{1,2}, H. Čermáková^{1,2}, T. Fischer^{1,3} and J. Horálek¹

¹ Institute of Geophysics, Academy of Sciences of the Czech Republic, Prague, michalek@ig.cas.cz

² Faculty of Mathematics & Physics, Charles University in Prague

³ Faculty of Science, Charles University in Prague

The static source parameters like size of the fault plane, seismic moment and stress drop are important quantities for understanding the earthquake processes. The static stress drop is commonly accepted to be almost constant but recent studies show that this is not valid in many cases and stress drop can vary between 0.2-20 MPa (e.g. *Shearer et al., 2006*). Thus the confirmation of the validity of scaling laws in the case of small earthquakes can significantly contribute to the assessment of the seismic potential of a particular fault zone. One of the areas with such small intraplate earthquakes is the West Bohemia/Vogtland region in the Central Europe where earthquake swarms occur.

The area is continuously monitored since 1991 by WEBNET seismic network which nowadays consists of 13 permanent stations and similar amount of temporary stations. The main instrumentally recorded swarms occurred in 1997 ($M_L \leq 3.0$), 2000 ($M_L \leq 3.2$), 2008 ($M_L \leq 3.8$) and 2011 ($M_L \leq 3.5$). Each swarm consists of about thousands of events and is characterized by abrupt onset with high rate of events lasting hours to several days with recurrence period of weeks to months. About 80% of the seismic energy is released in the epicentral zone near station NKC. The main fault plane is steeply dipping towards west at 80° and striking to the south at 171° . Hypocentral distances to the stations ranges between 6 - 30 km (for details see *Fischer et al., 2010*). In this study we analyzed 40 events from the 2000 swarm which passed all the selection criteria (see below). These events are evenly distributed along the main focal zone covering approximately 6 km². The events were selected to comprehend almost whole magnitude range ($0.5 \leq M_L \leq 3.0$).

For determination of source parameters we used absolute spectral approach after *Brune (1970)*. We assume the source geometry to be circular with high-frequency falloff $n = 2$ and all differences in spectral shape from this value we attribute to Q (frequency independent). We used displacement amplitude spectra of P wave on vertical component in 1 sec window (250 samples) and tried to find two source parameters for each event, i.e. one common corner frequency f_c and N values of attenuation factors Q (at N stations). Mean Q values for the whole network are between 200-300. The low frequency plateau Ω_0 was determined as a mean of $\Omega(f)$ for the three lowest frequencies (i.e. 1-3 Hz). The spectra were computed using the multitaper technique then interpolated in such a way to have the frequencies evenly distributed in the logarithmic scale and fitted by minimizing the sum of residuals to the model in L2 norm. The criteria for selecting events were signal-to-noise ratio > 2 in analyzed frequency band 1-80 Hz and minimum number of stations equal to 3. As a second approach for f_c determination we used method after *Snoke (1987)*. Advantage of this method is that the integral of the square of the ground velocity spectrum after attenuation correction can be used directly for determination of f_c without running the whole inversion process (see Fig. 1). The inversion procedure was implemented in the SEISMON processing package (*Mertl & Hausmann, 2009; Michálek et al., 2011*).

The rupture radius a is calculated according to equation $a = k \alpha / f_c$ where $k = 0.24$ (Aki & Richards, 2002) and $\alpha = 6.0$ km/s. Seismic moment is derived using the formula in Brune (1970) with application of radiation correction term for the known typical fault plane orientation (strike = 171, dip = 80, rake = 30). Stress drop is calculated using Eshelby (1957) and is ranging between 0.1 - 30 MPa and decreasing with seismic moment (see Fig. 2).

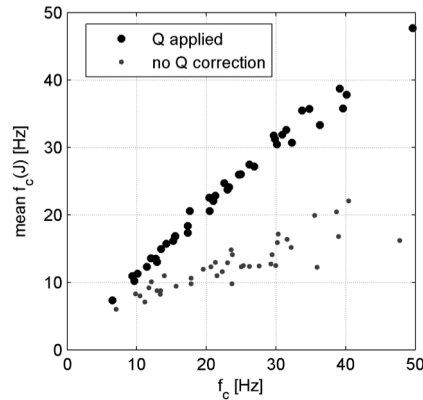


Figure 1. Comparison of two approaches of determining f_c . After sufficient attenuation correction both methods seem to be equivalent.

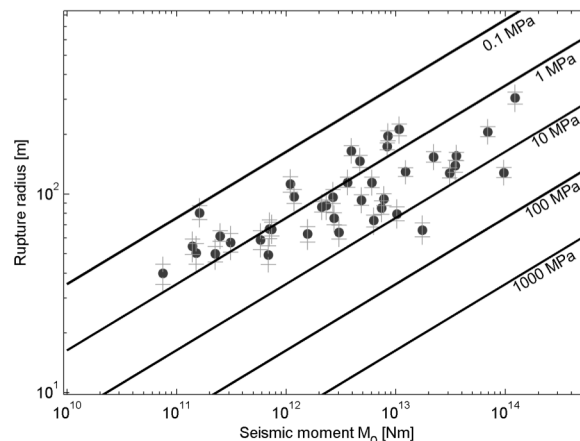


Figure 2. The rupture radius is ranging between 35 - 300 m. The error bars indicate the uncertainty of rupture radii.

References

- Aki, K. & Richards, P.G. *Quantitative Seismology. Book II*, 700 (University Science Books: 2002).
- Brune, J. (1970). Tectonic stress and the spectra of seismic shear waves from earthquakes. *Journal of Geophysical Research* 75, 4997-5009.
- Eshelby, J.D. (1957). The Determination Of Elastic the Field of an ellipsoidal inclusion, and related problems. *Proceedings of the Royal Society of London*, 376-396.
- Fischer, T., Horálek, J., Michálek, J., Boušková, A. (2010). The 2008 West Bohemia earthquake swarm in the light of the WEBNET network. *J Seismol*, 14:665–682, DOI 10.1007/s10950-010-9189-4.
- Mertl, S. & Hausmann, H. (2009). Seismon – a flexible seismic processing software. *Geophysical Research Abstracts* 11, 4266.
- Michálek, J., Doubrovová, J., Mertl, S. (2011). Usage of SEISMON within the WEBNET seismic network. *Geophysical Research Abstracts* 13, 6264.
- Shearer, P.M., Prieto, G. a. & Hauksson, E. Comprehensive analysis of earthquake source spectra in southern California. *Journal of Geophysical Research* 111, 1-21 (2006).
- Snoke, J. (1987). Stable determination of (Brune) stress drops. *Bulletin of the Seismological Society of America* 77, 530-538.

Scalar Moment Variations and Isotropic Characteristics of the Main- and After- Shock Earthquakes in Transform Fault System

Roberto Ortega¹ and Luis Quintanar²

¹ Centro de Investigación Científica y de Educación Superior de Ensenada, CICESE. Unidad La Paz. México. ortega@cicese.mx

² Instituto de Geofísica. Universidad Nacional Autónoma de México. luisq@ollin.igeofcu.unam.mx

Full moment tensor inversions of main- and after- shock earthquakes with non-double couple component in the Gulf of California Transform Fault System are presented in this work. In general, the isotropic constant volume parameter k of the main shock is positive indicating that tensile opening cracks are the initial processes of the seismic sequences. After the main shock, the aftershock sequence initiates. For many aftershocks, the k parameter is negative, implying that closing cracks are the principal source mechanisms. In addition, the dilatational component T-ISO remains almost constant for both main- and after- shock sequences. Therefore, some aftershocks are the effect of a healing process over a weaken crust previously affected by the main shock. On the other hand, the scalar moment is highly sensitive to the amount of non-double couple component and it is very different when is compared with the pure deviatoric inversion. We are interested to describe variations in k reversals, since the main shock shows that the fault mechanism represents a positive isotropic component (opening crack), whereas the aftershocks represent closing cracks. When closing cracks occur, the aftershock distribution at the fault is at least 2 times larger than the predicted slip distribution obtained by a kinematics analysis at the source. We relocated all the aftershocks of different examples and the general trend shows that they are scattered outside the rupture region, implying that rupture characteristics are different. The region that comprise the rupture zone is not only affected by asperities, but also at the vicinity, the aftershocks are the result of a strong stress interaction between the main event and the fault rupture effects over a weak crust. The total moment release cause instability of the young and thin lithosphere, therefore studies based on scalar moment analysis need to be adjusted if they are used to relate the characteristics of the source. Main- and after- shocks have in some cases very different source characteristics and care should be taken if they are used for scaling studies.

The fault stiffness as the key parameter that controls EQ efficiency scaling law

Gevorg G. Kocharyan

Institute of Geospheres Dynamics, Russian Academy of Sciences, Leninskii pr. 38/1, Moscow, 117334
Russia. E-mail gevorgkidg@mail.ru

One of the well known problems in seismology for a long time has been the formulation of scaling laws for earthquakes. The question of whether radiation efficiency of earthquakes scales or it is constant and doesn't depend on event size is widely debated and is still essentially unresolved.

Studies of earthquake scaling relations involve source parameters such as seismic moment M_0 , source radius r_0 , radiated energy E_s , static stress drop $\Delta\sigma$ etc.

Radiation efficiency of the earthquake $\eta_R = \frac{E_s}{E_s + \Delta E_{fr}}$ is the ratio of radiated energy E_s to the sum of radiated and fractured ΔE_{fr} energies. This parameter is proportional to the ratio E_s/M_0 [Kanamori, Brodsky, 2004].

After consideration of the rupture energy budget one can conclude that η_R can roughly be expressed by means of media properties and event scale as $\eta_R = 1 - \frac{\mu}{\alpha \cdot L \cdot k_f}$. Here μ is the rock rigidity (shear modulus), k_f is unloading stiffness of the fault with the length equal to L , and α is the empirical coefficient. Coefficient α depends on the tectonic environments.

We have investigated normal and shear stiffnesses of fractures and fault zones in a wide scale range from several meters to hundreds of kilometers. For this purpose we used the results of seismic measurements along lines crossing discontinuities in rock. We used explosions of various scale from 10^{-3} kg to 10^8 kg of TNT as seismic sources for our experiments. Processing measured data revealed noticeable sudden variations in the amplitudes and periods of seismic waves, which are confined to the zones of fractures and faults. These jumps were used to estimate the normal $k_n = d\sigma/dW_n$ and shear $k_s = d\tau/dW_s$ stiffnesses of each discontinuity. Here σ and τ are normal and shear stresses acting at the discontinuity; W_n and W_s are relative normal and shear displacements of the opposite sides of the discontinuity.

Such an approach gives us the possibility to investigate properties of both rock joints and deep faults. Analyzing the results of measurements we concluded that the fault shear stiffness decreases with the scale not proportional to the fault length, but $k_s \sim L^{-(0.25+0.5)}$.

Under the assumption that the unloading stiffness decreases according to the same law, one can easily obtain the following relation: $\eta_R \sim 1 - \frac{G}{\alpha \cdot L^{0.5+0.75}}$. It shows a gradual increase of the efficiency of earthquake with scale.

Therefore, the self similarity law, which is correct for the first approximation for events of all sizes, in fact is violated, when data series obtained in similar tectonic conditions are considered. This effect remains valid even with account for underrating the contribution of high frequencies to the radiated energy.

Self-similar rupture growth and its break due to the finite seismogenic layer: Revisit of the cumulative moment and moment rate functions of large earthquakes

Takahiko Uchide¹ and Chen Ji²

¹ Disaster Prevention Research Institute, Kyoto University, Gokasho, Uji, Kyoto, 611-0011 Japan, uchide@eqh.dpri.kyoto-u.ac.jp

² Department of Earth Science, University of California, Santa Barbara, Santa Barbara, CA 93106, USA, ji@geol.ucsb.edu

One of issues discussed for a long time in earthquake seismology is if some feature indicating the final magnitude exists during the rupture growth. If yes, such feature should be related to a factor to control the final magnitude, and will help us know the final magnitude earlier and improve the earthquake early warning technique.

Uchide and Ide [2010] proposed the scaling studies of earthquake growth in time by comparing cumulative moment and moment rate functions. They investigated six earthquakes (M_w 1.7 – 6.0) in Parkfield by slip inversion analyses, and discussed a self-similar rupture growth and its limitation due to the finite thickness of the seismogenic layer. This is the only example, and it is important to examine this framework to other earthquakes.

Based on the framework of *Uchide and Ide* [2010], we revisit the moment rate functions and the cumulative moment functions of large earthquakes estimated by slip inversion analyses. The four large earthquakes we study are the 1999 Chi-Chi earthquake (M_w 7.6) [*Ji et al.*, 2003], the 2002 Denali earthquake (M_w 7.9) [*Ji et al.*, 2004a], the 2003 San Simeon earthquake (M_w 6.6) [*Ji et al.*, 2004b], and the 2008 Wenchuan earthquake (M_w 7.9) [*Parsons et al.*, 2008].

Figure 1 shows the cumulative moment functions of these four earthquakes. The Chi-Chi, San Simeon, and Denali earthquakes show the t -cubic growth at the beginning. The Denali earthquake continues for more than 100 s after the deviation from the self-similar rupture growth, similar to the 2004 Parkfield earthquake, while the Chi-Chi and San Simeon earthquakes stops immediately after the deviation, similar to smaller earthquakes in Parkfield which are not affected by the seismogenic limit. This fact reflects the different seismogenic limit relative to the fault length, as *Uchide and Ide* [2010] proposed. The faults of Chi-Chi and San Simeon earthquakes are enough wide and the ruptures reach the seismogenic limit around the half of their source durations. Therefore the effect of the finite seismogenic layer is limited. On the other hand, the Denali earthquake has a narrow fault: 300-km long and 36-km wide. And the break of the self-similar rupture growth is clearly observed.

The Wenchuan earthquake does not fit the t -cubic self-similar scaling. This earthquake has a weak initial rupture in the first 0.8 s, and skipping the first 0.8 s, this earthquake also follows the self-similar rupture growth up to 6 s (Figure 2). This fact may imply that at 0.8 s the rupture restarted to grow self-similarly.

The shape of the normalized moment rate functions (Figure 3) implies the effect of the seismogenic limit. The moment rate function of the Chi-Chi earthquake is close to a bell shape, which implies again that the effect of the finite seismogenic zone is limited. Those of the San Simeon and the Wenchuan earthquakes have a bell

shaped part and a short tail. That of the Denali earthquake is very different from a bell shape due to the narrow fault, which breaks the self-similar rupture.

This study supports the hypothesis that earthquake grows self-similarly unless affected by the seismogenic limit. Earthquakes may have an initial rupture, after which they restart the self-similar growth.

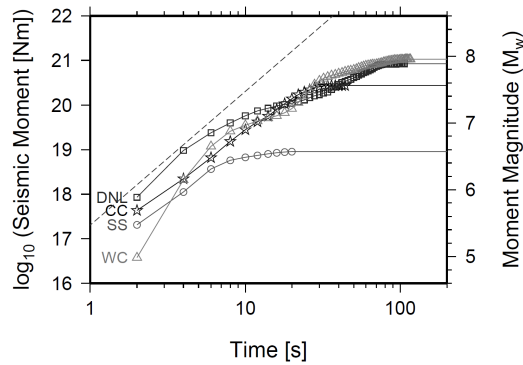


Figure 1. Cumulative moment functions of the 1999 Chi-Chi (CC), the 2002 Denali (DNL), the 2003 San Simeon (SS), and the 2008 Wenchuan (WC) earthquakes. Dashed line indicates the self-similar scaling relationship for earthquakes in Parkfield [Uchide and Ide, 2010], $M_o(t)[Nm] = 2 \times 10^{17}(t [s])^3$.

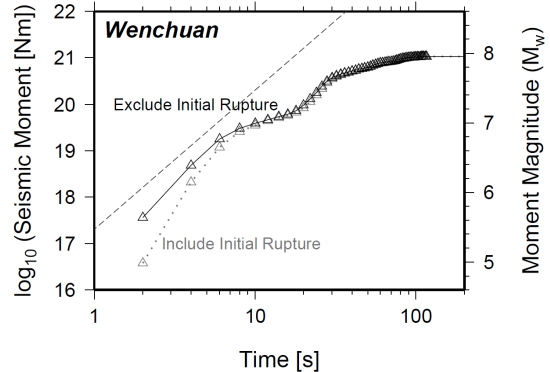


Figure 2. Original (gray) and 0.8-s shifted (black) cumulative moment rate functions of the Wenchuan earthquake.

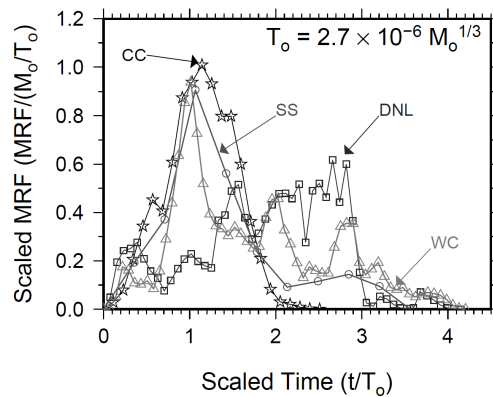


Figure 3. Scaled moment rate functions of the four large earthquakes. Time and moment rate are normalized by a reference source duration, $T_o[s] = 2.7 \times 10^{-6}(M_o[Nm])^{1/3}$, and the total seismic moment divided by T_o , respectively.

References

- Ji, C., D. V. Helmberger, D. J. Wald, and K.-F. Ma (2003), Slip history and dynamic implications of the 1999 Chi-Chi, Taiwan, earthquake, *J. Geophys. Res.*, *108*, 2412, doi:10.1029/2002jb001764.
- Ji, C., D. V. Helmberger, and D. J. Wald (2004a), A Teleseismic Study of the 2002 Denali Fault, Alaska, Earthquake and Implications for Rapid Strong-Motion Estimation, *Earthquake Spectra*, *20*, 617-637.
- Ji, C., K. M. Larson, Y. Tan, K. W. Hudnut, and K. Choi (2004b), Slip history of the 2003 San Simeon earthquake constrained by combining 1-Hz GPS, strong motion, and teleseismic data, *Geophys. Res. Lett.*, *31*, L17608, doi:10.1029/2004GL020448.
- Parsons, T., C. Ji, and E. Kirby (2008), Stress changes from the 2008 Wenchuan earthquake and increased hazard in the Sichuan basin, *Nature*, *454*, 509-510.
- Uchide, T., and S. Ide (2010), Scaling of earthquake rupture growth in the Parkfield area: Self-similar growth and suppression by the finite seismogenic layer, *J. Geophys. Res.*, *115*, B11302, doi:10.1029/2009JB007122.

Three-stage magnitude-area scaling supported by slip inversions and dynamic rupture simulations

Hiroe Miyake¹, Kojiro Irikura², Luis A. Dalguer³ and Satoko Murotani¹

¹ Earthquake Research Institute, University of Tokyo

² Aichi Institute of Technology

³ ETH Zurich)

Source scaling of seismic moment and rupture area is a fundamental issue to understand earthquakes. For the source scaling of seismic moment and fault length, the L -model (Scholz, 1982) and the W -model (Romanowicz, 1992) had been proposed for crustal earthquakes over the magnitude range of the circular-crack model. Recent development of slip inversions enabled us to improve quantitative estimates of the magnitude-area scaling.

Based on the source characterization of slip inversions, the magnitude-area scaling for crustal earthquakes has been constructed:

The first circular-crack model stage of
 $S \text{ (km}^2\text{)} = 2.23 \times 10^{-15} \times (M_0 \text{ (Nm)} \times 10^7)^{2/3}$ (Somerville *et al.*, 1999)
 for $M_0 < 7.5 \times 10^{18}$ Nm,

the second L -model stage of
 $S \text{ (km}^2\text{)} = 4.24 \times 10^{-11} \times (M_0 \text{ (Nm)} \times 10^7)^{1/2}$ (Irikura and Miyake, 2001, 2011)
 for $M_0 \geq 7.5 \times 10^{18}$ Nm,

and the third W -model stage of
 $S \text{ (km}^2\text{)} = 5.30 \times 10^{-25} \times (M_0 \text{ (Nm)} \times 10^7)$ (Irikura *et al.*, 2004)
 for $M_0 \geq 7.5 \times 10^{20}$ Nm,

that was recently revised into
 $S \text{ (km}^2\text{)} = 1.0 \times 10^{-17} \times M_0 \text{ (Nm)}$ (Murotani *et al.*, 2010)
 for $M_0 \geq 1.8 \times 10^{20}$ Nm.

The above three-stage source scaling shows bending without significant gaps that pointed out by several 2-D numerical simulations (Figure 1). The scaling supports $L \sim W_{max}$, not $L = 2W_{max}$. There were less evidence of the differences seen in cascade and scaling earthquake ruptures. The second L -model stage is similar to Hanks and Bakun (2002) well constraint by megafault systems.

It is very important to quantify stress drop for the stages of the scaling. We performed a series of dynamic rupture simulations for strike-slip faulting using 3-D FDM of Dalguer *et al.* (2008). Stress drops were assumed for 2.3, 3.0, 5.0, and 10.0 MPa for rectangular crack models with maximum fault width W_{max} of 20 km. Aspect ratios of the faults ranged 1 to 20. Our dynamic rupture simulations naturally reproduced the three-stage magnitude-area scaling (Figure 2). Those are compatible with the static models by Fujii and Matsu'ura (2000) and Shaw and Scholz (2001). To fit the scaling between slip inversions and dynamic rupture simulations, slight increase of stress drop from 2.3 to over 3.0 MPa is required in the second L -model stage, where the stress drop increases from 2.3 to 5.7 MPa for the circular-crack calculation by Eshelby (1957).

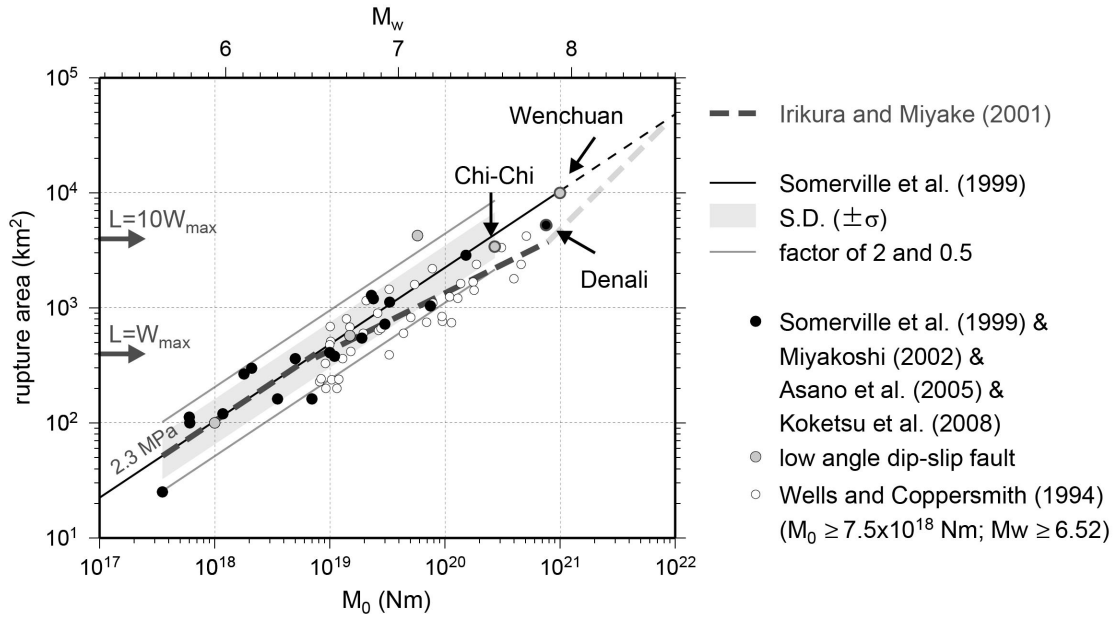


Figure 1. Magnitude-area scaling for crustal earthquake from slip inversions (Irikura and Miyake, 2011).

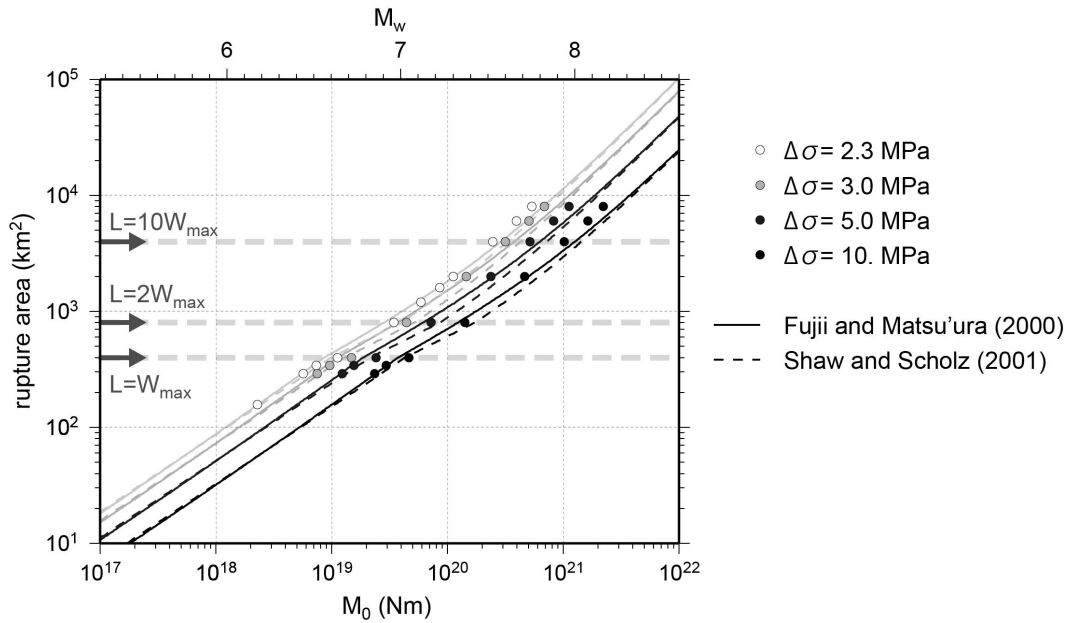


Figure 2. Magnitude-area scaling from dynamic rupture simulations for rectangular crack models with maximum fault width W_{max} of 20 km.

Seismic source properties extracted from a new global and complete catalogue of earthquake source time functions

Martin Vallée

Geoazur, University of Nice Sophia Antipolis, IRD-CNRS-OCA, Valbonne, France

Earthquake source time functions (STFs) offer a direct insight on the seismic source properties, integrated over the fault plane. In classical earthquake models, variations of the STFs properties (duration, maximum amplitude) for earthquakes of a given magnitude imply variations in stress drop or rupture velocity. Information extracted from STFs is less rich than the one given by the description of the rupture scenario on the fault plane (extended source analysis). But compared to the latter approach, study of STFs presents a strong advantage in an exhaustive perspective of the seismicity analysis: they can be reliably and efficiently derived from teleseismic data alone, provided earthquakes have a magnitude larger than 5.5-6. This opens the possibility to analyse conjointly, in a consistent way, the ~2400 earthquakes with $M > 6$ of the last 20 years.

We make use of a recently developed approach - called SCARDEC (*Vallée et al.*, 2011) -, based on the deconvolution of the teleseismic P and S body waves. Using physical constraints on the STFs, SCARDEC resolves simultaneously the source parameters (depth, focal mechanism and seismic moment) and the STF of the earthquake. This method works well for all earthquake depths and for all magnitudes larger than 5.5-6 (including the very large events). SCARDEC is used today in near-real time, to provide rapid information on the source characteristics. We here apply the method to the catalogue, previous mentioned, of earthquakes with magnitude larger than 6 in the period 1992-2011. Thanks to the good quality, global coverage, and easy access of the broadband data of the global networks (IRIS arrays IU, II and IC, GEOSCOPE, GEOFON, USGS), we obtain reliable STFs for about 1700 earthquakes spanning the whole depth range, and the [6-9] magnitude range.

As a first application of this STFs catalogue, we examine how the STF maximum amplitude (called F_m) evolves with magnitude and depth. In a model where stress drop and rupture velocity is constant, it can be simply shown that F_m scales with $M_0^{2/3}$, where M_0 is the seismic moment. This is closely related to the better-known scaling relation between T , the rupture duration, and $M_0^{1/3}$. We choose to work with F_m rather than T , because its determination on the real STFs is much less subjective. When selecting only the shallow earthquakes of the catalogue (implying that there should not be a systematic variation related to the rigidity), F_m evolves as $M_0^{0.68}$, very close to the expected relation (Figure 1). At a given M_0 , the dispersion of F_m is smaller than one order or magnitude, while M_0 varies on about 5 orders of magnitude. This implies that stress drop and rupture velocity are on average independent of the seismic moment, and that most shallow earthquakes share similar values for these two source properties.

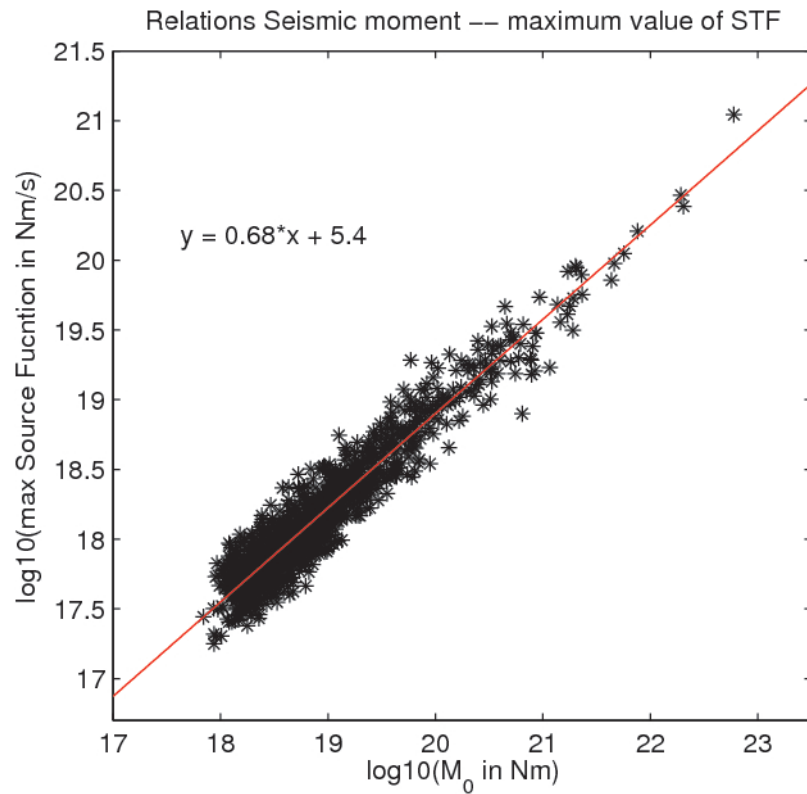


Figure 1. Relation between seismic moment M_0 and maximum of the STF F_m , for the 1170 shallow earthquakes (depth < 45km) of the new catalogue. The relation is shown in log-log representation. The straight line indicates the best linear fitting, and its corresponding equation is shown on the figure.

This observation allows us to scale F_m to the seismic moment (we note F_m' this scaled value), in order to study its variations with depth, independently of the earthquake size. We find that F_m' values present internal variations at a given depth, but (1) for depths larger than 90km, they are always above the average value determined for shallow earthquakes and (2), the averaged values of F_m' (average made for earthquakes with similar depths) increase with depth. Hypotheses explaining this behaviour will be discussed during the meeting.

References

Vallée, M., J. Charléty, A.M.G. Ferreira, B. Delouis, and J. Vergoz, SCARDEC : a new technique for the rapid determination of seismic moment magnitude, focal mechanism and source time functions for large earthquakes using body wave deconvolution, *Geophys. J. Int.*, 184, 338–358, 2011.

Areas of slip of recent earthquakes in the Mexican subduction zone

Vala Hjörleifsdóttir, Hugo S. Sánchez-Reyes, Shri Krishna Singh, Xyoli Pérez-Campos, Arturo Iglesias

Departamento de Sismología, Instituto de Geofísica, Universidad Nacional Autónoma de México

The Mexican subduction zone is unusual: the width of the seismogenic zone is relatively narrow and a large portion of the co-seismic slip generally occurs below the coast, ~ 45 to 80 km from the trench. The earthquake recurrence interval is relatively short and almost the entire length of the zone has experienced a large ($M_w \geq 7.4$) earthquake in the last 100 years (Singh et al., 1981).

In this study we present detailed analysis of the areas of significant slip during several recent (last 20 years) large earthquakes in the Mexican subduction zone. The most recent earthquake of 20 March 2012 ($M_w 7.4$) occurred near the Guerrero/Oaxaca border. The slip was concentrated on the plate interface below land and the epicentral PGAs ranged between 0.2 and 0.7g. The updip portion of the plate interface had previously broken during the 25 Feb 1996 earthquake ($M_w 7.1$), which was a slow earthquake and produced anomalously low PGAs (Iglesias et al., 2003). This indicates that in this region the area close to the trench is at least partially locked, with some earthquakes breaking the down-dip portion of the interface and others rupturing the up-dip portion.

The Jalisco/Colima segment of the subduction zone seems to behave in a similar fashion. The 9 October 1995 ($M_w 8.0$) earthquake generated small accelerations relative to its size. The energy to moment ratio, E_0/M_0 , is $4.2e-6$ (Pérez-Campos, Singh and Beroza, 2003), a value similar to the Feb, 1996 earthquake. This value is low compared to other thrust events in the region. The earthquake also had the largest (M_s - M_w) disparity along the Mexican subduction zone, 7.4 vs 8.0. The event produced relatively large tsunami. On the contrary, the 3 June 1932 earthquake ($M_s 8.2$, $M_w 8.0$), that is believed to have broken the same segment of the subduction zone, appears to be “normal.” Based on the available evidence, it may be concluded that the 1932 event broke a deeper patch of the plate interface relative to the 1995 event.

The mode of rupture in the subduction zone between the two areas mentioned above is not known. This part of the subduction zone includes the rupture area of the 1985 Michoacán earthquake ($M_w 8.0$) and the “Guerrero Gap” which is a section of the subduction zone that has not had a large earthquake in the last 100 years.

The downdip and updip patches on the plate interface, which, generally, rupture independently may slip during one great earthquake. This possibility must be accounted for in the estimation of maximum-magnitude earthquake along the subduction zone.

Tremor activities and thermal structures in various subduction zones

Suguru Yabe¹, Satoshi Ide¹ and Shoichi Yoshioka²

¹ The University of Tokyo, EPS

² Kobe University, RCUSS

Various phenomena of slow earthquakes, deep tremor and low frequency earthquakes (LFEs), very low frequency earthquakes (VLFs), slow slip events (SSEs), have a different scaling law from that of usual earthquakes (Ide et al., 2007), which indicate the mechanism of slow earthquakes are different from that of ordinary earthquakes. The difference may arise from the difference of governing rheology: i.e., slow earthquakes occur in brittle-ductile or ductile regime while ordinary earthquakes occur in brittle regime, controlled by depth-dependent temperature along plate interface. However, some studies imply that tremor is not controlled by temperature (e.g. Brown et al., 2007) and it is still open question whether slow earthquakes are mainly controlled by temperature. Here we investigate the source locations of deep tremor using the envelope correlation method of Ide (2010; 2012) and compare them with the temperature and shear strength profiles along the plate interface calculated using a numerical model (Yoshioka and Sanshadokoro, 2002), in several subduction zones with the various age of subducting plate.

Beneath the North Island in New Zealand, the characteristics of seismicity and tectonics change along strike, and deep tremor and slow slip have been identified (e.g. Wallace and Beavan, 2010; Kim et al., 2011, Fry et al., 2011, Ide, 2012). We reanalyze these detected tremors and confirm that tremors in North Island are on the plate interface, which was not apparent in the previous studies. Thermal modeling of the Hikurangi subduction zone suggests that change of seismic coupling depth is due to the change of temperature profile, fluid distribution, and convergence rate. The tremor sources are located near brittle-ductile transition, which implies that tremor genesis is controlled by temperature.

Near the triple junction of the southern Chile subduction zone, and in the Colima-Jalisco region of the Mexican subduction zone, the depth of tremors becomes deeper as the subducting plate age increases (Ide, 2012). Since old plate is cool, this result also implies that tremors are controlled by the temperature along the plate interface. We plan to carry out the tremor relocation and thermal modeling to these subduction zones, and clarify the dependence of tremor on the plate interface temperature.

Envelope inversion for the spatio-temporal distribution of high-frequency energy radiators of the M9.0 Tohoku-Oki earthquake

A. Inbal¹, J.-P. Ampuero¹, S. Lui¹, D. Helmberger¹ and R. W. Graves²

¹ Division of Geological and Planetary Sciences, California Institute of Technology, Pasadena, California, USA

² U.S. Geological Survey, Pasadena, California, USA

The March 11, 2011 M9.0 Tohoku-Oki earthquake was recorded by dense seismological and geodetical networks deployed in Japan, as well as by a vast number of seismic stations worldwide. These observations allow us to study the properties of the subduction interface with unprecedented accuracy and resolution. In particular, depth-dependent variations of fault behavior, a feature that has long been masked by strong heterogeneities along the fault strike, can now be probed successfully. Back-projection analysis of teleseismic data suggests that coherent high frequency energy (> 1 Hz) was mainly emitted from deep portions of the megathrust, at the bottom extent of the rupture zone (Meng et al., 2011). Here we study the details of high-frequency energy radiation during the M9.0 mainshock from local observations.

In order to better constrain the timing, location and amplitude of high-frequency radiators, we invert waveform envelopes recorded by the dense Kiban Kyoshin borehole accelerometers network located in northeastern Japan. Conventional inversions of acceleration data suffer from the lack of resolution of local Earth models, and are thus capable of modeling only signals with periods of a few seconds or longer. Waveform envelopes, on the other hand, are less sensitive to structural complexities, and may be used efficiently to model signals at high frequencies. We compute theoretical envelopes for waves travelling in a heterogeneous scattering medium using the method of Nakahara et al. (1998). We assume constant rupture velocity, and perform a search for rupture velocity and rise time that will minimize the misfit between the observed and calculated envelopes in several frequency bands. A major difficulty in the inversion procedure is the separation of the source and the site effects. Strong trade-offs between these parameters render the inversion non-linear and thus extremely sensitive to the response of individual stations. We address this issue by two means. First, we adopt an empirical approach and iteratively separate the source and receiver terms from the stacked spectra of numerous events recorded by the network. Second, we perform forward modeling of several M~6 aftershocks to identify stations that systematically deviate from our predictions. Estimates of site responses obtained from these tests are used as input for the inversion. Preliminary results are consistent with far-field observations and suggest that the origin of high-frequency energy emitted during the M9.0 event is at the down-dip extent of the rupture zone.

References

- L. Meng, A. Inbal and J.-P. Ampuero (2011). A window into the complexity of the dynamic rupture of the 2011 M_w9.0 Tohoku-Oki earthquake. *Geophys. Res. Lett.*, 38, L00G07, doi:10.1029/2011GL048118.
- H. Nakahara, T. Nishimura, H. Sato and M. Ohtake (1998). Seismogram envelope inversion for the spatial distribution of high-frequency energy radiation from the earthquake fault: Application to the 1994 far east off Sanriku earthquake, Japan. *J. Geophys. Res.*, 103 (B1).

Radiation efficiency and breakdown work in a dynamic rupture model for the 2011 Tohoku earthquake considering recent stress accumulation and thermal fluid pressurization

Mitsui Yuta¹, Yoshihisa Iio² and Yukitoshi Fukahata²

¹ Grad. Sci., Hokkaido Univ.

² DPRI, Kyoto Univ.

Mitsui et al. (Earth Planets Space, accepted for the special issue “The 2011 Tohoku earthquake”) constructed a dynamic rupture simulation model for the 2011 Tohoku earthquake, referring to the moment release rate obtained by seismic slip inversions. Their simulation raised importance of recent shear stress changes around the epicenter of the mainshock, owing to four M7-class earthquakes during 2003-2011, and nonlinear weakening friction for the occurrence of the M9 earthquake. In particular, dynamic thermal pressurization of pore fluid on the fault was assumed. Figure 1 shows a calculation result for “larger fault model” in that study.

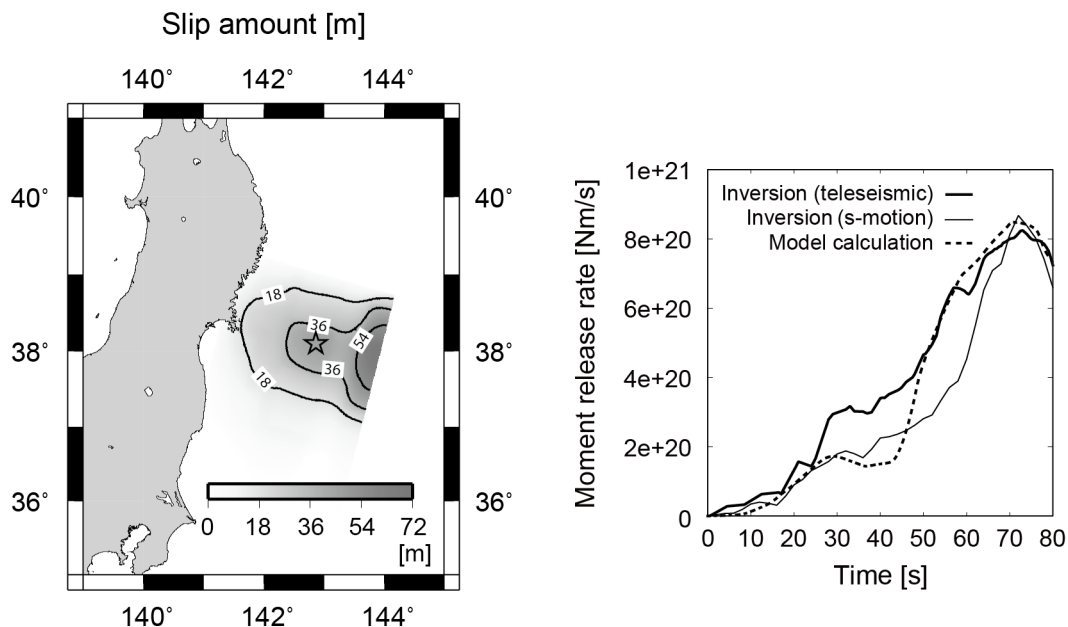


Figure 1. Calculated slip distribution and moment release rate, in comparison with the moment-rate function in a slip inversion study (Yoshida et al., 2011).

Besides, their dynamic rupture simulation did not use any constraint about radiation energy or breakdown work on the fault. Such values are of significance in terms of earthquake scaling. Thus we checked the mean radiation efficiency, which is defined as the radiation energy from the whole fault divided by the seismic moment. For the above model, the radiation efficiency is almost 9×10^{-5} . This value seems larger than many earthquakes but within the range of a scaling that is valid over several orders of seismic moment (Baltay et al., 2011). Moreover, we measured the whole breakdown work on the model fault. The value is almost 3×10^{18} J, smaller than a power law scaling (Tinti et al., 2005) by one order of magnitude. The value of the breakdown work in our simulation corresponds to that for Mw8.3 earthquake in the scaling line.

In conclusion, our dynamic rupture model for the 2011 Tohoku earthquake, constraint by the moment release in the seismic inversions, has a slightly larger value of the radiation efficiency and smaller value of the breakdown work in comparison with the previously proposed earthquake scaling. We will examine this point also in other parameter set with the same observational constraint.

References

- Baltay, A., S. Ide, G. Prieto, and G. Beroza, "Variability in earthquake stress drop and apparent stress", *Geophys. Res. Lett.*, 38, L06303, 2011
- Mitsui, Y., Y. Iio, and Y. Fukahata, "A scenario for the generation process of the 2011 Tohoku earthquake based on dynamic rupture simulation: role of stress concentration and thermal fluid pressurization", *Earth Planets Space*, accepted
- Tinti, E., P. Spudich, and M. Cocco, "Earthquake fracture energy inferred from kinematic rupture models on extended faults", *J. Geophys. Res.*, 110, B12303, 2005
- Yoshida, Y., H. Ueno, D. Muto, and S. Aoki, "Source process of the 2011 off the Pacific coast of Tohoku Earthquake with the combination of teleseismic and strong motion data", *Earth Planets Space*, 63, 565–569, 2011

Compressional rupture branching in a weakened oceanic lithosphere during the 11 April 2012 M8.6 Sumatra earthquake

L. Meng*, J-P. Ampuero, J. Stock, Z. Duputel, Y. Luo and V.C. Tsai

Seismological Laboratory, Division of Geological and Planetary Sciences, California Institute of Technology, Pasadena, CA 91125, USA.

* Corresponding author, email: lsmeng@gps.caltech.edu

Seismological observations of the 2012 Mw 8.6 Sumatra earthquake reveal unprecedented complexity of dynamic rupture. The surprisingly large magnitude results from the combination of deep extent, high stress drop and rupture of multiple faults. Back-projection source imaging indicates that this multiple fault rupture occurs on distinct planes in an orthogonal conjugate fault system, with relative slow rupture speed. The ESE-WNW ruptures add a new dimension to the seismotectonics of the Wharton Basin which was previously thought to be controlled by N-S strike-slip faulting. The rupture turns twice into the compressive quadrant, against the preferred branching direction predicted by Coulomb stress calculations. The earthquake also had low radiation efficiency. We attribute these features to a low friction coefficient, possibly due to serpentinization of the oceanic crust.

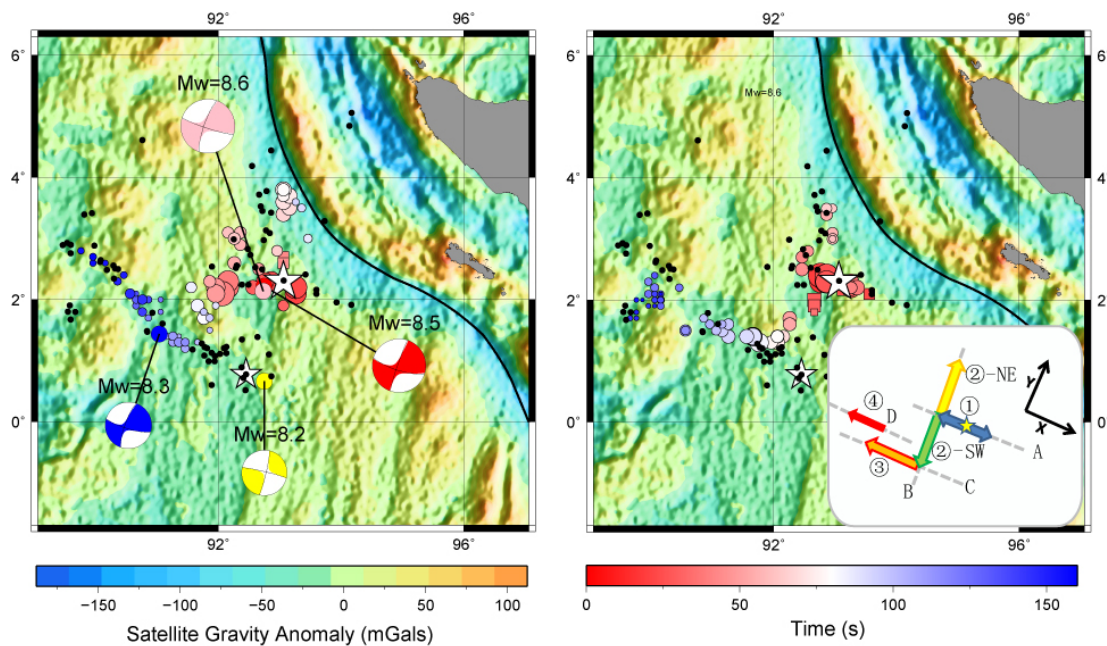


Figure 1. Spatio-temporal distribution of high-frequency radiation as seen from Japan (left) and Europe (right). Colored circles and squares indicate the position of primary and secondary peak high-frequency radiation (from movies S1 and S2, respectively) with size scaling with beamforming amplitude and color indicating timing relative to hypocentral time (color scale on bottom-right). The secondary peaks of MUSIC pseudo-spectrum are at least 50% as large as the main peak in the same frame. The background is colored by the satellite gravity anomaly $v. 18.1$ from the UCSD TOPEX database (color scale on bottom-left). Black dots are the epicenters of the first day of aftershocks from the NEIC catalog. The big and small white stars indicate the hypocenter of the mainshock and M8.2 aftershock. The focal centroid of the M8.6 mainshock, M8.2 aftershock and double CMT solutions of the mainshock are colored pink, yellow, red and blue beach balls. Inset shows the interpreted fault planes (grey dashed lines) and rupture direction (colored arrows).

The Slip Pulse Equation for Multi-scale Simulation of Strong-Rate-Weakening Friction

Heaton, Th.¹ and A. Elbanna²

¹ California Institute of Technology

² Univ. of Calif. at Santa Barbara

We investigate the implications of strong-rate-weakening friction using a 1-d spring-block slider model. Recently, Goldsby and Tullis (2011) presented experimental evidence for strong-rate-weakening friction that they interpret as evidence for flash heating (Rice, 2006). Although we can conjecture that strong-rate-weakening friction may be the key to understanding the heat flow paradox, it has not been possible to simulate the dynamic behavior of two half-spaces that are sliding with strong-rate-weakening friction. In particular, Rice and others (2001) argued that pure-rate-weakening friction produces ruptures with unstable characteristics and that it leads to ill posedness.

Aagaard and Heaton (2008) used 3-d finite element dynamic rupture models to investigate the possibility that spatially heterogeneous slip evolves from the dynamic complexity that comes from strong-rate-weakening friction. Although strong-rate-weakening friction did indeed produce instability, the size of the computation necessary to achieve multi-scale simulations was far too large for current computational resources. Because the 3-d elastic problem proved numerically intractable, we chose to investigate the spring-block-slider problem of Burridge and Knopoff (1968). While this problem model has been extensively studied by Carlson and others (1991), we were especially interested in describing prestress conditions that are compatible with strong-rate-weakening friction.

We found that if we tune the spring stiffnesses appropriately, then the system fails in self-similar slip pulses that are spatially complex and multi-scale with power law statistical distributions. This is a strong indication of chaos. Figure 1 shows a representative simulation where the rupture length segments (vertical axis) are shown for each of 5,000 consecutive events in the system (the event number is on the horizontal axis).

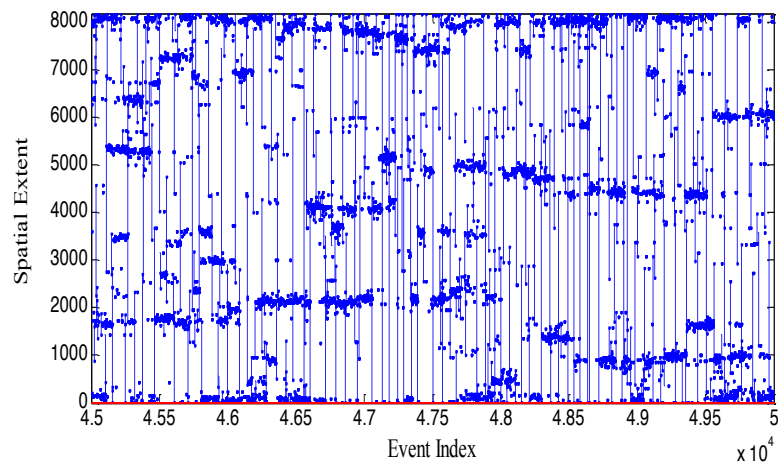


Figure 1. The rupture lengths (vertical axis) of a sequence of 5,000 events (event index on the horizontal axis). Notice the multi-scale and chaotic nature of the sequence.

We discovered a remarkable new approach to solving this problem. We realized that, with the exception of event nucleation, the events all consisted of slip pulses that were self-similar with respect to slip amplitude. This allowed us to find power-law relationships between the slip amplitude, the slip rate, the frictional work done by a pulse, and the kinetic energy of a pulse. We could then write a single difference equation that balances potential, kinetic, and dissipative energy changes as a pulse propagates through the system. That is, the change in the size of a propagating pulse depends on the prestress through which it propagates and also on the present size of the slip pulse which determines the frictional work (remember ... the friction depends on the slip rate which correlates with the slip). That is, we could replace n nonlinear coupled equations by a single 1-d difference equation. Furthermore, since the balance of energy equation was exact, and since the slip pulses were very close to self-similar with respect to slip amplitude, the new difference equation predicted the system very well and over a very broad range of length scales. The equation given below tells how the amplitude of a propagating slip pulse of present slip D will change dD in the next increment of rupture dx .

$$\frac{dD}{dx} = \frac{-(\gamma\xi D^{\xi-1} - \sigma_{oc}) + \sqrt{(\gamma\xi D^{\xi-1} - \sigma_{oc})^2 - 2k_c(\frac{1}{2}k_l D^2 - \sigma_{ol}D + \alpha D^{\beta+1})}}{k_c}$$

The prestress at x is given as the sum of the prestress from the coil springs, σ_{oc} , and the leaf springs, σ_{ol} . The full numerical solution is used to empirically determine that pulse kinetic energy $\approx \gamma D^\xi$ and pulse friction energy $\approx \alpha D^{1+\beta}$. We see that ξ and β are similarity coefficients in this fractal problem. Figure 2 shows an example of the use of this equation. The prestress in the top box is a critical prestress that results from running the model for a long time (many events).

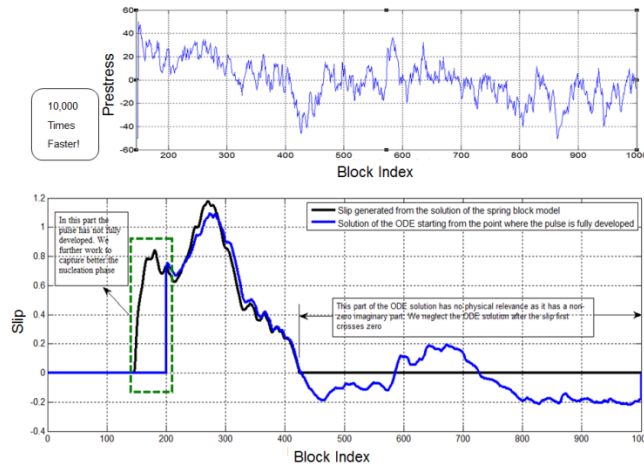


Figure 2. (Top): Prestress distribution for the test case. (Bottom): The solution of the proposed differential equation (in blue) mimics the slip solution from the spring block model in the pulse-like region (between blocks 200 and 420). The initial condition for the equation was taken as the slip value at the point where the nucleation phase is over and the pulse has fully developed. The nucleation phase is handled by the full calculation.

The success of the hybrid scheme is a very exciting development. The computation time is thousands of times smaller than for the full solution. Furthermore, it illuminates the physics of this problem; namely the slip pulses carry energy that is redistributed along the rupture surface.

Earthquake Sequences on Faults with Heterogeneous Compressive Stress and Enhanced Co-seismic Weakening

Junle Jiang¹ and Nadia Lapusta^{1,2}

¹ Division of Geological and Planetary Sciences, California Institute of Technology, Pasadena, CA, United States.

² Division of Engineering and Applied Science, California Institute of Technology, Pasadena, CA, United States.

In numerical simulations of isolated dynamic earthquake rupture, heterogeneous stress is often used to produce complex earthquake scenarios, and fault prestress and frictional strength are usually assigned independently. Real earthquakes are recurring events on faults with a variety of heterogeneities in fault properties, and fault prestress and strength are physically related through stress redistribution due to prior slip. Therefore, simulating earthquake sequences on faults with heterogeneity is important for understanding the characteristic seismic behavior of faults and for assessing seismic hazard.

We study the long-term slip history on faults with kilometer-scale variation in fault compressive stress which follows characteristic power spectra possibly related to geometric complexity, pore pressure variations and etc. The entirety of earthquake cycles, including fully dynamic seismic rupture and aseismic tectonic loading, are simulated on 2D faults governed by Dieterich-Ruina rate-and-state friction with enhanced co-seismic weakening due to shear heating. Initial shear stresses are pre-assigned and developed into physically-consistent distribution through many cycles.

In our simulations, incorporation of enhanced co-seismic weakening generally results in events with larger slip and enables the fault to operate at lower average stress level. Increasing heat production, and hence larger co-seismic weakening at the places of higher normal confinement, tends to partially compensate for the effect of heterogeneous static strength. As an example, Figure 1 and 2 showcase the behavior of a fault with heterogeneous normal stress that's typical of a mature fault. Despite the heterogeneity in the normal confinement, the earthquake sequences consist of all fault-spanning seismic events. Shear stresses evolve and redistribute on the ruptured fault, in accordance with the fault strength, hence to reduce the subsequent effect of the introduced heterogeneity in dynamic rupture in the long-term fault behavior. While some variations in rupture speed are observed in the models, coseismic slip and stress drop over the fault are approximately uniform in space.

Our current work is directed towards quantifying the effect of fault heterogeneity level on the earthquake behavior and patterns. The work would be used to: (1) draw implications for the realistic state of stress on heterogeneous faults and how it would affect earthquake nucleation conditions, with an eye towards explaining the apparent lack of seismicity on some faults such as Southern San Andreas, and (2) understand the effect of stress redistribution on rupture propagation, with consequences for ground shaking.

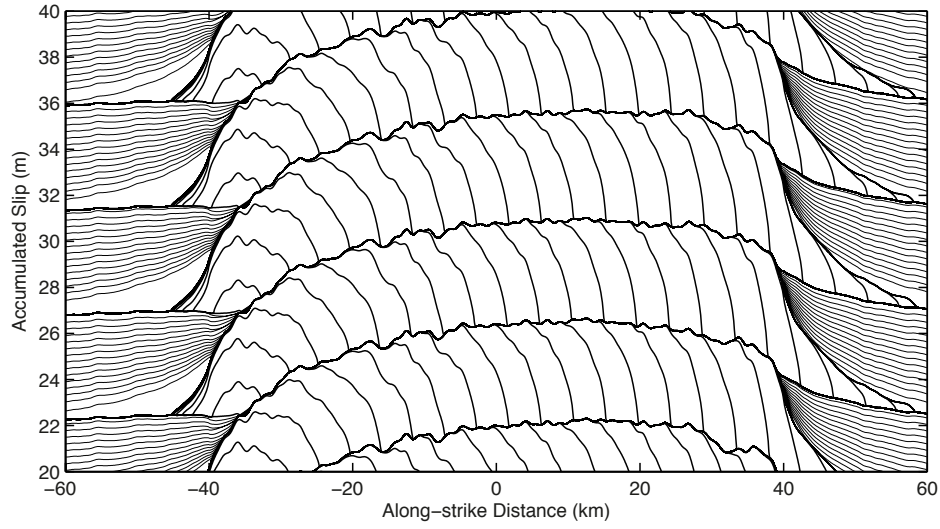


Figure 1. Slip accumulation in seismogenic regions (thick lines plotted for every 1 second) surrounded by stably creeping regions (thin lines plotted for every 5 years) on a fault with heterogeneous compressive stress.

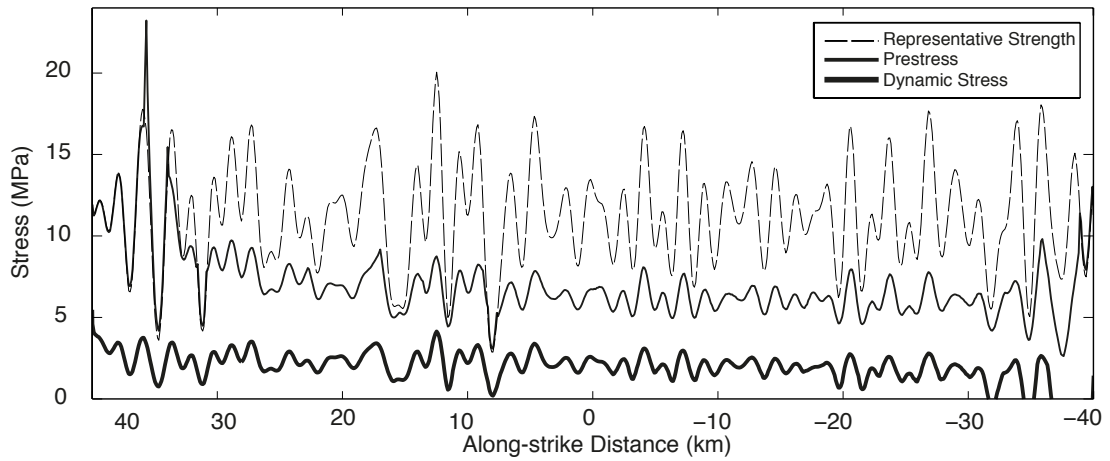


Figure 2. Characteristic stress state (representative static strength, prestress and minimal dynamic stress) for a seismic event in the long-term behavior of the heterogeneous fault.

The seismic cycle at subduction thrusts: Implications of geodynamic simulations benchmarked with laboratory models

Ylona van Dinther^{1,2}, Taras Gerya², Luis A. Dalguer², Fabio Corbi³,
Francesca Funicello³ and P. Martin Mai⁴

¹ Swiss Seismological Service, ETH Zurich, Sonneggstrasse 5, CH-8092, Zurich, Switzerland, ylona.vandinther@tomo.ig.erdw.ethz.ch

² Institute of Geophysics, ETH Zurich, Sonneggstrasse 5, CH-8092, Zurich, Switzerland

³ LET-Laboratory of Experimental Tectonics, Univ. "Roma Tre", L.S.L. Murialdo 1, 00146 Roma, Italy.

⁴ Division of Physical Sciences and Engineering, 4700 King Abdullah University of Science and Technology, Thuwal 23955-6900, Saudi Arabia.

We benchmark a quasi-static, visco-elasto-plastic numerical model to a new laboratory approach, and demonstrate the applicability of geodynamic models in earthquake cycle research. Our results show that slip rate-dependent friction needs to be included to spontaneously simulate frictional instabilities. We analyze the physical framework in terms of underlying physics, parameter space, and several intensely debated dynamic rupture features, including self-healing pulses and re-rupturing. Finally, we show surface displacements capture the most characteristic features of the inter-, co-, and postseismic phase observed in geodetic measurements via afterslip.

The physics governing the seismic cycle at seismically active subduction zones remains poorly understood because direct observations are limited in space and time. Therefore, reliable and realistic numerical simulations are needed to shed light into subduction zone seismicity. To investigate subduction zone dynamics and associated interplate seismicity, we benchmark a quasi-static, visco-elasto-plastic numerical model to a new laboratory approach presented in Corbi et al. [submitted]. Our modeling setup includes a visco-elastic gelatin wedge underthrust by a plate with defined velocity-weakening and -strengthening regions.

Our novel approach includes velocity-weakening friction into a geodynamic modeling framework, and spontaneously generates series of fast frictional instabilities that correspond to analog earthquakes (Figure 1). A match between numerical and laboratory source parameters is obtained if velocity-strengthening is applied in the aseismic regions to stabilize and limit the rupture extent, while still promoting slip complexity.

Spontaneous nucleation by coalescence of neighbouring slip patches occurs mainly at evolving asperities near the seismogenic zone limits, with a preference for the downdip region. Consequently, a crack-, or occasionally even pulse-like, rupture propagates toward the opposite side of the seismogenic zone by overcoming stress heterogeneities through increasing stresses ahead of its rupture front.

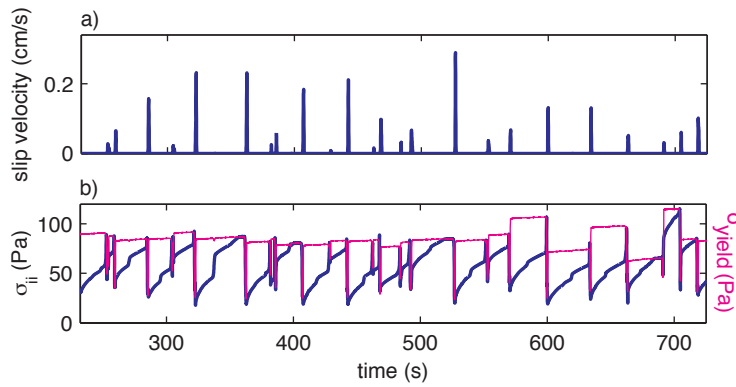


Figure 1. Lagrangian evolution of physical properties at a central particle.

The resulting surface displacements qualitatively agree with geodetic observations, and show landward and, from near the downdip limit, upward interseismic motions (Figure 2). These are rebound and reversed coseismically as the fault slips. Slip produces stress shadows that are subsequently relaxed by postseismic afterslip.

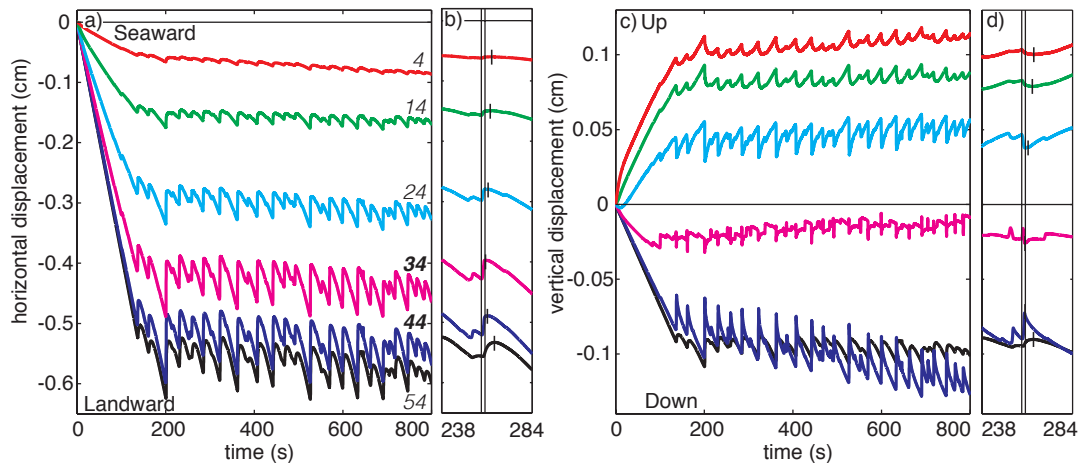


Figure 2. Particle displacements w.r.t. their original location measured along an array at the surface in (a,b) surface-parallel, and (c,d) surface-perpendicular direction. Italic numbers indicate distance to the laboratory backstop in centimeters.

The agreement of our simulations with laboratory results and a wide range of observed physical phenomena, including back-propagation and repeated slip, demonstrate that visco-elasto-plastic geodynamic models with rate-dependent friction represent a powerful new approach that may greatly contribute to our understanding of the seismic cycle at subduction zones.

References

Corbi, F., Funicello, F., Moroni, M., van Dinther, Y., Mai, P.M., Dalguer, L.A., Faccenna, C. (submitted). The seismic cycle at subduction thrusts: 1. insights from laboratory models, *Journal of Geophysical Research*.

The seismic cycle on spontaneously evolving subduction faults in realistic geometry geodynamic simulations

Ylona van Dinther^{1,2}, Taras Gerya², P. Martin Mai³, Luis A. Dalguer² and Gabriele Morra⁴

¹ Swiss Seismological Service, ETH Zurich, Sonneggstrasse 5, CH-8092, Zurich, Switzerland, ylona.vandinther@tomo.ig.erdw.ethz.ch

² Institute of Geophysics, ETH Zurich, Sonneggstrasse 5, CH-8092, Zurich, Switzerland

³ Division of Physical Sciences and Engineering, 4700 King Abdullah University of Science and Technology, Thuwal 23955-6900, Saudi Arabia

⁴ School of Earth and Environmental Sciences and Quality of Life Technology, Seoul National University, Seoul, South Korea

Earthquakes occur over a large range of spatial and temporal scales. While abundant data are available to gain understanding of short-term behavior of earthquakes, the long-term evolution of subduction zone seismicity remains elusive due to the limited observational time span. Additional complexities arise for the seismically active subduction zones due to their inaccessibility and a complex setting. Realistic numerical modeling of subduction zone physics can help to improve our understanding of the long-term seismic cycle.

The potential to model seismic cycles with a quasi-static, visco-elasto-plastic, continuum-mechanics based numerical model typically used in geodynamics (I2ELVIS) was demonstrated in van Dinther et al. (submitted). Their work (presented at this conference as well) demonstrates that cycles of analog earthquakes can be simulated if velocity-weakening friction is included. The present study incorporates such slip-rate dependent friction, but uses a spontaneously evolving, more realistic geometrical and rock physical setup of a continental margin (Figure 1a). We thus, for the first time, fully include the three previously proposed ingredients to simulate the seismic cycle in subduction zones: a) a rate-dependent friction, b) visco-elastic mantle relaxation, and c) slow tectonic loading (Wang, 2007).

We demonstrate that seismic cycles can be realistically modeled in this complex, spontaneously evolving setup, and verify and extend previous results obtained for a static friction coefficient. Our results reveal the presence of several spontaneously formed clusters of plastic strain localizations (Figure 1c) whose activity is coupled through the thrust interface. Spatio-temporal relations between these clusters and their periodicity vary with different subduction regimes, and most likely are distinguished by thrust coupling.

Based on an event detection algorithm, we observe a heterogeneous distribution of slip within the weakest basaltic crustal layer, in which the high slip patches (asperities) are located at its thinnest, most coupled section (down to depths of 45 km). The corresponding seismogenic zone is roughly bounded by the 200 and 450 degrees Celsius isotherms. The events are governed by a Gutenberg-Richter like power law distribution if their rupture sizes are larger than the most strongly coupled segment. We also analyze surface displacements, and quantify the relative contributions of visco-elastic mantle relaxation and deep postseismic afterslip.

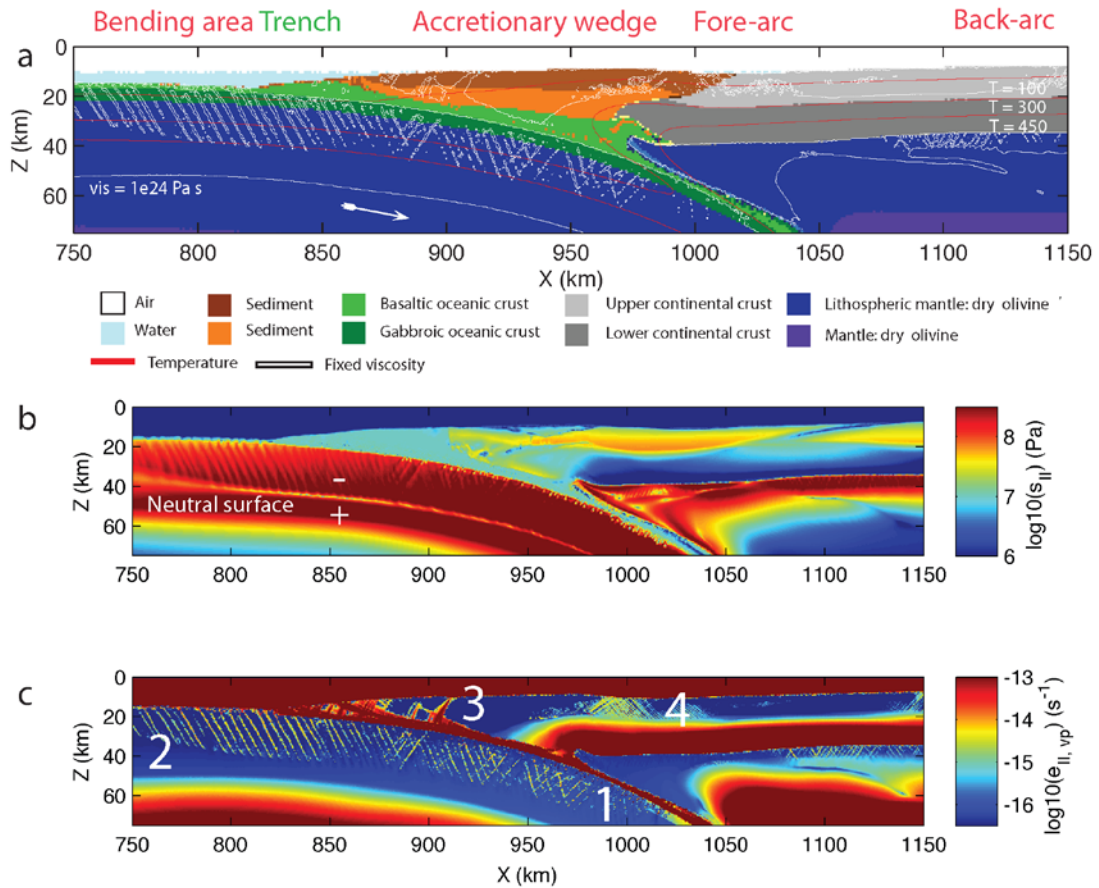


Figure 1. Subduction zone structure from a) rock composition overlain by temperature and viscosity contours showing the localizations, b) second invariant of the deviatoric stress tensor, and c) visco-plastic strain rate with four clusters of plastic strain localizations; 1) main thrust, 2) trench-ward dipping extensional bending localizations in the outer-rise, 3) faults within the accretionary wedge (including a backthrust and several splay faults that are important for tsunami generation), and 4) the overriding plate localizations within the fore- and back-arc.

References

- van Dinther, Y., Gerya, T., Dalguer, L., Corbi, F., Funicello, F., and Mai, P. (submitted). The seismic cycle at subduction thrusts: 2. Dynamic implications of geodynamic simulations benchmarked with laboratory models, *Journal of Geophysical Research*.
- Wang, K., 2007. Elastic and Viscoelastic Models of Crustal Deformation in Subduction Earthquake Cycles, *in The Seismogenic Zone of Subduction Thrust Faults* edited by T.H. Dixon and J.C. Moore.

Inferring earthquake source properties from dynamic rupture models by means of non-linear kinematic source inversion

Youbing Zhang, Seok Goo Song, Luis Angel Dalguer and John Clinton

Institute of Geophysics, ETH Zurich, youbing.zhang@sed.ethz.ch

An essential element of understanding earthquake source processes is obtaining a reliable source model via geophysical data inversion. Spontaneous dynamic rupture modeling, that incorporates conservation laws of continuum mechanics and constitutive behavior of rocks under frictional sliding, is capable of producing physically self-consistent kinematic descriptions of earthquake faulting and its associated seismic wave propagation, resulting in ground motions on the surface. Therefore, testing kinematic source inversion techniques by inverting synthetic ground motions obtained from dynamic rupture simulations is a solid step to explore the reliability of source inversion techniques to explore the physics of real earthquake source.

We use 24 models of Mw 6.5~7.0 from a large spontaneous dynamic source models database. This set of models is characterized with stochastic initial stress distribution for three classes of faulting (thrust, normal and strike slip) with buried and surface rupturing faults. The state of initial stress and frictional strength are parameterized using two different cases of normal stress: depth-dependent, and depth-independent (Dalguer and Mai, 2011). Compsyn code (Spudich and Xu, 2002) was deployed to generate forward synthetic waveforms, and an Evolutionary Algorithm was used to search for the source parameters: peak slip velocity, rupture time, rise time, and rake angle at low frequency (up to 1Hz). As a first attempt, the regularized Yoffe function is applied as a single window slip velocity function, which is a flexible slip velocity function defined by three independent parameters: the final slip, the slip duration and the duration of the positive slip acceleration, Tacc (Tinti, et al. 2005).

Our preliminary results show that we can obtain better solutions with the regularized Yoffe function, consistent with the overall properties of dynamic rupture models, and the inversion models could capture large slip patches of the dynamic models with better velocity waveform fitting than the widely used boxcar and triangular functions. However, details of slip velocity complexities resulted from the dynamic rupture models are not well captured by the inversion procedure. Besides, the model spaces could be significantly perturbed, depending on data and modeling schemes used in the inversion. In the next step, we will try to examine how the station geometries effects the source inversion result, and more geodetic data such as high-rate GNSS data will be included to source inversion research.

Initiating spontaneous rupture propagation in dynamic models with linear slip-weakening friction – a parametric study

Martin Galis¹, Christian Pelties², Jozef Kristek^{3,4}, Peter Moczo^{3,4} and P. Martin Mai¹

¹ KAUST – King Abdullah University of Science and Technology, Thuwal, Saudi Arabia

² Ludwig-Maximilians-University Munich, Munich, Germany

³ Comenius University Bratislava, Slovakia

⁴ Slovak Academy of Sciences, Bratislava, Slovakia

Numerical simulations of earthquake ruptures require artificial procedures to initiate spontaneous dynamic propagation under linear slip-weakening friction. A frequently applied technique uses a stress asperity for which effects of the forced initiation depend on size and geometry of the asperity, the spatial distribution of stress in and around the asperity, and the maximum stress-overshoot value. To properly study the physics of earthquake rupture processes, it is mandatory to understand, and then minimize, the effects of the artificial initiation on the subsequent spontaneous rupture propagation.

Numerical and analytical studies show that asperity size is an important parameter that should be chosen as small as possible. Criteria for estimating this minimum size have been proposed for 2D in-plane and anti-plane rupture modes (Andrews, 1976; Day, 1982; Campillo & Ionescu, 1997; Favreau et al., 1999; Uenishi & Rice, 2003) and in 3D (Uenishi & Rice, 2004). Using too small an initiation zone will lead to premature rupture arrest. Other studies suggest that these estimates do not provide general rules for designing simulations. Consequently, it is desirable to define guidelines to estimate the minimum size of the rupture initiation region for spontaneous dynamic rupture propagation.

The geometry or shape of the initiation region is another important parameter in 3D dynamic rupture problems. A square initiation patch has been frequently chosen (e.g. Harris et al. 2009), Uenishi & Rice (2004) and Dunham (2007) suggested an elliptical initialization zone, while Ripperger et al. (2007) tested arbitrarily shaped initiation regions. Galis et al (2010) introduced an elliptical initiation patch with the goal to mimic (1) different required sizes of asperities to generate spontaneous 2D in-plane and anti-plane ruptures; (2) the elliptical shape that 3D cracks exhibit soon after propagating spontaneously. Recently, Bizzarri (2010) tested different rupture initiation approaches, and showed that (a) forced rupture propagation with proper rupture speed leads to gradual transition from the imposed initiation to spontaneous rupture propagation; (b) an elliptical stress asperity with smooth stress is a valid alternative to the forced-rupture-propagation initiation.

Most published studies that use the stress-asperity parameterization for rupture initiation assume a stress discontinuity at the asperity edge, where the asperity stress suddenly drops to the level of the initial background stress. Two recent studies applied a smooth spatial distribution of stress in and around the asperity (Galis et al., 2010; Bizzarri, 2010). Within the stress asperity the stress is chosen larger than the yield stress. The stress overshoot (difference between prescribed stress and yield stress) inside the asperity is assumed small, usually not larger than 1% over the static stress.

Thus, the model space of possible parameterizations for rupture initiation is large, but a detailed parametric study of their effects on the resulting dynamic crack propagation has not yet been conducted. We therefore extend our previous work to define the optimal initiation parameterization that ensures spontaneous rupture propagation. We consider different sizes and shapes of the initiation region as well as different stress-overshoot values and different spatial sampling to investigate the conditions for spontaneous rupture propagation. This study does not examine in detail the stress distribution within the initiation patch as the required additional parameters greatly expand the model space; this is left for future work.

We perform extensive numerical simulations of 3D rupture propagation governed by linear slip-weakening friction. We find that the boundary delimiting regions of the spontaneous rupture propagation and premature rupture arrest appears to be determined only by the area of the initiation patch. At present, effects of larger over-shoot values seem to be of lesser importance, but simulations with a wider parameter space are needed to confirm our initial result. Additionally, we compare our numerical results with 2D and 3D analytical estimates (Andrews, 1976 a,b; Day, 1982; Campillo & Ionescu, 1997; Favreau et al., 1999; Uenishi & Rice, 2003, 2004), and conclude that the transition between propagating and non-propagating ruptures is incompatible with theoretical estimates of the critical half-lengths. We conjecture that these discrepancies are due to 3D effects and less idealized boundary/initial conditions in the numerical simulations. Our study thus guides the appropriate choice of the rupture initiation zone, to reduce unsuccessful but costly dynamic rupture simulations, and to minimize the effects of forced initiation on the subsequent spontaneous rupture propagation.

References:

- Andrews, D. J., 1976a. Rupture propagation with finite stress in antiplane strain, *J. Geophys. Res.* 81, 20
- Andrews, D. J., 1976b. Rupture velocity of plane strain shear cracks, *J. Geophys. Res.* 81, 32
- Bizzarri, A., 2010. How to Promote Earthquake Ruptures: Different Nucleation Strategies in a Dynamic Model with Slip-Weakening Friction, *Bull. Seism. Soc. Am.* 100, No. 3, doi: 10.1785/0120090179
- Campillo, M. & Ionescu, I.R., 1997. Initiation of antiplane shear instability under slip dependent friction, *J. Geophys. Res.* 102, No. B9
- Day, S.M., 1982. Three-dimensional finite difference simulation of fault dynamics: rectangular faults with fixed rupture velocity, *Bull. Seis. Soc. Am.*, Vol. 72, No. 3
- Day, S.M., Dalguer, L.A., Lapusta, N. and Liu, Y., 2005. Comparison of finite difference and boundary integral solutions to three-dimensional spontaneous rupture, *J. Geophys. Res.* 110, B12307, doi:10.1029/2005JB003813
- Dunham, E. M., 2007. Conditions governing the occurrence of supershear ruptures under slip-weakening friction, *J. Geophys. Res.* 112, no. B07302, doi 10.1029/2006JB004717.
- Favreau, P., Campillo, M. and Ionescu, I.R., 1999. Initiation of In-Plane Shear Instability under Slip-Dependent Friction, *Bull. Seism. Soc. Am.* 89, 5
- Harris, R. A., et al., 2009. The SCEC/USGS dynamic earthquake rupture code verification exercise, *Seism. Res. Lett.* 80, no. 1, doi 10.1785/gssrl.80.1.119, 119–126.
- Galis, M., Moczo, P., Kristek, J. and Kristekova, M., 2010. An adaptive smoothing algorithm in the TSN modeling of rupture propagation with the linear slip-weakening friction law, *Geophys. J. Int.* 180, doi 10.1111/j.1365-246X.2009.04427.x
- Pelties, C., de la Puente, J., Ampuero, J.-P., Brietzke, G.B. and Käser, M., 2012. Three-dimensional dynamic rupture simulation with a high-order discontinuous Galerkin method on unstructured tetrahedral meshes, *J. Geophys. Res.* 117, B02309, doi:10.1029/2011JB008857
- Ripperger, J., J.-P. Ampuero, P. M. Mai, and D. Giardini (2007), Earthquake source characteristics from dynamic rupture with constrained stochastic fault stress, *J. Geophys. Res.*, 112, B04311, doi:10.1029/2006JB004515
- Uenishi, K., Rice, J.R., 2003. Universal nucleation length for slip-weakening rupture instability under nonuniform fault loading. *J. Geophys. Res.* 108(B1), doi:10.1029/2001JB001681
- Uenishi K., Rice, J.R., 2004. Three-dimensional rupture instability of a slip-weakening fault under heterogeneous loading. *Eos Trans. AGU*, 85(46), Fall Meet Suppl, Abstract S13E-04

Scaling Properties of Critical Slip Distance Within the Framework of Rate- and State-Dependent Friction Law

Takahiro Hatano

Earthquake Research Institute, University of Tokyo

Rock friction may be regarded as an elementary ingredient of the crustal deformation processes including earthquakes and therefore it has been extensively investigated mainly by means of laboratory experiment. These results are formulated as a simple empirical law, which is now referred to as the rate- and state-dependent friction (RSF) law:

$$\mu = \mu_* + a \log V/V_* + b \log \Theta V_*/L, \quad (1)$$

$$\Theta = f(\Theta, V, L), \quad (2)$$

where μ is the friction coefficient, a , b positive nondimensional constants, V_* the reference sliding velocity, V the sliding velocity, μ_* the friction coefficient at steady-sliding state with V_* , L the length constant. The value of $a-b$ determines the stability of steady-sliding state as demonstrated by Ruina [1983]. The length constant L is regarded as the characteristic slip distance, over which the friction coefficient relaxes to its steady-state value. This length scale also scales the rupture nucleation size [Dieterich 1992], as well as the critical slip distance [Cocco and Bizzarri, 2002]. Therefore, estimate of these parameters beyond the laboratory scale is very important in earthquake physics.

Quite a few attempts have been made to estimate these parameters for natural faults by means of seismic [Ide and Takeo, 1997; Yamada et al., 2005] and geodetic inversions [Miyazaki et al., 2004; Fukuda et al., 2009]. The length constant L estimated in these observational studies is much (typically three to five orders of magnitude) larger than that in laboratory experiments, but few explanation has been given on this wide discrepancy. Therefore, complementary to such observational studies, it may be also important to deduce these parameters from a materials-science point of view; namely, to estimate these parameters theoretically under given tectonic conditions. Nevertheless, the RSF in its present form should be regarded as an empirical law because it has not been derived or deduced from the subscale ingredients. It is thus natural that no mathematical expressions are known for these important parameters. For example, conventionally, the length constant L has been interpreted as a *typical* dimension of the microscopic junctions (i.e., true contact patches), but the definition of *typical* has not been given explicitly. Therefore, L depends on a statistical averaging method over microscopic asperities and the difference is considerable as the patch size distribution is a power law [Dieterich and Kilgore, 1994, 1996].

In this talk, a full account is given of the microscopic basis of the RSF law. As the macroscopic friction force is accommodated by the microscopic asperities, the macroscopic friction law should be derived from constitutive laws of such asperities. With this procedure one can overview the micro-macro correspondence in friction and understand the physical meaning of the phenomenological parameters in a macroscopic friction law. Here we derive the RSF from constitutive laws of the microscopic asperities. Consequently, the microscopic expressions of the RSF

parameters are given. In particular, we obtain the microscopic expression for the length constant L . This expression illustrates the statistical nature of the critical slip distance. It is found that L is the *0th weighted power means* of the corresponding microscopic quantities: a linear dimension of asperities. We discuss some remarkable statistical properties of L in the context of fractal topography.

It is also found the state variable is given as the 0th weighted power mean of contact duration of each asperities. This finding leads us to the systematic derivation of evolution laws for the state variable. As a demonstration, the two major evolution laws (the aging and the slip laws) are derived and the implicit assumptions and approximations behind them are clarified.

References

- Cocco, M., and A. Bizzarri (2002), On the slip-weakening behavior of rate-and state-dependent constitutive laws, *Geophysical Research Letters*, 29, 1516.
- Dieterich, J. H., and B. D. Kilgore (1994), Direct observation of frictional contacts: New insights for state-dependent properties, *Pure and Applied Geophysics*, 143(1-3), 283–302.
- Dieterich, J. H. (1992), Earthquake nucleation on faults with rate- and state-dependent strength, *Tectonophysics*, 211(1-4), 115-134.
- Dieterich, J. H., and B. D. Kilgore (1996), Imaging surface contacts: power law contact distributions and contact stresses in quartz, calcite, glass and acrylic plastic, *Tectonophysics*, 256, 219–239.
- Fukuda, J., K. Johnson, K. Larson, and S. Miyazaki (2009), Fault friction parameters inferred from the early stages of afterslip following the 2003 Tokachi-oki earthquake, *Journal of Geophysical Research*, 114, B04412.
- Ide, S., and M. Takeo (1997), Determination of constitutive relations of fault slip based on seismic wave analysis, *J. Geophys. Res.*, 102(B12), 27379–27391.
- Miyazaki, S., P. Segall, and J. Fukuda (2004), Space time distribution of afterslip following the 2003 Tokachi-oki earthquake: Implications for variations in fault zone frictional properties, *Geophys. Res. Lett.*, 31, L06623.
- Yamada, T., J. J. Mori, S. Ide, H. Kawakata, Y. Iio, and H. Ogasawara (2005), Radiation efficiency and apparent stress of small earthquakes in a South African gold mine, *Journal of Geophysical Research*, 110, B01305.

Dynamics of Slip Fronts at Frictional Interfaces: Analysis of Slip Precursors and Rupture Velocity

Mathilde Radiguet, David S. Kammer*, Vladislav A. Yastrebov, Jean-François Molinari

Computational Solid Mechanics Laboratory (LSMS), School of Architecture, Civil and Environmental Engineering (ENAC), Ecole Polytechnique Fédérale de Lausanne (EPFL), Station 18, 1015 Lausanne, Switzerland

* Presenting author; david.kammer@epfl.ch

The rupture dynamics of earthquakes span a considerable range, from slow to super-shear ruptures. Rupture speed has a major influence on the generation of strong ground motions, yet our understanding of the mechanisms causing these variations in the rupture speed are still elusive. Laboratory friction experiments also bring evidences of the variability in rupture speed [*Rubinstein et al., 2006; Ben-David et al., 2010*]. Compared to real earthquakes, experimental ruptures occur in a controlled environment and can thus provide dense information to study the dynamics of slip events.

We use a finite element method, which allows us to access detailed information on the dynamics of friction, to simulate the propagation of slip fronts at frictional interfaces. The studied setup is similar to the experimental setup used by *Ben-David et al. [2010]*. It consists of a block of viscoelastic material in contact with a rigid body. A velocity-weakening friction law controls the friction at the interface. We apply a shear load to the block, either on the top surface of the block or on one side. In both cases, the resulting shear tractions at the interface are non-uniform. The stress distribution presents a high concentration close to the edge when the load is applied on the side. The speed of the applied shear load, which is displacement controlled, is several orders of magnitude slower than the elastic shear wave speed.

Applying a non-uniform shear loading, we observe a sequence of slip precursors, which initiate at shear levels well below the global static friction threshold. These precursors stop before propagating over the entire interface, and their lengths increase with increasing shear force (Figure 1). Our results are consistent with previous experimental observations [*Rubinstein et al., 2007*].

We also show that the velocity of the slip front varies with changing static stress state along the interface, as recently observed experimentally [*Ben-David et al., 2010*]. However, a simple static stress criterion is not enough to describe the propagation speed. We thus show that an energetic criterion, relating the slip front speed with the relative rise of the energy density at the slip tip is more appropriate [*Kammer et al., 2012*].

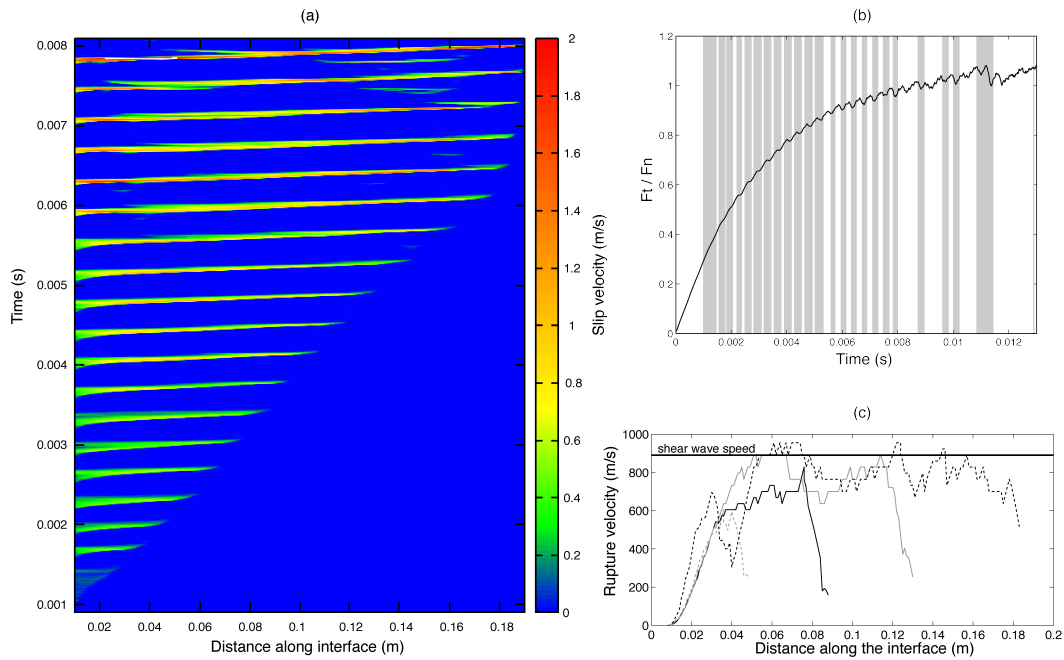


Figure 1. (a) Temporal evolution of the slip velocity along the interface, where blue indicates zero velocity and red highest velocity. The shear loading is applied at $x=0$ (left side). Precursors of increasing length can be observed. (b) Evolution of the ratio of the shear force (F_T) over the normal force (F_N) with time for the same simulation. Gray rectangles mark the occurrence of precursor events, which are associated with a decrease in F_T/F_N . (c) Rupture front velocity for precursors of different length.

References

- Ben-David, O., Cohen, G., Fineberg, J.: The dynamics of the onset of frictional slip. *Science* 330, 211 (2010)
- Kammer D.S., V. A. Yastrebov, P. Spijker, and J.-F. Molinari. On the propagation of slip fronts at frictional interfaces. *Tribol. Lett.* (2012).
- Rubinstein, S., Cohen, G., Fineberg, J.: Dynamics of precursors to frictional sliding. *Phys. Rev. Lett.* 98, 226103 (2007)
- Rubinstein, S.M., Shay, M., Cohen, G., Fineberg, J.: Crack-like processes governing the onset of frictional slip. *Int. J. Fract.* 140, 201–212 (2006)

Modeling Jumping Rupture and Rupture through Stable-Sliding Zones using Various Friction Laws

Kenny Ryan and David Oglesby

Department of Earth Sciences, University of California Riverside, USA

It is well known that fault stepovers can under some circumstances facilitate jumping rupture, and under other circumstances cause rupture termination (e.g., Harris and Day 1993; Kase and Kuge 1998; Duan and Oglesby 2006). Additionally, it is known that faults contain stable-sliding zones that may be a result of velocity-strengthening friction (e.g. Hyndman et al. 1997; Scholz 1998). However, there has been no extensive investigation into how different frictional parameterizations can affect rupture propagation over stepovers and through stable-sliding zones. In this study, we investigate rupture in such locations under 3 different frictional parameterizations, including 2 forms of rate- and state-dependent friction (Dieterich 1978, 1979; Ruina 1983): the ageing law and slip law, as well as simple slip-weakening friction. We use the dynamic finite element method (Barall 2008) to model 2D ruptures along strike-slip stepovers and dip-slip faults. Specifically, we look at the friction laws in relation to their corresponding energy budgets, since the weakening curve associated with each friction law can give a simplified view of the energy partitioning. We find that the fracture energy has a first order effect on whether or not rupture propagates over stepovers or through stable regions. In particular, ruptures with equal fracture energy densities have similar maximum jumping distances and can tunnel through similar-sized stable zones. However, the shape of the weakening curve of each friction law has a smaller, second order effect. The ageing law and slip-weakening friction have very similar slip-weakening curves, while the slip law has a relatively non-linear slip-weakening curve. It is worth noting that looking at the energy budget through time may provide some insight into this second order effect. Furthermore, we change the energy budget by adding a normal-stress-dependent state variable (of which a change in normal stress leads to a change in state variable of the opposite sign) to the rate- and state-dependent parameterizations. This frictional parameterization hinders jumping rupture across stepovers, for both compressional and extensional regimes, but has a smaller effect on the total slip and slip velocity of the dip-slip ruptures (Oglesby et al. 1998; Oglesby et al. 2000).

Propagation of 1-point and 2-point statistics from dynamic source through kinematic to ground motions

Seok Goo Song* and Luis A. Dalguer

Swiss Seismological Service (SED), ETH Zurich

* Presenting author, email: song@sed.ethz.ch

Both rupture and wave propagation affect strong ground motions on the surface. The complexity of finite faulting rupture processes may play a significant role in determining near-source ground motion characteristics, especially for large events. Numerous researchers have successfully adopted spontaneous dynamic rupture modeling for the last several decades for physics-based source and ground motion modeling although input dynamic parameters and friction laws are not well constrained in general. Furthermore it is not well defined how to characterize or quantify the heterogeneity of input dynamic parameters. We claim that at least two statistical measures, i.e., 1-point and 2-point statistics, are needed to quantify the heterogeneity of spatial data and that 1-point statistics such as mean, variance, and shape of probability density function (PDF) of dynamic input parameters at a given point on the fault, is a separate quantity that we need to consider and constrain in addition to 2-point statistics, i.e., 2-point correlation. We demonstrate that 1-point statistics of input dynamic parameters such as stress drop can significantly affect several aspects of resulting kinematic source motions and also near-source ground motions. Dynamic rupture modeling with varying 1-point statistics of input stress drop clearly shows that 1-point and 2-point statistics of both kinematic source motions on the fault and near-source ground motions on the surface are significantly and systematically affected by 1-point statistics of input parameters, in particular standard deviation of input stress drop. For example, the upper tails of 1-point probability density function (PDF) for three kinematic source parameters (slip, rupture velocity and peak slip velocity) are all pushed up with increasing standard deviation in input stress drop. The increasing standard deviation also leads to the decrease of correlation length especially for temporal kinematic source parameters such as rupture velocity and peak slip velocity. It is encouraging that cross-correlations between kinematic source parameters show consistent patterns with the findings by Song et al. (2009) and Song and Somerville (2010). For example, significant correlations are observed between these parameters and correlation maximum points are often shifted in the forward rupture direction rather than being located at zero-offset points. More interestingly these cross-correlation patterns are systematically changed with increasing standard deviation in input stress drop. The main strength of this study is to characterize the heterogeneity of earthquake source parameters and ground motion intensity parameters in the same format of 1-point and 2-point statistics. 1-point statistics is a basic form in empirical ground motion prediction equations (GMPEs). In other words, ground motion intensity parameters such as peak ground velocity (PGV) and spectral acceleration (SA) are supposed to follow the Lognormal distribution and constraining their median and sigma as a function of magnitude and distance is a great concern in empirical GMPEs. Recently earthquake engineers started looking at 2-point statistics of ground motion parameters, such as spatial correlation of epsilon. The spatial correlation of epsilon is an important factor for risk assessments of spatially distributed structures and also loss estimation for a certain region. In our modeling, the increase in standard deviation in input stress drop also increases peak ground velocity (PGV) significantly, in particular, fault normal component in the

forward rupture directivity region. We believe that quantifying the characteristics of earthquake source and ground motions in the same format of 1-point and 2-point statistics will provide us with a great opportunity to study the effect of earthquake rupture processes on near-source ground motion characteristics in a systematic sense.

Experimental investigation of frictional stick-slip, stable sliding and runaway under earthquake deformation conditions

Elena Spagnuolo¹, Stefan Nielsen¹, Giulio Di Toro^{1,2}, Marie Violay¹, Steven Smith¹ and Fabio Di Felice¹

¹ Istituto Nazionale di Geofisica e Vulcanologia, Roma, Italy

² Dipartimento di Geoscienze, Università di Padova, Padova, Italy

Earthquake nucleation on pre-existing surfaces is governed by frictional instabilities. The evolution of the system (slipping zone-wall rocks in nature and slipping zone-apparatus in the laboratory) throughout those instabilities is usually described by the rate & state friction law (Dieterich & Ruina). The rate & state friction law is based on few parameters (a, b, etc.) which can either lead to stable sliding (aseismic creep) if friction increases with increasing slip velocity (rate hardening), or to catastrophic failure (seismic slip) if friction decreases with slip velocity (rate weakening).

To investigate the transition from stable to unstable slip regimes we performed a series of experiments under either shear stress-controlled (shear stress increased stepwise on the sample) or velocity-controlled (velocity steps imposed on the sample) conditions using a rotary shear apparatus called SHIVA (Slow to High Velocity Apparatus recently installed at INGV, Rome). Experiments were performed on pre-cut ring-shaped samples (50/30 mm ext./int. diameter) of micro-gabbro and calcite marble under various (constant) normal stresses σ_n in the range of $10 < \sigma_n < 30$ MPa and slip velocities V in the range of $10^{-6} < V < 1$ m/s. Experiments were performed at room temperature and room-humidity conditions at acquisition rates up to 2.5 kHz.

Here we show that, in both rocks, a transition from stable (rate hardening) to unstable (rate weakening) regime occurs when a slip velocity threshold of few cm/s is overcome. A detailed mapping of the steady-state friction vs. the whole velocity range is provided. At $V < 3$ cm/s friction has a log-linear positive velocity dependence (in agreement with the rate & state friction law for positive a-b values); as velocity increases, friction gradually evolves towards a negative dependence and eventually it merges into a $1 / V^{0.5}$ dependence for $V > 0.1$ m/s.

The experimental configuration used here (shear stress-controlled) allows, like in nature, the spontaneous nucleation of frictional instabilities and to identify the deformation conditions responsible for earthquake nucleation. The extrapolation to natural conditions of the above experimental results might also explain the propagation of seismic ruptures in faults patches characterized by conditionally stable regimes (e.g., shallow portions of tsunamigenic megathrusts faults).

Frictional behavior of simulated anhydrite fault gouge and the effects of supercritical CO₂

A. Pluymakers, J. Samuelson and C. Spiers

HPT Laboratory, Faculty of Geosciences, Utrecht University, Utrecht, Netherlands

An attractive option for mitigating climate change is to store anthropogenic CO₂ in the Earth's subsurface, particularly in depleted oil and gas reservoirs. To ensure safe storage and avoid potential leakage of CO₂, rigorous testing of the frictional properties of faults within and adjacent to potential reservoirs is necessary to determine the conditions under which such faults might be reactivated, and if such reactivation has the potential to be seismic.

Anhydrite is a common caprock to many potential CO₂ storage sites worldwide as well as in the Netherlands. We specifically will investigate the frictional properties of Zechstein anhydrite, obtained from the bottom of the Permian Zechstein Formation which is caprock to many gas reservoirs in the Netherlands and North Sea. Intact core material was powdered and sieved at 50µm to simulate fault gouge. Experiments will be conducted using a direct shear configuration in a triaxial pressure vessel on a 1mm thick gouge layer, over a range of temperatures (80 - 150°C) and sliding velocities (0.2-10µms⁻¹) and at a fixed effective normal stress ($\sigma_{n,eff}=25\text{MPa}$). Pore fluid conditions also are varied, with experiments being run dry, saturated with DI water or supercritical CO₂, or with CO₂ saturated DI water (in the case of pressurized pore fluid: $P_f=15\text{MPa}$).

First results of direct shear experiments on dry anhydrite gouge without CO₂ indicate a friction coefficient of approximately 0.64; results further show a transition from velocity strengthening frictional behavior at temperatures of 80 and 100°C to stick-slip and/or velocity weakening behavior at 120 and 150°C. In contrast, a first wet experiment at 120°C indicates that the presence of water leads to velocity strengthening. One possible implication for a transition from velocity strengthening in wet anhydrite gouge to weakening in dry gouge is that desiccation of fault gouge by migrating CO₂ could potentially result in earthquake nucleation in faults rich in anhydrite gouge. Our continuing investigation will scrutinize the capacity of CO₂ to desiccate anhydrite fault gouge and determine if such desiccation can lead to velocity weakening behavior, as occurs in dry gouge.

Gutenberg-Richter law, giant earthquakes and slow events in laboratory experiment

Tetsuo Yamaguchi

Department of Mechanical Engineering, Kyushu University

We report on experimental studies of spatio-temporally heterogeneous stick-slip motions in the sliding friction between a hard poly-methyl methacrylate (PMMA, plexiglass) block and a soft poly-dimethyl siloxane (PDMS, silicone) gel plate. [1] In our experiment, the statistics of the slip size shows the Gutenberg-Richter law as well as the peak at a size corresponding to giant slip events, as shown in the Figure 1(a). We also prepared gels having more viscous characters, and studied the size-duration relation. It obeys $T \propto M_0^{1/2}$ (Figure 1b), which is similar to that reported by Ide. [2] By applying the PIV technique to visualize 2D distributions of the particle velocity during slip events and of the shear stress during stick-slip cycles, we succeeded in visualizing the rupture process of slip events and also heterogeneous accumulation of the stress fields towards a large slip event. In the presentation, we will report more details of our results.

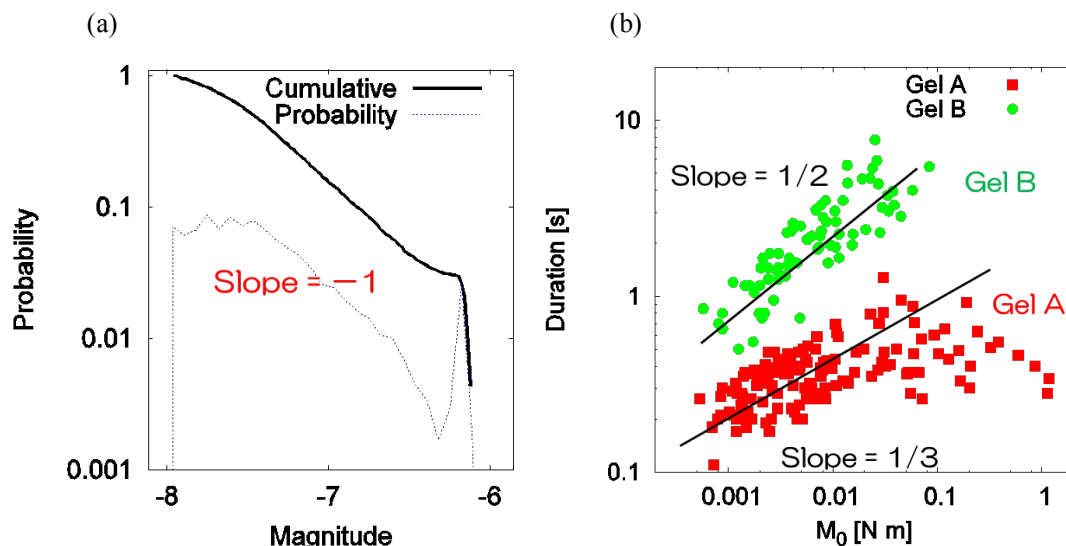


Figure 1. (a) Event size distributions (cumulative and probability distributions), and (b) Size – Duration relation in our experiments ($V = 10 \mu/s$).

References

- [1] T. Yamaguchi, M. Morishita, M. Doi, T. Hori, H. Sakaguchi, J. P. Ampuero, Gutenberg-Richter law in sliding friction of gels, *J. Geophys. Res. Solid Earth*, **116**, B12306 (2011)
- [2] S. Ide, A Brownian walk model for slow earthquakes, *Geophysical Research Letters*, **35**, L17301 (2008)

Full waveform analysis and micromechanics of source processes at nanoseismic scale

Gilles Hillel Wust-Bloch¹ and Michael Tsesarsky²

¹ Department of Geophysics, Tel Aviv University, Israel

² Department of Structural Engineering & Department of Geological and Environmental Sciences, Ben-Gurion University, Israel

By lowering detection threshold within ground noise, getting unusually close (10^2 - 10^{-1} m) to source processes and applying advanced sonogram analysis, nanoseismic monitoring (NM) links rock mechanics lab experiments with the observation of very low-magnitude ($-1.9 < M_L < 0.0$) local seismicity or geomaterials failure ($-4.3 < M_L < 0.0$). NM was used to determine the load-time function and the spatio-temporal evolution of pre-failure waveforms. Unreinforced concrete beams and limestone plates undergoing four-point bending tests were used to examine pre-failure microcracking under constant loading. Repeated tests show that constant-force loading triggers a wide range of impulsive signals whose frequency and rate patterns evolve until complete material failure. A high sampling rate (2000 Hz) permits the discrimination of four different types of pre-failure nano-events: quakes, spikes, puffs and tremor. It was observed that within the 1-200 Hz window, signal energy concentration is not uniform and that its time distribution is not random. Although the imposed stress differs from that of natural earthquakes, the frequency-time relationship of these sub-signals relates to standard micromechanics processes reported in material testing. Scaling tests between these lab observations and signals generated by very low-magnitude local seismicity and structural health monitoring of geomaterials, which have been recorded in situ by the same platforms, show stability over several magnitude orders. With adequate scaling, the link we have been able to establish between controlled material failure and naturally generated seismicity will help understanding earthquake nucleation processes.

Fault zone structure of the central Alpine Fault revealed during the first phase of the Deep Fault Drilling Project (DFDP-1)

J. Townend¹, R. Sutherland², V.G. Toy³, S.C. Cox⁴ and C.J. Boulton⁵

¹ School of Geography, Environment, and Earth Sciences, Victoria University of Wellington, PO Box 600, Wellington 6140, New Zealand (john.townend@vuw.ac.nz)

² GNS Science, PO Box 30368, Lower Hutt 5040, New Zealand

³ Department of Geology, University of Otago, PO Box 56, Dunedin 9054, New Zealand

⁴ GNS Science, Private Bag 1930, Dunedin 9054, New Zealand

⁵ Department of Geological Sciences, University of Canterbury, Private Bag 4800, Christchurch 8140, New Zealand

Understanding what conditions prevail within the interiors of active faults is crucial for elucidating the mechanisms governing long-term fault evolution and, in particular, the earthquake-rupture processes that are of vital interest to society. The Alpine Fault is a mature, transpressive plate-bounding structure that has accommodated >460 km of dextral offset since 24 Ma and which has a late Quaternary of c. 26 mm/yr. Paleoseismic observations indicate that the Alpine Fault produces large earthquakes ($M_w \sim 8$) every 200–400 years and that it last slipped in 1717 AD. The Deep Fault Drilling Project (DFDP) is focused on determining the conditions under which faults evolve and generate earthquakes, via a sequence of drilling operations and long-term monitoring permitting analysis of ambient conditions and fault rock lithologies adjacent to the central Alpine Fault. In contrast to several fault zone drilling experiments undertaken following large earthquakes, DFDP addresses conditions in a fault zone prior to an anticipated large earthquake¹.

In early 2011, the first phase of DFDP drilling (DFDP-1) was successfully completed with the construction and instrumentation of two shallow boreholes intersecting the central Alpine Fault at Gaunt Creek². Core analysis and wireline logging data reveal the presence of a mineralogically and hydrologically distinct 15–20 m-thick “alteration zone” in the hanging wall formed by fluid-rock interaction and mineralization. This alteration zone is formed of cemented low-permeability fractured ultramylonite and cataclasite, and obscures the boundary between the damage zone and fault core. The fault core contains a <0.5 m-thick principal slip zone identified on the basis of core analysis and wireline logging data, near the base of a 2 m-thick layer of gouge and ultracataclasite. Hydraulic observations made during drilling, piezometer measurements made over 12 months as fluid pressures equilibrated, and laboratory data all yield consistent estimates of the fault core’s permeability of c. 10^{-23} to 10^{-21} m². In contrast, the permeability of the distal damage zone determined from slug tests is approximately 10^{-14} m²; in other words, a six order-of-magnitude permeability difference exists across the alteration zone.

The extremely low permeability and meter-scale width of the fault core are likely to play a significant role in governing earthquake rupture on the central Alpine Fault. In particular, the permeability of $<10^{-21}$ m² we infer for the 2 m-thick fault core enclosing the PSZ suggests that the fault may undergo extreme thermal pressurization behavior in response to small amounts (possibly submillimeter) of slip at low slip rates ($\ll 1$ mm/s) well before the onset of seismic radiation^{3,4}.

A second observation made during DFDP-1 that may have an important bearing on earthquake rupture processes is the macroscopic (10–100 m-scale) asymmetry of the fault revealed by sonic velocity measurements and core analysis. The P-wave velocity of the hanging wall is higher than that of the footwall by approximately 0.5 km/s. The significance of this difference in fault rock compliance on either side of the dipping fault zone for coseismic changes in fault strength or ground motion distributions⁵, or for preferred rupture propagation directions^{6,7}, remains to be examined. Further characterizing the structural and hydraulic architecture of the fault zone will improve our understanding of the relationship between in situ conditions, earthquake rupture processes, and the specific hazards posed to South Island communities by future Alpine Fault earthquakes.

References

- ¹Townend, J., et al., 2009, *Sci. Drilling.*, doi: 10.2204/iodp.sd.8.12.2009
²Sutherland, R., et al., 2012, submitted
³Segall, P., & Rice, J., 2006, *J. Geophys. Res.*, doi: 10.1029/2005jb004129
⁴Schmitt, D., et al., 2011, *J. Geophys. Res.*, doi: 10.1029/2010jb008035
⁵Ma & Beroza, 2008, *Bull. Seismol. Soc. Am.*, doi: 10.1785/0120070201
⁶Dor, O., et al., 2006, *Earth Planet. Sci. Lett.*, doi: 10.1016/j.epsl.2006.03.034
⁷Mitchell, T.M., et al., 2011, *Earth Planet. Sci. Lett.*, doi: 10.1016/j.epsl.2011.04.023

What can microstructural observations of natural faults tell us about dissipative mechanisms that operated at the earthquake source?

V.G. Toy¹, C.J. Boulton¹, N.C. Barth¹, B. Carpenter², IODP Expedition 343 Scientists and IODP-MI³, D. Goldsby⁴, A. Kopf⁵, T. Mitchell², C. Marone⁶, R. Sutherland⁷, J. Townend⁸ and T. Tullis⁴

¹ Department of Geology, University of Otago, Dunedin, New Zealand. virginia.toy@otago.ac.nz

² Istituto Nazionale di Geofisica e Vulcanologia, Rome, Italy

³ Multiple; c/- Centre for Deep Earth Exploration (CEDX), JAMSTEC, Yokohama, Japan.

⁴ Department of Geological Sciences, Brown University, Providence, RI, USA.

⁵ MARUM, Universität Bremen, Germany.

⁶ Geoscience, The Pennsylvania State University, State College, PA, USA.

⁷ GNS Science, Lower Hutt, New Zealand.

⁸ School of Geography, Environment, and Earth Sciences, Victoria University, Wellington, New Zealand.

Some proportion of the elastic strain energy stored in the crust is dissipated on and around fault planes both co- and aseismically, rather than converted to radiated energy. We have examined outcrop to microscale fabrics of active natural fault rocks from principal slip zones (psz; defined as the zones that accommodated most shear displacement) in various tectonic settings, and obtained laboratory data about frictional behaviour and microstructural evolution. Here we consider how observed microfabrics broadly reflect the dissipative processes that operated within these psz.

1. New Zealand's Alpine Fault is capable of generating $M_w \sim 8$ earthquakes with a return period of 200-300 years and is near the end of a major earthquake cycle. Continuous core of the fault psz recently recovered from its locked central section demonstrates most coseismic slip was localised to a cm-thick layer of highly comminuted ultracataclasite derived from a quartzofeldspathic protolith. This layer contains recycled gouge clasts illustrating it remains the locus of slip through multiple earthquakes, despite displaying velocity-strengthening behaviour in laboratory tests¹. It is surrounded by more permeable but cemented cataclasites into which psz gouge has been injected, suggesting thermal pressurisation occurred. The main dissipative mechanisms in this environment are inferred to be particle fragmentation and frictional heating resulting in thermal pressurisation of free fluids, both accompanying seismic slip. However, we recognise fragmentation probably ceased with the advent of thermal pressurisation, and that it is generally unlikely a significant proportion of available elastic strain energy is dissipated on-fault by these mechanisms.

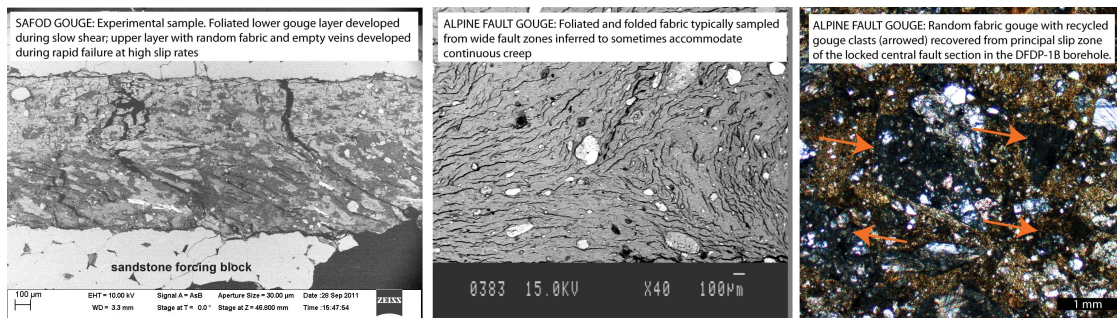
2. Elsewhere, the Alpine Fault's psz is metres thick and composed of a gouge of foliated clay minerals (including Mg-rich smectites). This difference in structural style reflects protolith mineralogy since in this region the fault cuts a mixture of quartzofeldspathic and ultramafic rocks². Foliated and folded packages of gouge are common and microstructural evidence strongly suggests solution-transfer is an important deformation mechanism in these gouges, which are frictionally weak and velocity strengthening in experiments. Some proportion of energy dissipation on this part of the fault therefore occurs aseismically, although there is also evidence for some coseismic energy release³.

3. The microfabric of natural fault gouge from the creeping segment of the San Andreas Fault, ('SDZ' sample from the SAFOD borehole) comprises packages of foliated and folded clay minerals (including Mg-rich smectites). Others have inferred

this microstructure is characteristic of material that deforms by continuous creep⁴. This is consistent with our experimental observations at intermediate slip velocities, where disaggregated gouge re-develops a microstructure comprising foliated and folded packages of clay minerals when shear is distributed throughout the gouge layer. At faster experimental slip rates, localised through-going slip surfaces and hydrofractures form, indicating increasing importance of thermal pressurisation and rock fragmentation as coseismic dissipative mechanisms.

4. The Tohoku plate boundary interface subduction thrust, which we recently sampled during IODP Expedition 343, also comprises >1m thickness of foliated, sheared clay with a variably intense scaly fabric and occasional microfolds. We infer this material would have accommodated continuous creep under strain hardening conditions. Embedded within it are rare, through going, zero thickness planar surfaces along which we infer strain localised to accommodate rapid loading (possibly including earthquake-rate slip). Elsewhere in the core, we observed structures more likely to result from recent coseismic slip. These are localised (mm-thickness) zones of ultracomminuted material surrounded by fractured breccias. In these zones both rock fragmentation and frictional heating were important on-fault dissipative processes.

To summarise, natural faults display a range of microfibrils within psz that may be localised or distributed through metre thicknesses. Creeping faults generate distributed zones of foliated and folded material, whereas faults that slipped seismically generate more localised zones of comminuted material, and dissipate some energy coseismically via fragmentation. Finally, there is evidence frictional heat was generated coseismically on most of the localised faults, but we have not observed pseudotachyrites so infer this heat is dissipated into fluids or by mineral decomposition reactions.



References

1. Boulton, C.J., Carpenter, B.M., Toy, V.G., Marone, C., 2012. Physical properties of surface-outcrop cataclastic fault rocks, Alpine Fault, New Zealand. *Geochemistry, Geophysics, Geosystems* 13, Q01018, doi: 10.1029/2011GC003872.
2. Boulton, C., Barth, N., Carpenter, B., Toy, V.G., 2011. Significant along-strike variations in fault gouge thickness, friction coefficient and mineralogy, Alpine Fault, New Zealand. Abstract T41C-04 presented at 2011 Fall Meeting, AGU, San Francisco, Calif.
3. Berryman, K., Cochran, U., Clark, K., Biasi, G., Langridge, R., and Villamor, P., submitted. Great earthquakes occur regularly on an isolated plate boundary fault? *For Science*, Jan 2012.
4. Holdsworth, R.E., van Diggelen, E.W.E., Spiers, C.J., de Bresser, J.H.P., Walker, R.J., Bowen, L. 2011. Fault rocks from the SAFOD core samples: Implications for weakening at shallow depths along the San Andreas Fault, California. *Journal of Structural Geology* 33 (2), 132-144.

Observations of isotropic moment tensor components and scaling with seismic moment in TauTona Mine, South Africa

Deborah Kane¹, Margaret Boettcher¹, Art McGarr² and Joe Fletcher²

¹ University of New Hampshire

² US Geological Survey

Earthquakes are well monitored in TauTona Mine, South Africa, where underground near-source stations record smaller events and higher frequency energy than can generally be observed with surface recordings. This unique environment hosts earthquakes spanning a range of magnitudes ($-4 < M_w < 4$) and shows evidence for a variety of source mechanism types, including double-couple tectonic-like sources at all magnitudes observed (Boettcher et al., 2009). Extensive ground motion recording and event cataloging provides a detailed dataset for observing source scaling over this range. We use data collected between 2004 and 2009 from the in-mine array (1-6 kHz), the Natural Earthquake Laboratory in South African Mines (NELSAM) project (6-12 kHz), and a short-term PASSCAL experiment (200 Hz) to study source mechanism variability via moment tensor solutions over the complete magnitude range.

Our previous analysis of 43 mining-induced earthquakes has suggested that the contribution of isotropic components to the moment tensor solutions is dependent on magnitude (Kane et al., 2012). Specifically, small ($M_w < 0$) earthquakes exhibit a greater degree of explosive isotropic components whereas larger ($M_w > 1.5$) earthquakes occur with a greater degree of implosive isotropic components (Figure 1). A possible model to explain these observations relates the explosive small events to cracks forming in manmade structures, and implosive larger events to collapse of mining excavations adjacent to rupture zones.

Here, we expand our dataset of moment tensor solutions obtained by measuring peak amplitudes of picked phases (e.g., McGarr 1992) to offer further insight to this evidence for scaling. We also investigate two other methods for obtaining moment tensor solutions. First, we apply a full waveform inversion using the same overall method as for the individual phase amplitudes; this provides more tightly constrained results by incorporating many more data points and by minimizing errors due to mis-picked phases. Second, we compute time-dependent moment tensors following the methods described by Sileny et al (1992). This time-dependent approach allows detailed analysis of the rupture process and can resolve evolution of rupture from one type of source (e.g., shear crack) into another type (e.g., implosive source). These observations provide evidence for physical processes such as coseismic collapse of the mining stope.

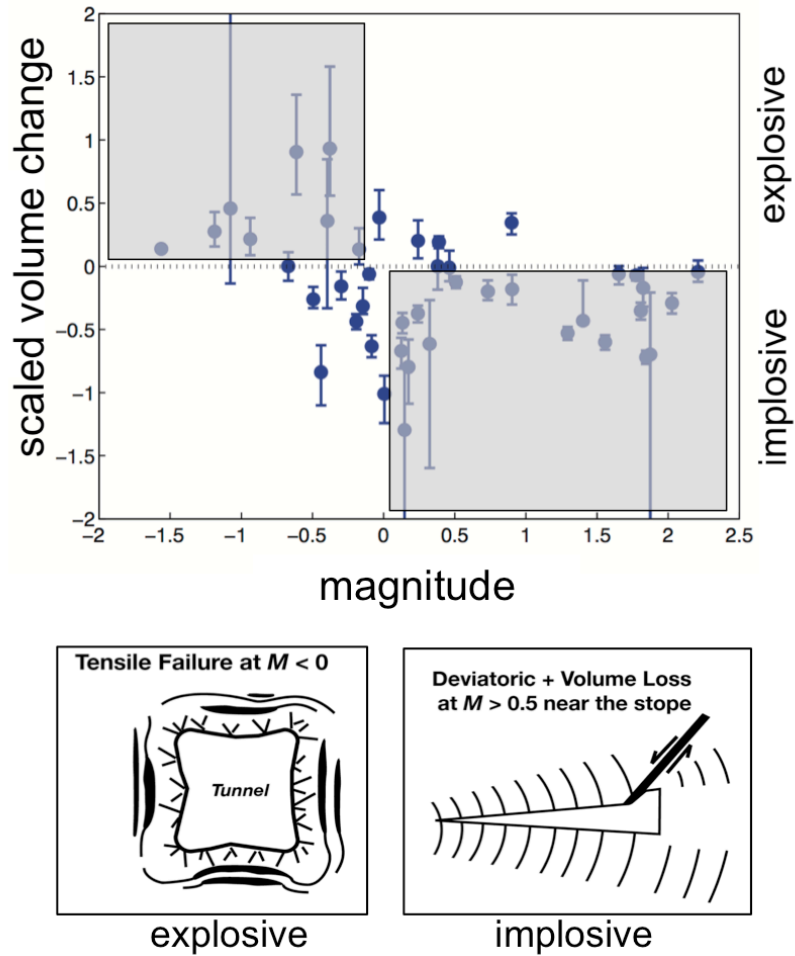


Figure 1. Preliminary results showing trend of isotropic component of moment tensor solution with event magnitude (top). Gray boxes highlight explosive and implosive results, and sketches (bottom) illustrate simple model explanations for the observed trend.

References

- Boettcher, M.S., A. McGarr, and M. Johnston, Extension of Gutenberg-Richter distribution to M_w -1.3, no lower limit in sight, *Geophys. Res. Lett.*, 36, L10307, doi:10.1029/2009GL038080, 2009.
- Kane, D., M. Boettcher, A. McGarr, J. Fletcher, M. Johnston, and Z. Reches, Effect of earthquake location and magnitude on moment tensors in a South African gold mine, *Seism. Res. Lett.*, Vol. 83, No. 2, oral presentation at 2012 SSA Meeting.
- McGarr, A., Moment tensors of ten Witwatersrand mine tremors, *Pure Appl. Geophys.*, 139, 781–800, 1992.
- Sileny, J., G.F. Panza, and P. Campus, Waveform inversion for point source moment tensor retrieval with variable hypocentral depth and structural model, *Geophys. J. Int.*, 109, 259-274, 1992.

Quasi-static and dynamic deformations of the rocks associated with mining induced seismic events around deep level mining in South Africa

A. Milev^{1,4}, R. Durrheim^{1,3,4}, M. Nakatani^{1,7}, Y. Yabe^{1,6,7}, H. Ogasawara^{1,2}, M. Naoi^{1,5} and SATREPS¹

¹ JST-JICA, Science and Technology Research Partnership for Sustainable Development (SATREPS), Japan

² Ritsumeikan University, Japan

³ University of Witwatersrand (WITS), South Africa

⁴ Council for Scientific and Industrial Research (CSIR), South Africa

⁵ ERI, Tokyo University, Japan; ⁶Tohoku University, Japan

Two underground sites in a deep level gold mine in South Africa were instrumented by the Council for Scientific and Industrial Research (CSIR) with tilt meters and seismic monitors. One of the sites was also instrumented by Japanese-German Underground Acoustic emission Research in South Africa (JAGUARS) with a small network, approx. 40 m span, of eight Acoustic Emission (AE) sensors.

The rate of tilt, defined as quasi-static deformations, and the seismic ground motion, defined as dynamic deformations, were analysed in order to understand the rock mass behavior around deep level mining. In addition the high frequency AE events recorded at hypocentral distances of about 50m were analysed. This was the first implementation of high frequency AE events at such a great depth (3300m below the surface).

A good correspondence between the dynamic and quasi-static deformations was found. The rate of coseismic and aseismic tilt, as well as seismicity recorded by the mine seismic network, are approximately constant until the daily blasting time, which takes place from about 19:30 until shortly before 21:00. During the blasting time and the subsequent seismic events the coseismic and aseismic tilt shows a rapid increase indicated by a rapid change of the tilt during the seismic event. Much of the quasi-static deformation, however, occurs independently of the seismic events and was described as 'slow' or aseismic events.

During the monitoring period a seismic event with M_w 2.2 occurred in the vicinity of the instrumented site. This event was recorded by both the CSIR integrated monitoring system and JAGUARS acoustic emission network. The tilt changes associated with this event showed a well pronounced after-tilt. Most probably this is a result of the aftershock sequence following the event. The aftershock activities were also well recorded by the acoustic emission and the mine seismic networks. More than 21,000 AE aftershocks were located in the first 150 hours after the main event. The mine seismic network which has a resolution of $M-0.5$ in this area detected only 9 aftershocks. Using the distribution of the AE events the position of the fault in the source area was successfully delineated. The distribution of the AE events following the main shock was related to after tilt in order to quantify post slip behavior of the source. There was no evidence found for coseismic expansion of the source after the main slip.

An attempt to associate the different type of deformations with the various fracture regions and geological structures around the stopes was carried out. A model, was introduced in which the coseismic deformations are associated with the stress regime outside the stope fracture envelope and very often located on existing

geological structures, while the aseismic deformations are associated with mobilization of fractures and stress relaxation within the fracture envelope.

Further research in this direction is currently in progress under the Joint South African Japanese program, SATREPS. This involves long term underground monitoring using a wide variety of instruments such as tilt, closure and strain meters, a highly sensitive AE fracture monitoring system, as well as strong ground motion monitors.

Magnitude-frequency distributions of AEs associated with the mining front and pre-existing faults –cases from SATREPS array operating in a South African gold mine

Makoto Naoi¹, Masao Nakatani¹, Joachim Philipp², Shigeki Horiuchi³, Kenshiro Otsuki⁴, Thabang Kgarume⁵, Gilbert Morema⁶, Sifiso Khambule⁷, Thabang Masakale⁷, Koji Miyakawa¹, Atsushi Watanabe¹, Hirokazu Moriya⁴, Osamu Murakami⁸, Yasuo Yabe⁴, Hironori Kawakata⁸, Nana Yoshimitsu⁸, Tony Ward⁸ and Hiroshi Ogasawara⁸

¹ Univ. of Tokyo

² GMuG

³ Home seismometer corp.

⁴ Tohoku univ.

⁵ CSIR

⁶ Seismogen

⁷ OHMS

⁸ Ritsumeikan univ.

We recently established an extensive 3D AE (Acoustic Emission) monitoring array at 1 km depth in the Ezulwini mine in South Africa, which consists of 24 AE sensors (covering 1-40 kHz) and 6 tri-axial accelerometers (three of them have a flat frequency response up to 25 kHz, others are up to 10 kHz). The extent of the array is about 100m x 50m x 30m. Waveforms are recorded at 500 kS/s over a duration of ~65ms for each trigger. We picked P- and S-wave arrivals using an automated algorithm (Horiuchi et al. 2011, JpGU). From approximately net 44 days observation (8 August, 2011 ~ 10 October, 2011), we obtained high-quality hypocenters for approx. 370,000 events mostly located within 200 m from the array. Moment magnitude (Mw) could be determined for about 98% of them. The smallest Mw was -5.3.

More than 80% of the AEs were located close to the mining front. In addition, several isolated planar AE clusters were found in places other than mining front. Almost all AEs occurred in these two types of clusters. Eight major planar clusters, which have 20~100 m extent and consist of 300~10,000 AEs, were identified in places other than mining front. Positions and attitudes of five of them were consistent with geological faults known by our/mine's survey. We presume the other three are also associated with pre-existing structures.

Five of the eight major planar clusters were distant (> 40 m) from the mining front. In and around these clusters, we could confirm that no events greater than Mw 0.5 occurred since the mine's routine monitoring (detectability down to Mw -1.5) started in April, 2009. Therefore, we can deny the possibility that the present AE activities of these 5 clusters are aftershocks of a large event with the rupture area comparable or greater than the AE cluster size. For the analyzed period of approx. 2 months, seismicity of these clusters were remarkably constant, which may suggest the loading rate by mining was fairly constant.

We investigated the magnitude-frequency distributions of AEs in the eight planar clusters and also AEs close to the mining front. During non-working time (Sunday and 17:00-9:00 in weekday), the size distribution of AEs close to the mining front followed the Gutenberg-Richter law (hereinafter referred to as "GR law") with $b \sim 1.3$ down to Mw -3.9. This result is consistent with a study of Kwiatek et al. [2010] in the Mponeng mine in South Africa, who reported that the size distribution of AEs

close to mining front in 11 hours following blasts obeyed the GR law ($b \sim 1.17$) down to $M_w -3.5$. AEs belonging to the 8 planar clusters also basically followed the GR law down to $M_w -4.2$ with b -values varying between $1.27 \sim 1.79$ from cluster to cluster, though depletion of larger events might be suggested. Kwiatek et al. [2010] has shown the validity of the GR law down to $M_w -4.4$ for aftershocks of an M2 event in the Mponeng mine, which clusters also showed a planar distribution as in the present case. However, note that the present case is concerned about steady activity, whereas the M2 aftershock sequence studied by Kwiatek et al. [2010] largely consisted of on-fault events [Naoi et al. 2011] that are expected to be influenced by large stress disturbance introduced by complex main fault rupture [Helmstetter and Shaw, 2006].

Throughout the data presently analyzed, lower limit of magnitude range (M_c) for the GR law to hold was found to increase linearly with the distance from our AE array (e.g., $M_c \sim -4.2$ at 30m from the center of our array; $M_c \sim -3$ at 100m). This indicates that these M_c reflect detection limit of the array. Hence, we conclude that the self-similar statistics of the GR law has been extended down to $M_w -4.2$ for steady activity associated with geological faults, which may be regarded as a very good analogue of natural tectonic seismicity.

Second degree moments: a tool for fault plane detection

Petra Adamová¹, Jan Štílený¹ and Ernest Lötter²

¹ Institute of Geophysics of the Academy of the Sciences, Czech Republic, Prague

² Institute of Mine Seismology, Australia, Hobart

The standard moment tensor does not contain information about the tempo-spatial structure of the source, and cannot be related to finite-extent source parameters like fault geometry, average rupture velocity along the fault or duration of the source process. The information on geometry of the focus and simplified insight into the dynamics of the source process are contained in quantities called second degree moments. We can retrieve them by inverting records using frequencies beyond the low-frequency plateau. There are several approaches describing higher degree moments. We follow the formalism developed by Doornbos (1982) for its clarity and straightforward relevance to simple fault models. Despite the method was originated in 80ies, second degree moments were applied in seismology rarely till now, and exclusively to crustal earthquakes: from small to strong events (e.g. McGuire et al. 2001, 2002 and 2004). Never have they been applied to local induced events in local applications like mining tremors. The major benefit for the practice is foreseen in the capability of the approach to remove the ambiguity of the two nodal planes within the double-couple part of the traditional moment tensor solution, i.e. to distinguish the genuine fault plane from the auxiliary one. Compared to earthquake seismology, monitoring in mines underground frequently has an additional advantage, namely that stations are often not constrained to a single level - the Earth surface, and are situated both above and below the focus of the event. This improves the quality of the focal sphere coverage, which is of crucial importance for reconstruction of the second degree moments. To demonstrate the application of the method, we selected five local events from the deep-level gold mine Ridgeway in East Australia. This data has been processed on a routine basis for the standard moment tensor by the Institute of Mine Seismology (IMS). We can advantageously compare their spectral amplitude inversion with our solutions from the full waveform inversion (see Fig. 1). Second degree moments cannot be compared with any previous study because they haven't been evaluated yet. We studied resolution of these parameters using jack-knife test. Fault-plane solutions are very compatible with the known local geology. Moreover, the orientation of source ellipsoids (including errors obtained from jack-knife test) – second degree moments which describe the spatial extent of the focus – can be well correlated with the existing fault planes. It clearly demonstrates the anticipated benefit of the approach in detecting the fault from the two nodal planes of the traditional beachball (see Fig. 2).

References

- Doornbos, D. J. (1982). Seismic moment tensors and kinematic source parameters, *Geophys. J. R. Astr. Soc.* 69, 235–251.
- McGuire J. J., Zhao L., Jordan T.H. (2001). Teleseismic inversion for the second-degree moments of earthquake space-time distribution, *Geophys. J. Int.* 145, 661–678.
- McGuire, J. J., Zhao L., Jordan T.H. (2002). Predominance of unilateral rupture for a global catalog of large earthquakes, *Bull. Seismol. Soc. Am.* 92, no. 8, 3308–3317.
- McGuire, J. J. (2004). Estimating finite source properties of small earthquake ruptures, *Bull. Seismol Soc. Am.* 94, no. 2, 377-393.

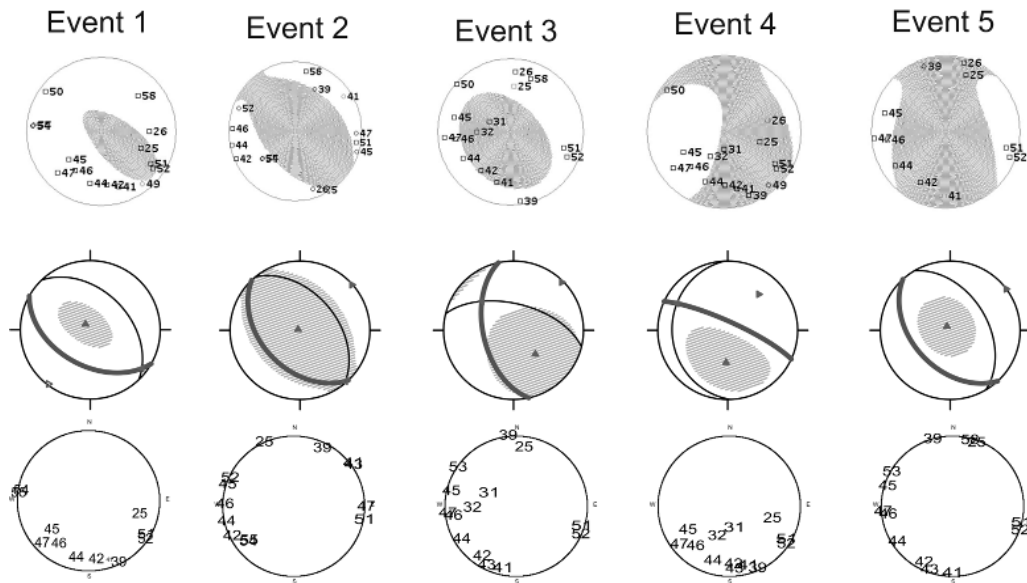


Figure 1. Standard MTs for the 5 mining events investigated. Top: IMS fault-plane solutions from spectral amplitudes together with the stations providing the data; compressions - grey. Middle: fault-plane solutions obtained in this study. Solid lines represent nodal lines. The plane determined as the fault from the SDM solution is the thick line. Bottom: station coverage used in this study.

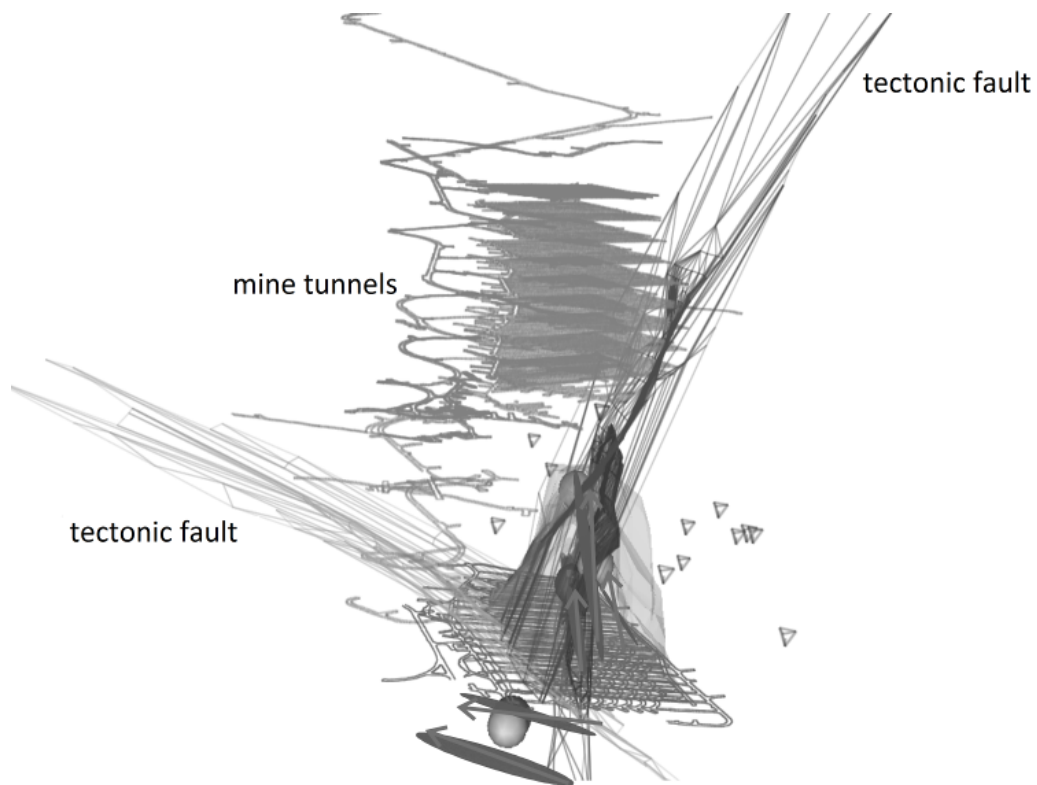


Figure 2. Location of all events with source ellipsoids in view looking east. Geological faults in Ridgeway mine are plotted in the same figure.

Samples of micro-earthquake mechanisms induced by fluid injection at the Hot Dry Rock site Soultz (Alsace) in 2003 using alternative source models

Zuzana Jechumtálová and Jan Šílený

Institute of Geophysics, Academy of Sciences of the Czech Republic, Prague, Czech Republic

The geothermal reservoir at Soultz-sous-Forêts is a valuable natural laboratory for understanding the mechanism of the micro-earthquakes generated during stimulation and circulation tests. There is an ongoing effort towards detecting of the type of fracturing of the rock massif through the retrieval of the micro-earthquake mechanisms, however it remains rather ambiguous yet. Recent studies indicate prevalingly shear slip but rarely also a non-shear pattern is observed.

Moment tensor – used today as a universal tool for description of the mechanism – captures general balanced dipole sources. However, its generality may sometimes be inconvenient, as it intrinsically includes also non-physical sources. Advantageously, the MT inversion is linear, allowing a fast retrieval of the six independent components. Unluckily, in the case of noisy or insufficient data they may represent spurious non-double-couple components. Therefore, simultaneously we also invert for an alternative source model, which can simulate a tensile crack, optionally combined with a shear slip. The model was originally designed by Dufumier & Rivera (1997) and revisited and theoretically explored by Vavryčuk (2001, 2011). This type of source avoids non-physical combinations of the moment tensor components a priori. A slip along the fault with an off-plane slip component can be described by four angles pointing the fault plane normal and non-orthogonal slip vector, and by a magnitude. It results in five model parameters: strike, dip, rake, off-plane angle and a magnitude. We call it a simple shear-tensile/implosion (STI) source model. When we decrease the number of model parameters from six to five, inversion is robust even for less input parameters, but unfortunately becomes non-linear, which largely slows down the inversion. To estimate reliability of inverted STI parameters, we used the model space mapping in the course of the inversion and displayed the ‘confidence zones’ – areas where the normalized residual sum (NRMS) remains below a certain percentage of the best value.

From the bulk of the seismicity recorded during stimulation in 2003, we concentrated on the first phase of the injection when only a single borehole GPK3 in the site was stimulated. We processed thirteen micro-earthquakes with magnitudes bigger than 1.4 and not processed previously by Horálek et al. (2010). The records had low signal-to-noise ratio and were not detected by all 15 stations of Soultz surface network. It means that MTs need not be always well constrained and noise contamination and structure mismodelling may produce spurious non-shear components. Inversion into the shear-tensile/implosion source model, which consists of physical components exclusively, can reveal this. The orientations of double-couple part of the MT are in a very good agreement with source lines of the STI model (Fig.1). Moment tensors possess non-DC parts between 4% and 68%. The STI model results in off-plane angles between -3.5° and 4.5° and the pattern of their distribution indicates that the non-zero values are not significant. This fact demonstrates that non-DC components of MT were spurious, caused by noise

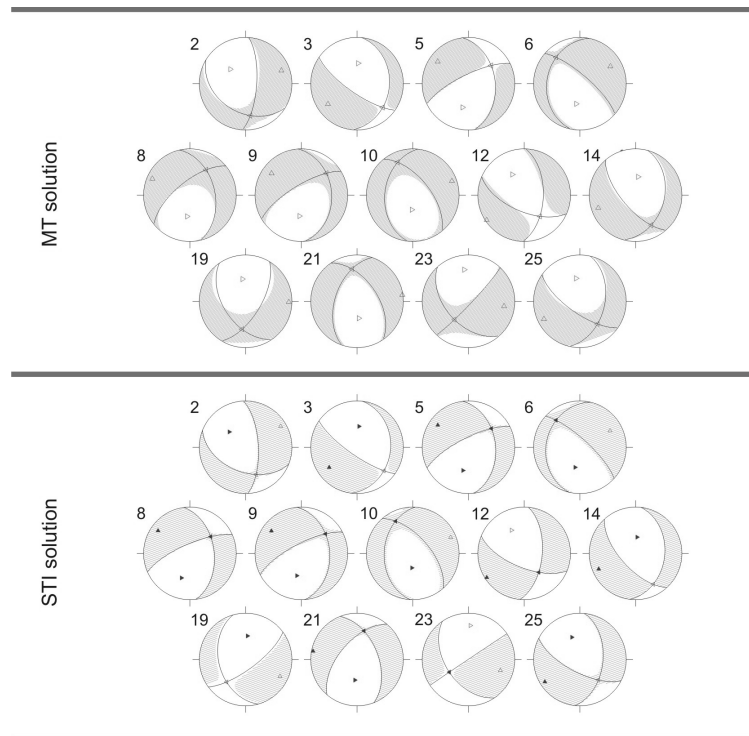


Figure 1 Comparison of moment tensor (MT) solutions and shear-tensile/implosion (STI) solutions. The source mechanisms are represented in a traditional fault-plane solution plots. The nodal lines of the DC part of the retrieved MTs, the source lines of STI are displayed using grey lines and corresponding principal axes T, P and N using a triangle apex up, right and left respectively, in equal-area, lower-hemisphere projection.

contamination, structure mismodelling and lack of input data. Thus, our investigation of weaker events suggests that again their source mechanisms are dominantly pure shears (dip-slip and oblique normal) just like the stronger micro-earthquakes processed by Horálek et al. (2010). Directions of T-axes are stable and sub-horizontal in E-W direction. On the other hand, the directions of P-axes vary from vertical to horizontal in N-S direction. All these results are very similar to previous analysis (Horálek et al., 2010) and are in agreement with the stress pattern from in-situ measurements (Evans, 2005). We can conclude that even weaker micro-earthquakes from the first phase of the injection in 2003 with magnitudes larger than 1.4 were pure shear slips on pre-existing faults.

References

- Dufumier, H. and Rivera, L. [1997] On the resolution of the isotropic component in moment tensor inversion. *Geophys. J. Int.*, **131**, 595-606, doi:10.1111/j.1365-246X.1997.tb06601.x.
- Evans, K. F. [2005] Permeability creation and damage due to massive fluid injections into granite at 3.5 km at Soultz: Part 2 - Critical stress and fracture strength, *J. Geophys. Res.*, **110**, B04204, doi:10.1029/2004JB003169.
- Horálek, J., Jechumtálová, Z., Dorbath, L. and Šílený, J. [2010] Source mechanisms of micro-earthquakes induced in a fluid injection experiment at the HDR site Soultz-sous-Forêts (Alsace) in 2003 and their temporal and spatial variations. *Geophys. J. Int.*, **181**, 1547-1565, doi:10.1111/j.1365-246X.2010.04506.x.
- Vavryčuk, V. [2001] Permeability Inversion for parameters of tensile earthquakes, *J. Geophys. Res.*, **106**, 16339-16355, doi:10.1029/2001JB000372.
- Vavryčuk, V. [2011] Tensile earthquakes: Theory, modeling and inversion, *J. Geophys. Res.*, **116**, B12320, doi:10.1029/2011JB008770.

Relation between Stress Field changes and Fluid Injection at The Geysers Geothermal Field, California

Patricia Martinez, Marco Bohnhoff and Grzegorz Kwiatek

Helmholtz-Centre Potsdam German Research Centre for Geosciences GFZ, Potsdam, Germany
Contact: patricia@gfz-potsdam.de

Temporal variations of the crustal stress field associated with the release of coseismic stress are important towards an improved process understanding of induced seismicity in different types of reservoirs caused by massive fluid injection. However, an accurate and reliable determination of spatiotemporal stress rotations is difficult and requires local seismic networks with good azimuthal coverage and low magnitude-detection threshold.

The Geysers geothermal field is located close to the San Andreas Fault transform fault system in California, USA. The induced seismicity associated with the exploitation of the reservoir has been extensively monitored for more than 30 years. The reported seismicity rate includes 140 earthquakes/month with $M > 1.2$ and 14 earthquakes/year with $M > 3.0$ (e.g. Gritto and Jarpe, 2011). While it is evident that seismicity at The Geysers is related to injection and production operations it is difficult to relate the production parameters from individual wells to the spatial and temporal patterns of seismicity, partially due to insufficient location accuracy. Some attempts have been done in the past to calculate the local stress field in the area. Oppenheimer (1986) estimated the stress orientation by inverting 210 fault plane solutions. He obtained a result that was very consistent with the regional stress field, which might indicate that the regional tectonic stress field dominates over the stresses induced locally by geothermal activities. However, the focal mechanisms were estimated using limited number of first motions and in many cases the ambiguity between different fault plane solutions was unresolved.

In this study we aim at determining potential spatial and temporal variations of the local stress field orientation at The Geysers geothermal site using the triggered data provided by a permanent array of 34 stations from Lawrence Berkeley National Laboratory (LBNL) installed in 2007 along the area of The Geysers Geothermal Reservoir. The network is composed of 34 3C sensors (Oyo GS-11D short period geophones with natural frequency 4.5 Hz) located on surface and the data are recorded in triggering mode with sampling frequency 500 Hz (see Fig. 1). To determine the stress field orientation we apply the stress inversion algorithm of Abers and Gephart (2001), which is a non-linear approach using P-wave first motions polarities.

Potential rotations of the local stress field are then related to hydraulic parameters such as flow rate and injection pressure. In that respect we also address the relation to the occurrence of large magnitude events (LME) as observed in The Geysers field and in several other geothermal reservoirs. Preliminary results of the analysis and the procedures described above will be presented and discussed.

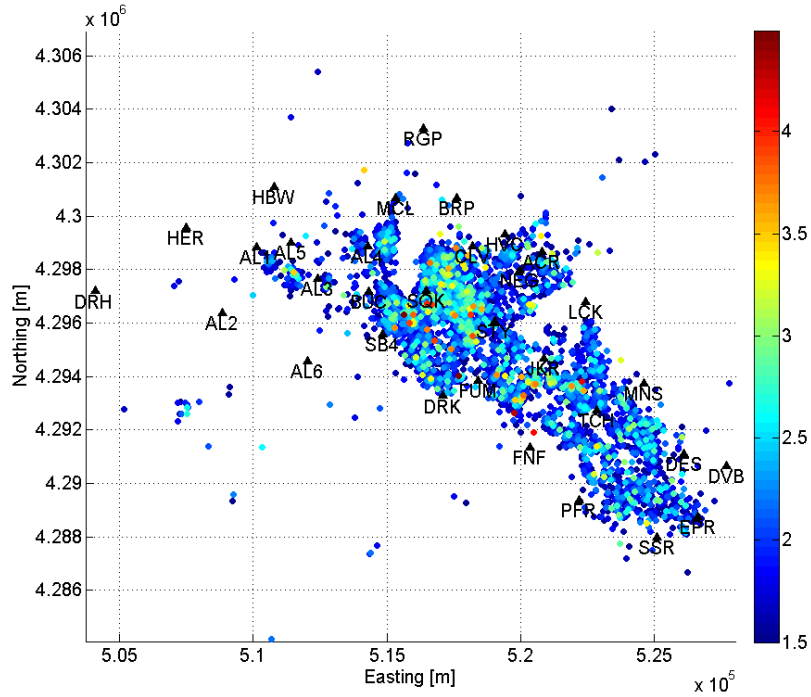


Figure 1. Location of the LBNL array and seismicity $1.5 < M$ from 2007 to 2012. Data source: BDSN and Northern HFN data, Berkeley Seismological Laboratory, University of California, Berkeley.

References:

- Abers, G. A. and Gephart, J. W. (2001). Direct inversion of earthquake first motions for both the stress tensor and focal mechanisms and application to southern California. *J. Geophys. Res.* 106, 26523-26540.
- Oppenheimer, David H. (1986). Extensional tectonics at The Geysers geothermal area, California. *J. Geophys. Res.* 91, 11463-11476.
- Majer, E. L. and Peterson, J. P. (2007). The impact of injection on seismicity at The Geysers, California Geothermal Field. *International Journal of Rock Mechanics & Mining Sciences*, 44, 1079 – 1090.

Shear-Tensile Model - A Prospective Alternative to Moment Tensor in Seismic Detection of Fracture Mode During Hydrofracture Treatment of Oil and Gas Wells

Jan Šílený

Institute of Geophysics, Academy of Sciences of the Czech Republic, Prague, Czech Republic

Recently, moment tensor has become a standard for description of seismic sources, both in earthquake seismology and for various types of induced seismicity. It is a general dipole source, but for practice it may be too general, its generality causing troubles during its reconstruction from noisy data in the inverse process, which may be additionally ill-conditioned due to inexact hypocenter location and/or availability of a rough velocity/attenuation model only. Then, the retrieved source may be biased, containing artifacts of a low-quality data or the inconsistent inverse problem. It seems reasonable to assume a simpler source model directly describing the physical phenomena anticipated in the particular focus. A simple combination of a shear slip with a tensile crack or 1D implosion – a shear-tensile/implosion model (STI) – may be a good model for natural earthquakes, where the tensile crack simulates a fault opening due to, e.g., its roughness or bending, for volcanic earthquakes, and especially for various types of seismic events induced by industrial activity like mining and hydro-fracturing in oil/gas and geothermal wells. The model simplification introduced is crucial in cases of depleted sensor configuration when the moment tensor fails, in single-azimuth monitoring in particular. This is just the case of application in oil and gas industry, where the monitoring of seismicity induced by hydrofracturing is typically performed from a single monitoring borehole. Then, moment tensor is able to provide constrained solutions only (e.g., a deviatoric solution or a pure shear slip model), but the STI detects also non-shear component correctly, providing important information on increase of permeability of the reservoir.

We demonstrate the resolving power of the STI model in the single-well vs. two well monitoring configuration and assuming noise contamination of the data, hypocenter mislocation and improper estimate of the velocity structure of the medium in synthetic experiments which mimic the Cotton Valley hydrofracture experiment (Fig.1).

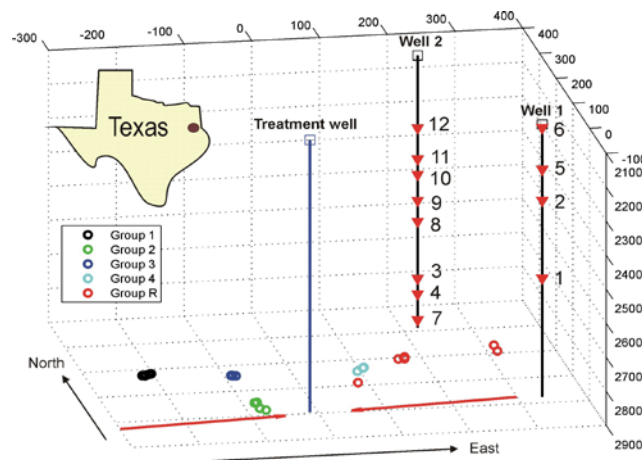


Figure 1. 3-D sketch of the Cotton valley, E.Texas gas field hydrofracture experiment. Seismicity originated by hydrofracturing of the treatment well observed from two monitoring boreholes. Hypocentra of several micro-earthquakes in classification (G1-G4,R) by Rutledge et al. (2004) marked by color circles. Synthetic data generated for event pointed by blue arrow. Red arrows – direction of maximum horizontal compression. Scales in meters.

The artificial “data” were synthesized for two types of the source mechanism: (i) a vertical strike-slip and (ii) a 45° dip-slip, both with the slip vector inclined by 5° from the fault plane (Fig.2).

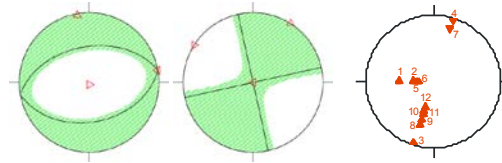


Figure 2. Theoretical source mechanisms for the synthetic experiment: vertical strike-slip (strike 80°, dip 90°, rake 0°, slope 5°)- left, inclined dip-slip (strike 80°, dip 45°, rake -90°, slope 5°)- middle. Right – station distribution of the focal sphere.

The mismodeling introduced is rather extreme: 1-D layered model for synthesizing the data, a homogeneous halfspace for the Green’s function. An error in localization was simulated by evaluating the GF out of the event hypocenter (33 m deeper). Fig.3 summarizes the combined mislocation and mismodeling: dip-slip source is resolved very well (including the slope) in both two-well and single well setups, while for strike-slip the reconstruction fails if only single-well data are available.

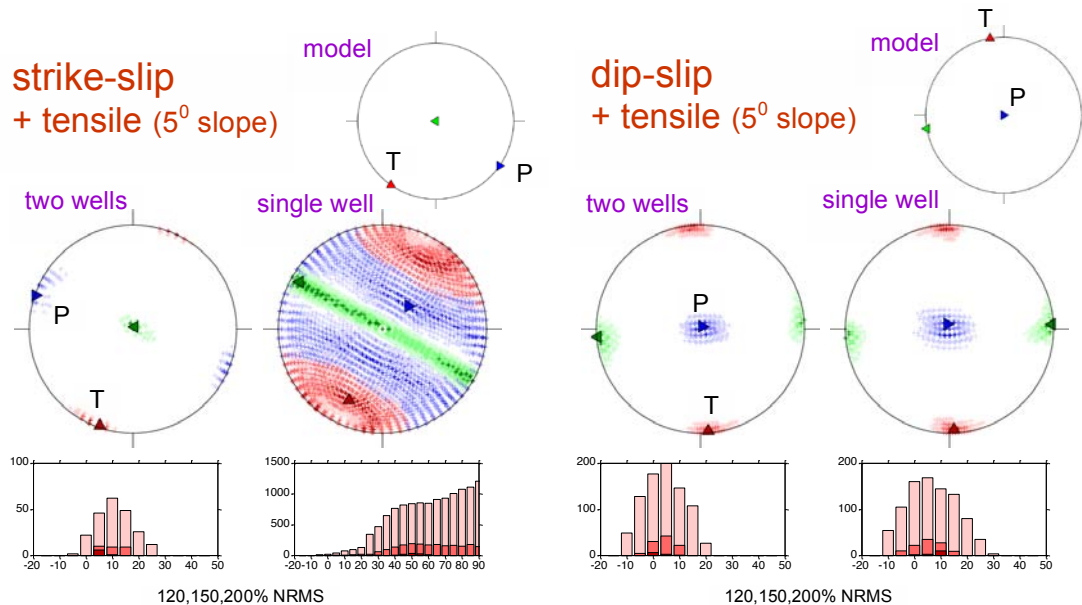


Figure 3. Resolution of the STI source model. Synthetic experiment simulating mislocation of the hypocenter and using improper velocity model in setups of two monitoring wells (see Fig.2) and a single well (# 2) only. Strike-slip and dip-slip theoretical source models considered for the data synthesis (top, also Fig.2). Resolved T,P,N axes and their confidence regions in the individual configurations – middle, histograms of the slope angle – bottom. Confidence region plotted for the levels of 120%, 150% and 200% of the minimum RMS

To much extent, success in determination of the mechanism of a seismic event depends on the configuration of the observational network. Monitoring of microseismicity due to hydrofracturing of oil/gas wells, realized by linear strings of sensors situated in monitoring boreholes, is mostly just the case of a deficient configuration. The extreme situation is a single well monitoring, when the data obtained (in the far field) cannot resolve the mechanism in the description of the

moment tensor. We demonstrated that a simpler source model, namely the shear-tensile/implosion source, has resolving power to reconstruct properly both the shear and non-shear components of the mechanism even in the case when the moment tensor fails. In addition, it is robust enough even with a high noise in the data, errors in localization of the hypocenter and estimation of the velocity profile of the reservoir.

Acknowledgements

This research was supported by the grant of the Grant Agency CR P210/12/2235 and by the European Community's FP7 Consortium Project AIM 230669.

Characterization of seismic velocity structure in the eastern Sea of Marmara region, NW Turkey, using ambient noise

D. Acarel, F. Bulut and M. Bohnhoff

Helmholtz-Centre Potsdam, German Research Centre for Geosciences GFZ, Potsdam
Contact: acarel@gfz-potsdam.de

We analyze the ambient seismic noise field in order to investigate crustal structure and seismic anisotropy at the North Anatolian Fault Zone (NAFZ) in NW Turkey. We focus on the eastern Sea of Marmara section of the NAFZ representing a pre-seismic phase of the seismic cycle just prior to an expected major ($M > 7$) earthquake. The target area has been monitored by the PIREs seismic network since autumn 2006 (Bulut et al., 2009; 2011). We apply a spatial autocorrelation and cross-correlation analysis of the seismic ambient noise to firstly determine spectral dependence of the seismic velocity in order to image crustal structure at near-surface and seismogenic depths. The time-domain cross-correlation of ambient noise recordings (diffuse wave field: isotropic random waves propagating with equal power in all directions) computed between a pair of receivers, will result in a waveform that differs only by a smooth frequency dependent amplitude factor from the Greens function between the receivers (Shapiro et al., 2005). The basic assumption is that the emerging signal from the noise correlation function will be dominated mainly by fundamental mode Rayleigh waves. Time-domain cross correlations are calculated for all available stations pairs (vertical component) in the target area (Figure 1). Greens functions are computed by stacking 2-min cross-correlation windows moving along one-year long data, obtained from 24 stations corresponding to approximately 270 correlation pairs. An example of stacked time domain correlations of 3-month data is shown in Figure 2.

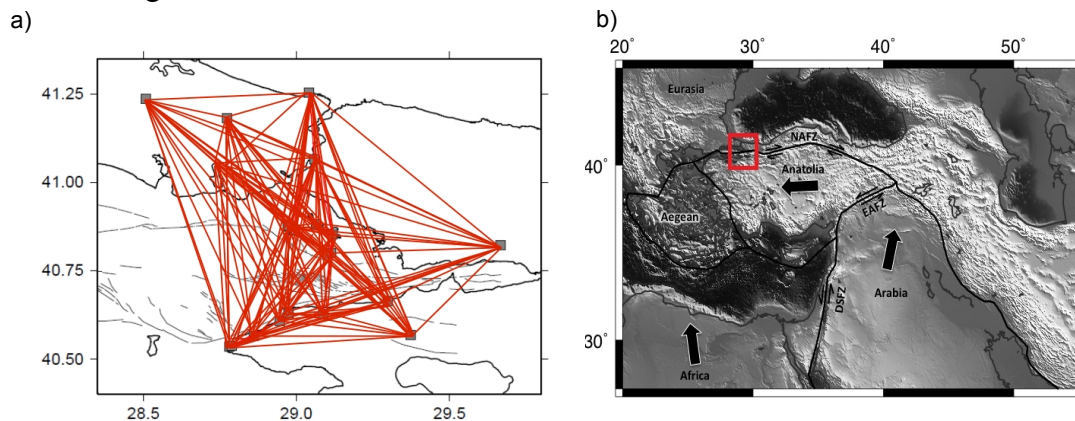


Figure 1. a) Tectonic framework of Turkey and surrounding regions. Tectonic boundaries are shown by black lines and relative plate motions by black arrows with respect to stable Eurasia. The red rectangle indicates the study area. b) Ray coverage obtained from all combinations of the correlation paths (red lines) and the station distribution (gray squares) in the target area.

Group velocity dispersion curves are obtained for all available correlation paths following the quality check step and eliminating the low-quality data. In a frequency band of 0.2 to 1.2 Hz, average group velocity ranges between ~ 2 to 3 km/s. Correlation-derived phase/group velocity dispersion curves will be inverted for shear wave velocity profiles. The obtained S-wave velocity model will be used to improve

the hypocenter precision for the earthquake catalogue along the Sea of Marmara segment of the NAFZ. Additionally we investigate the directional dependence of the seismic velocity field splitting the data set into subprofiles which samples different backazimuths. The crustal anisotropy is interpreted to represent the stress field orientation and/or structural heterogeneity along this section of the NAFZ. The observations will thereby allow to investigate physical parameters along and across the fault zone at pre-seismic phase of the seismic cycle providing insights into crustal characteristics and the role for earthquake generation. We plan to extend the study towards the ICDP-GONAF project (www.gonaf.de) using the borehole recordings providing a better signal to noise ratio and therefore a better detection of the ambient noise field.

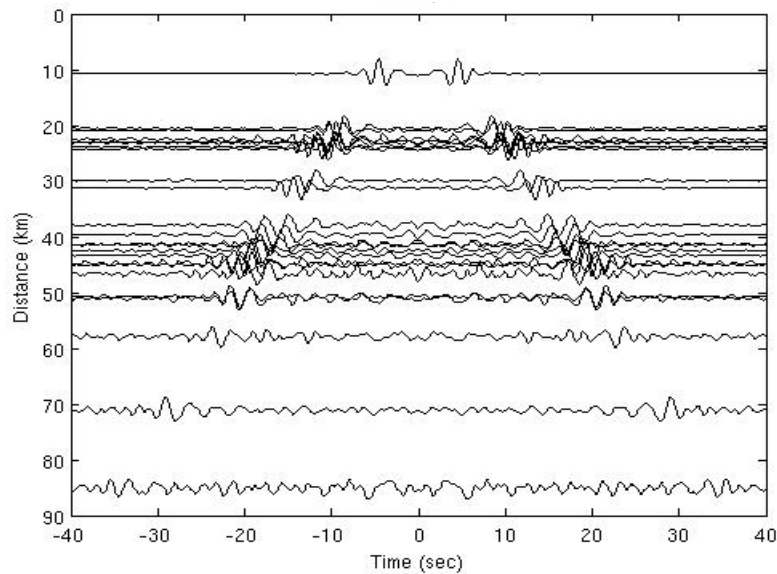


Figure 2. An example of time domain correlations obtained after stacking 3-month data. Correlations are ordered in terms of distance to investigate the velocity move-out. The data obtained from 3 master stations located in the northern part of the target area. Cross-correlations are band pass filtered between 0.5-2 Hz.

References:

- Bulut, F., Bohnhoff M., Ellsworth W. L., Aktar M. and Dresen G., (2009). Microseismicity at the North Anatolian Fault in the Sea of Marmara Offshore Istanbul, *Journal of Geophys. Res.*, doi: 10.1029/2008JB006244
- Bulut, F., Ellsworth W. L., Bohnhoff M., Aktar M. and Dresen G. (2011). Spatiotemporal earthquake clusters along the North Anatolian Fault Zone offshore Istanbul, *Bulletin of the Seismological Society of America*; August 2011; v. 101; no. 4; p. 1759-1768; DOI: 10.1785/0120100215
- Shapiro, N. M., M. Campillo, L. Stehly, and M. H. Ritzwoller, 2005. High resolution surface-wave tomography from ambient seismic noise, *Science*, 307 (5715), 1615– 1618.

High accuracy study of source scaling in Marmara Sea using seismic arrays

B. Can¹, M. Aktar¹, F. Bulut², M. Bohnhoff² and G. Dresen²

¹Bogazici University Kandilli Observatory & Earthquake Research Institute, Istanbul, Turkey

²GeoForschungsZentrum, Potsdam, Germany

The western part of the North Anatolian Fault Zone (NAFZ) is potentially considered to be one of the most seismogenic and possibly destructive fault in Turkey. The seismic activity of the Marmara Sea (Turkey) is monitored at a very low magnitude threshold level in order to understand the microseismic behavior of the major fault segments. In a cooperative project, Kandilli Observatory and Earthquake Research Institute of Bogazici University (Istanbul, Turkey) and GFZ German Research Centre for Geosciences, Helmholtz Centre (Potsdam, Germany) have installed seismic arrays on two islands (Sivriada and Yassiada) which are the closest land site locations to the inferred fault zone. These islands are located offshore Istanbul, within a 3-5 km distance to the Northern Boundary Fault of Cinarcik Basin. This is one of the major segments of the North Anatolian Fault Zone (NAFZ) and structurally constitutes a debate issue. Both seismic arrays have five 3-D short period seismographs, with an average station spacing of ~100 m. and a sampling frequency of 500 Hz. The network was recently enlarged to cover the neighbouring Islands (Balikciada, Burgazada, Heybeliada, Kinaliada and Buyukada) giving a unique opportunity for high resolution monitoring of the microseismicity at close distance.

We have observed in detail the cluster of earthquake sequences that have occurred at close distances to the PIREs arrays. We have used the largest magnitude events in the sequences as a waveform template for detecting the smaller ones. We have cross correlated the template with the continuous waveform from the same sensor, and then time shifted and stacked the cross-correlation traces from all of the stations from the two arrays. This type of beam forming approach has led to a very large improvement of the detection of the very small magnitude events, lowering the level down to $M=0.7$.

In terms of the location procedure, we have used a combination of the standard location approach, supported with the fk method in order to improve the backazimuth estimation. The location accuracy reached this way is considerably improved as compared to using only the land based observations using the standard location tools.

We have also focused on the scaling properties of event clusters. We have calculated the seismic moment, source size, stress drop, radiated seismic energy of the template events as well as the smaller magnitude events both individually and in a relative manner. Comparison of the results of constant Q analysis, spectral amplitude ratio method and stacking of the spectral amplitudes approaches are discussed. The use of multiple stations from the two different arrays allow us to carry independent estimations of different parameters which then permits a better statistical description of the overall accuracy. We evaluate the benefits of using arrays as compared to using single station observation. We also discuss accuracy issues regarding the use of arrays for observations which would normally be done in a borehole environment. In this context, we attempt a first order estimation of the seismic efficiency based on surface observations.

One of our goal is also to obtain a qualitative comparison of scaling properties in a seismic clustering observed in normal times. These clusters of low magnitude events are compared to the foreshock sequence observed for the 1999 Izmit Earthquake ($M_w=7.4$, 17.08.1999) which showed unusual scaling properties and was accepted to be a sign of slow deformation preceding a large rupture.

Spatiotemporal variations of the crustal stress field during the seismic cycle: Applications to the Marmara region, NW Turkey

Michèle Ickrath and Marco Bohnhoff

Helmholtz-Centre Potsdam German Research Centre For Geosciences GFZ, Potsdam, Germany.
Contact: ickrath@gfz-potsdam.de

Local rotations of the stress field may serve as an indicator to characterize the physical status of individual fault segments within the seismic cycle. The primary focus of our study is to contribute to the discussion whether or not local stress field rotations are a useful indicator for the loading status of individual fault segments during the seismic cycle. Furthermore, we want to test the different stress rotation models proposing long-term stress recovery or short-term decay of a rotation induced by a major earthquake (e.g. Michael, 1987; Hauksson, 1988).

The North Anatolian Fault Zone (NAFZ) in NW Turkey is one of the most active faults and has produced several destructive ($M > 7$) earthquakes during the last century. Currently the Sea of Marmara segments remain as the only section of the NAFZ that have not been activated since 1766. The Izmit 1999 $M = 7.4$ earthquake ruptured a ~ 140 km long segment of the NAFZ in NW Turkey between the Sea of Marmara and the Düzce area reflecting a right-lateral strike-slip mechanism consistent with the long-term regional stress field. To investigate the seismotectonic setting of the region and spatiotemporal variations of the stress field we focus on pre-, co- and postseismic phases of the 1999 Izmit earthquake using seismic recordings from all available local and regional networks. In particular we focus on the permanent seismic Sapanca-Bolu NETWORK (SABONET, Milkereit et al., 2000) consisting of 15 stations throughout the area in operation since 1996 and therefore covering the time span prior to the Izmit and Düzce events until several years after. During this time period ~ 9000 events were recorded. We also use data from the permanent Princes Islands Realtime Earthquake monitoring System (PIRES) network at the eastern part of the Marmara seismic gap where a $M > 7$ earthquake is expected (Bulut et al., 2009; 2011).

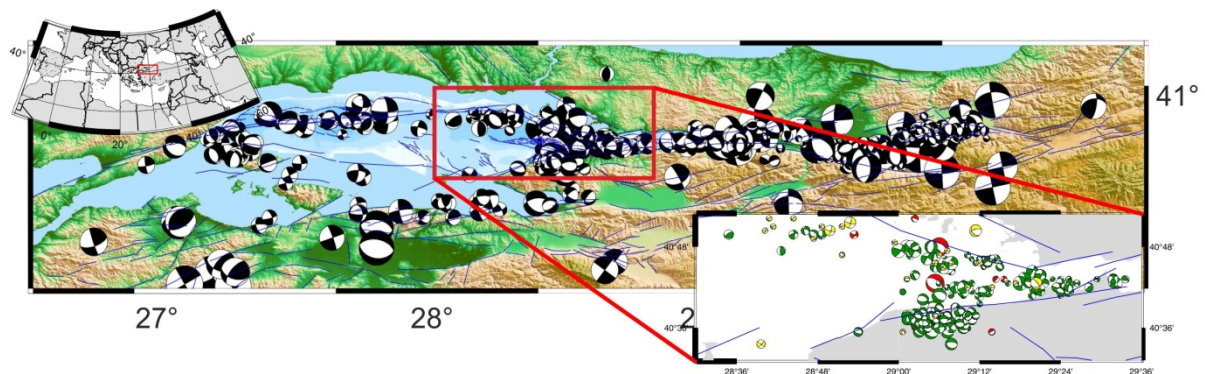


Figure 1. Overview map of the Focal Mechanism (FM) database of NW Turkey used in this study. Subplot (right): 216 FM from the eastern Sea of Marmara. FM are color-coded with time: prior to 1999, 1999 and post 1999 in red, green and yellow, respectively.

A compilation of all existing 750 Focal Mechanisms (FM) (e.g. Bohnhoff et al., 2006; Örgülü, 2010 and references therein) from previous investigations plus newly determined FM as well as P-wave polarities (this study) represent the basis for a stress tensor inversion (STI) inverting FM (Michael, 1984) and P-wave polarities (Abers and Gephart, 2001), respectively. Results for the whole Izmit/Düzce area reflect well-resolved strike-slip regimes during the pre- and postseismic phases of the Izmit event in 1999, whereas during the aftershock sequence an EW and a NE/SW-extensional normal faulting regime is observed dominated by the Akyazi and Düzce pull-apart structures, respectively. Both regions will be investigated in detail with regard to the postseismic recovery/decay as well as potential stress precursors preceding both mainshocks.

First results from the analysis of P-wave polarities for events at the Karadere-Düzce segment confirm a short-term change in the stress regime from strike-slip (preseismic) to normal faulting (aftershock period).

Results for the Eastern Sea of Marmara at the transition from the Izmit rupture to the Marmara seismic gap (red box Fig.1) indicate a significant $\sim 20^\circ$ clockwise rotation between the 3-month aftershock period in 1999 and the postseismic setting (since 2000).

This study will be extended using also acoustic emission data from rock-deformation experiments in the laboratory and considering different tectonic regimes such as the Andean subduction zone to elaborate on the impact of shear failure and the associated stress drop during large earthquakes for a rotation of the principal stresses acting on faults.

References

- Abers, G.A. and Gephart, J.W., 2001. Direct inversion of earthquake first motions for both the stress tensor and focal mechanism and application to southern California. *J.geophys.Res.*, 166, B11, 26,523-26,540.
- Bulut, F., Bohnhoff, M., Ellsworth, W., Aktar, M. & Dresen, G., 2009. Microseismicity at the North Anatolian Fault in the Sea of Marmara offshore Istanbul, NW Turkey, *J. geophys. Res.*, 114, doi:10.1029/2008JB006244.
- Bulut, F., Ellsworth, W., Bohnhoff, M., Aktar, M. & Dresen, G., 2011. Spatiotemporal Earthquake Clusters along the North Anatolian Zone Offshore Istanbul, *Bull. Seismol. Soc. Am.*, 101, doi: 10.1785/0120100215.
- Bohnhoff, M., Grosser, H. & Dresen, G., 2006. Strain partitioning and stress rotation at the North Anatolian fault zone from aftershock focal mechanisms of the 1999 Izmit $M_w = 7.4$ earthquake, *Geophys. J. Int.*, 166, 373–385.
- Hauksson, E., and L. M. Jones, The July 1986 Oceanside ($M_L = 5.3$) earthquake sequence in the Continental Borderland, Southern California, *Bull. Seismol. Soc. Am.*, 78, 1885-1906, 1988.
- Michael, A.J., 1987. Use of focal mechanisms to determine stress: a control study, *J. geophys. Res.*, 92, 357–368.
- Milkereit, C. *et al.*, 2000. Preliminary aftershock analysis of $M_w = 7.4$ Izmit and $M_w = 7.1$ Düzce earthquake in Western Turkey. In: Barka, A., Ö. Kozaci, S. Akyüz (Editors): The 1999 Izmit and Düzce Earthquakes: preliminary results. pp. 179–187, Istanbul Technical University.
- Örgülü, G., 2010. Seismicity and source parameters for small-scale earthquakes along the splays of the North Anatolian Fault (NAF) in the Marmara Sea, *Geophys. J. Int.*, doi: 10.1111/j.1365-246X.2010.04844.x.

Resolution of Non-Double-Couple Components in the Seismic Moment Tensor using Local Networks: Synthetic Case Study and Application to Aftershocks of the 1999 M_w 7.4 Izmit Earthquake

E. Stierle¹, V. Vavryčuk², J. Šílený² and M. Bohnhoff¹

¹ Helmholtz-Centre Potsdam - German Research Centre for Geosciences GFZ

² Institute of Geophysics, Academy of Sciences of the Czech Republic, Prague

The reliable detection of non-double-couple (NDC) components in the seismic moment tensor is facing increasing relevance in observational seismology and can substantially contribute to better understanding of seismic source processes involving non-shear rupture.

In this study we have analyzed the NDC components in aftershocks of the 1999 $M_w=7.4$ Izmit earthquake. The Izmit earthquake ruptured a ~140 km long segment of the North Anatolian Fault Zone in north-western Turkey and was followed by the $M_w=7.1$ Düzce earthquake that extended the rupture further to the East. A 35-station network of short-period seismometers was deployed only four days after the mainshock covering the entire rupture zone (Baumbach et al., 2003) (Figure 1). Propagation and focal mechanisms of aftershocks clearly indicate a segmentation of the fault plane into several segments (Bohnhoff et al., 2006). Of these, the Akyazi Plain is the most remarkable one. It reflects pure east-west extensional normal faulting in a regional strike-slip stress field indicating a small pull-apart structure. This region can be seen as a potential area, where significant real NDC components might exist. Therefore, we focus on this part of the Izmit rupture to analyze NDC components in moment tensors of earthquakes in a postseismic scenario.

Since the NDC components are sensitive to noise, velocity structure mismodeling or unfavorable azimuthal station coverage, they can be spurious being numerical errors of the inversion instead of a true part of the source mechanism (Šílený, 2009). Therefore real data analysis must be preceded by synthetic tests in order to define a confidence level, for which the NDC components can be considered statistically significant. We performed synthetic tests to analyze the ability of the network to detect physical (real) NDC components in seismic moment tensors of small earthquakes with a moment magnitude of $M_w=3$. We modeled synthetic P- and S-wave amplitudes using the geometry of the 35-station network that was deployed along the rupture after the Izmit earthquake (Figure 1). A shear-tensile source with a varying NDC content was adopted as a source model. When inverting for the full moment tensor, we contaminated the data with artificial random noise and we systematically incorporated an inaccurate knowledge of the velocity structure as well as of hypocenter locations. The tests were performed for various types of focal coverage and different focal mechanisms representing the regional tectonic settings. We found that the double-couple (DC) mechanisms can successfully be resolved for realistic errors and reasonable station configurations. However, the resolution of real NDC components remains limited due to the lack of observations from stations with epicentral distances less than 15 - 20 km. Spurious NDC components caused by velocity and hypocenter mismodeling, noise, and unfavorable focal coverage are non-negligible.

For studying aftershocks of the Izmit earthquake, data obtained by the 35-station network of 3-component short-period seismic stations are analyzed. We applied the full moment tensor inversion as well as the moment tensor inversion constrained to a shear-tensile source model using amplitudes of P- and S-waves. The stability of the moment tensor solution was accessed by a repeated inversion of data contaminated with random artificial noise. The quality of the solution was estimated from the scatter of P/T axes and nodal lines as well as from the difference between the NDC components of the solutions inverted from noise-free and noisy data. Large deviations in the NDC components and a high scatter of the P/T axes and of the nodal lines are an indicator of probably unstable and less accurate moment tensor solutions. The DC and NDC components of stable solutions are statistically analyzed and possible origins of the NDC components are discussed.

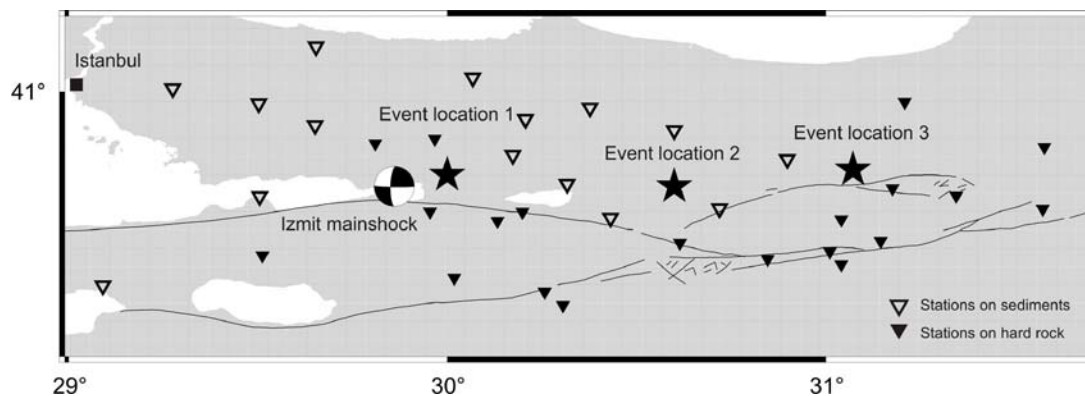


Figure 1. Configuration of stations of the seismic network deployed along the 1999 Mw=7.4 rupture of the North Anatolian Fault Zone to monitor aftershock activity (Baumbach et al., 2003). The stars mark the locations of the events considered in the synthetic test.

References

- Baumbach, M., D. Bindi, H. Grosser, C. Milkereit, S. Parolai, R. Wang, S. Karakisa, S. Zunbul, and J. Zschau (2003). Calibration of an ML scale in northwestern Turkey from 1999 Izmit aftershocks, *Bull. Seism. Soc. Am.* 93 2289-2295.
- Bohnhoff, M., H. Grosser, and G. Dresen (2006). Strain partitioning and stress rotation at the North Anatolian fault zone from aftershock focal mechanisms of the 1999 Izmit Mw= 7.4 earthquake, *Geophys. J. Int.* 166 373-385.
- Šílený, J. (2009). Resolution of Non-Double-Couple Mechanisms: Simulation of Hypocenter Mislocation and Velocity Structure Mismodeling, *Bull. Seism. Soc. Am.* 99 2265-2272.

Long-lasting aftershock activity of the 2011 Kutahya/Turkey Earthquake (Mw 5.8): Lessons learned from precise earthquake locations

Fatih Bulut¹, Marco Bohnhoff¹, Tugbay Kilic², Recai F. Kartal², F. Tuba Kadirioglu² and Georg Dresen¹

¹ Helmholtz-Centre Potsdam, GFZ Deutsches GeoForschungsZentrum

² Republic of Turkey Prime Ministry, Disaster and Emergency Management Presidency

We investigate pre- and aftershock activity of the 2011 Kutahya/Turkey Mw 5.8 earthquake in order to better understand the physical processes acting within the seismogenic layer of the crust before and after a moderate earthquake. Seismic activity has been monitored by local network that is operated by AFAD-Turkey. Approximately 7000 earthquakes have been detected typically ranging between magnitudes of 2.5 – 4.5 for the time period 2009 - 2012. The main-shock has been followed by ~4000 aftershocks above M 2.5 which is an extremely high number of aftershocks for a Mw 5.8 mainshock.. The area was hit by a Mw 5.4 earthquake in 2012, which occurred on the eastern-adjacent section of the fault ruptured in 2011. Using the double-difference algorithm, we improved the hypocenter locations to about 150 m. This allows to identify in greater detail the architecture of the normal fault that failed during the 2011 and 2012 main-shocks and also to characterize the pre- and post-seismic evolution of nearby seismicity.. The aftershock activity of the 2011 event clearly reveals a north-dipping normal fault that merges at a depth of about 10 km with a low angle normal fault. This observation is additionally confirmed by a rotation of well-resolved fault plane solutions with increasing depth... The pre-seismic activity is focused on the low-angle section of the fault below the subsequently occurring main-shock hypocenter. After the mainshock, the activity migrates upward during the aftershock period. We also observe a sideward migration of the activity towards the nucleation zone of the recent 2012 main-shock. We analyze the spatio-temporal evolution of the seismicity to unravel the interaction of different fault segments between the major events.

Comparison of the West Bohemia Earthquake Swarms in 2008 and 2011 from the Point of View of the Focal Migration and Source-Mechanism Variation

H. Cermakova^{1,2}, B. Ruzek¹, T. Fischer^{1,3}

¹ Institute of Geophysics, Academy of Science of the Czech Rep., Prague, Czech Republic, cermakova@ig.cas.cz

² Charles University, Faculty of Mathematics & Physics, Prague, Czech Republic

³ Charles University, Faculty of Science, Prague, Czech Republic

Earthquake swarms are specific type of seismic activity when the whole deformation energy is released by a sequence of weaker events, which are clustered in space and time without a mainshock. Western part of the Bohemian Massive (a border area between Czech Republic and Germany, called West Bohemia/Vogtland) ranks among the most active intraplate-earthquake-swarm areas in Europe. This region is monitored by a local seismic network WEBNET consisting of 13 telemetric and 10 autonomous stations. Since 1991, when WEBNET has been in operation, one medium (in 1997) and three intense swarms (in 2000, 2008 and 2011) have been recorded. All these swarms occurred on the same fault plane, close one to another, however, each of them shows different evolution. In this study we present results of analyses of the most intensive swarms in 2008 ($M_l < 3.8$) and 2011 ($M_l < 3.7$) of comparable size (similar seismic moment released), both consisting of more than 10 000 $M_l > 0$ events. First of all we focused on a space-time distribution of hypocenters. For this purpose we used the HypoDD code (Double-Difference Hypocenter Locations) by Waldhauser and Ellsworth (2000). The most important finding is that the swarm in 2008 occurred just on one plane whereas the swarm in 2011 activated two planes (maybe more). In 2008 events were spreading during two months from the bottom to the top of the plane. But the 2011 swarm showed much higher rapidity, the main activity on both planes lasted only a few days. Furthermore, we analysed a space-time distribution of focal mechanisms. We found that during both swarms a few types of mechanisms occurred. But the most dominant type is oblique normal faulting. In 2008 this was the main type during whole activity whereas in 2011 it was dominant only in the second half of the activity. In the first half mainly oblique thrust faulting appeared.

High-resolution fault tomography from accurate locations and focal mechanisms of swarm earthquakes

Vaclav Vavrycuk and Fateh Bouchaala

Institute of Geophysics, Academy of Sciences, Bocni II/1401, Praha 4, Czech Republic

We analyze 463 microearthquakes in the magnitude range from 0.5 to 3.7 that occurred during the 2008 earthquake swarm in West Bohemia, Czech Republic (Fig. 1), in order to image a detailed structure of the focal zone located at depths between 7 to 11 km. The double-difference location method was applied to records of 22 local stations in order to retrieve highly accurate locations of hypocenters with accuracy less than 20 m. The hypocenters are well clustered and distinctly map the system of activated faults. The fault geometry is surprisingly complex, the fault being composed of several segments with different orientations. The orientation of segments coincides well with the focal mechanisms (Fig. 2). The two principal fault segments are optimally oriented with respect to the tectonic stress and the associated microearthquakes are mainly double couple. The other fault segments are slightly misoriented (Fig. 3) being associated with microearthquakes displaying non-double couple mechanisms.

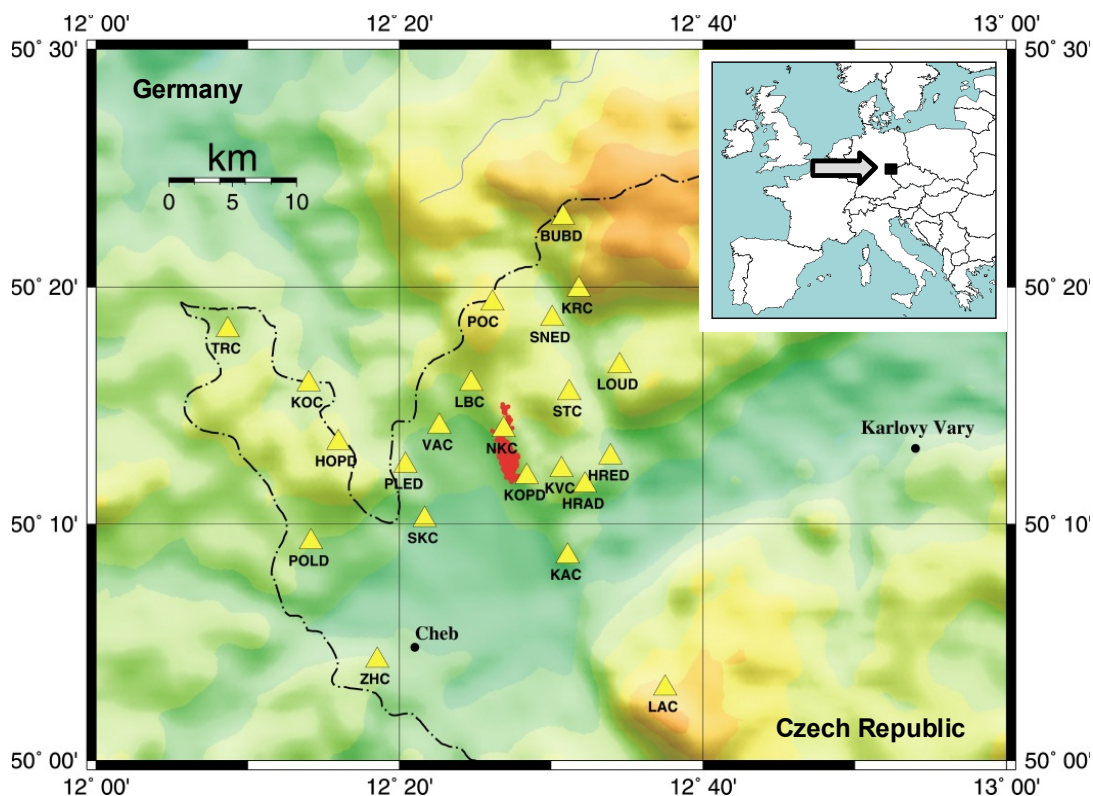


Figure 1. Topographic map of the West-Bohemia/Vogtland region. The epicentres of the 2008 swarm micro-earthquakes are marked by dots, the seismic stations are marked by triangles.

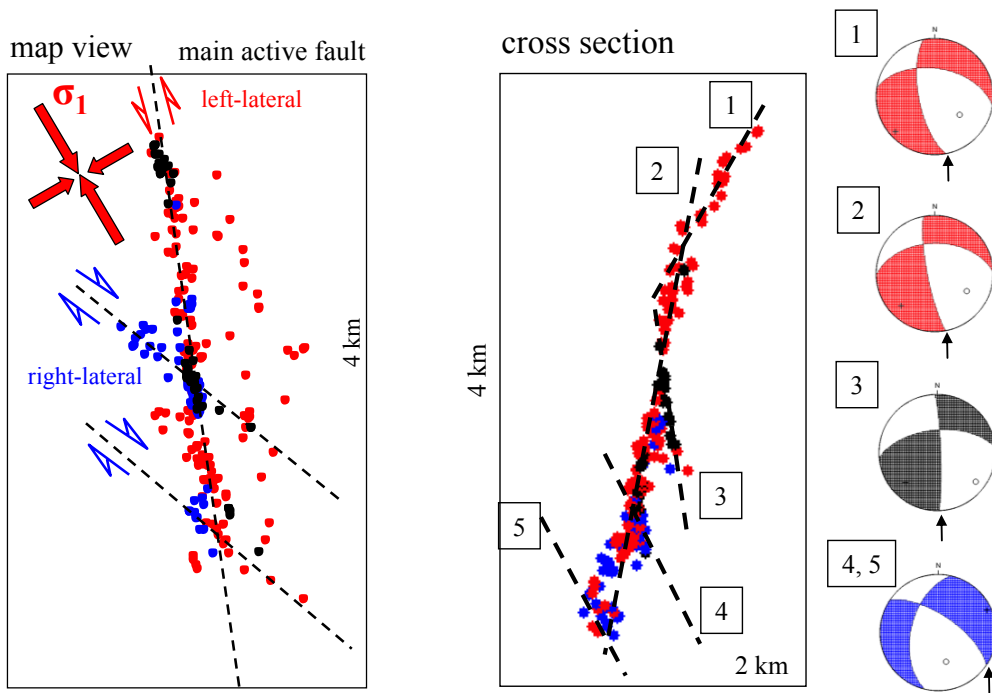


Figure 2. Complex fault geometry. Map view (left) and the cross section (right) of the focal zone showing activated fault segments together with associated focal mechanisms. Focal mechanisms (1), (2), (4) and (5) are associated with fault segments optimally oriented with respect to the stress field. Focal mechanism (3) is associated with a misoriented fault segment.

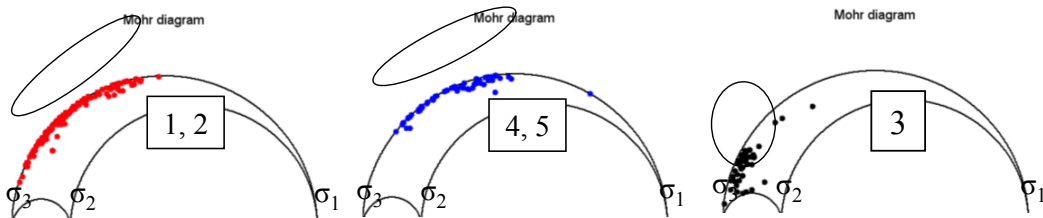


Figure 3. Mohr's diagrams for three basic families of focal mechanisms. Focal mechanisms (3) in the right-hand panel origin under significantly different stress conditions than the other focal mechanisms.

The statistical distribution of focal mechanisms is used for studying the stress conditions and the failure criterion in the focal zone. The direction of maximum compression is significantly inclined from the horizontal plane. The activated fault planes concentrate in the area of validity of the Mohr-Coulomb failure criterion. The distribution of the P/T axes reveals the 'butterfly' wing pattern. The average friction of faults is 0.5 and corresponds to a deviation of 32° of the principal fault segments from the maximum compression. The observed variability of focal mechanisms points to presence of a complex fault system with mutual interactions of fault segments rather than to presence of small scale stress heterogeneities or temporal changes of tectonic stress in the focal area.

Seismic observations of micro-earthquakes at small scale fractures

S.B. Kishkina

Institute of Geospheres Dynamics of RAS, Moscow, Russia

Location of variety scales earthquakes on fault zones is more distinct in cases with more accurately hypocenters determined. At the same time branched structures of major fault zones, it is assumed that some of the earthquakes occur at feathering fractures of smaller scale. It is thus possible to develop a “seismological” criterion for definition of a zone of “dynamic influence of faults”, i.e. the zone containing the majority of earthquakes associated with the fault zone under consideration [Kocharyan, 2011].

We used small-aperture arrays measurements from a various points at East-European Craton and Ural. We compare the seismic data processing results and regularities revealed during the analyses with the data obtained from geomorphology studies (or satellite image interpretation) of fault structures. The results confirm most small and micro-earthquakes locate in the fault zones and zones of “dynamic influence of faults”.

Figure 1 shows micro-earthquakes structural position for measurements from Karelian isthmus (a) and South Ural (b). The examples are considered to illustrate the most of variety scales earthquakes associated with the fault or fractures zones.

Fig.1a shows that the small earthquakes ($M \sim 1$) in Karelian isthmus area location are under zone of dynamic influence on cross-section stress control.

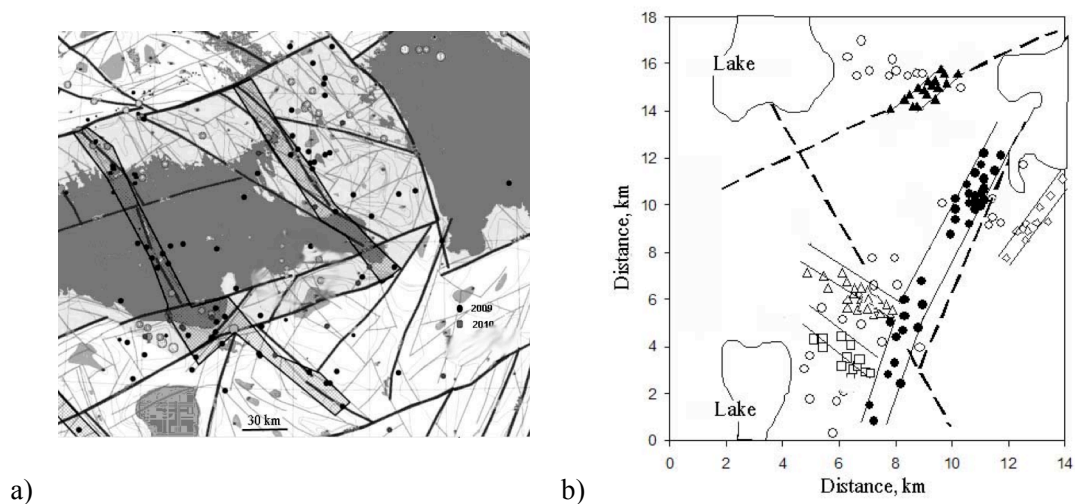


Figure 1. Most of variety scales earthquakes (different marks for different measurements) associated with the fault or fractures zones (solid and dash lines). Data for Karelian isthmus (a) and South Ural (b)

Similar results are obtained for aseismic Volga-region. Most micro-earthquakes ($M \sim -1$) are locate in the fault zone and in feathering fractures of smaller scale.

For Ural measurements the majority of micro-earthquakes locate the generalize fault along either. And some of the micro-earthquakes occur at feathering fractures

placed at an angle to the fault line. However, the precise location of small events in the areas with thick sedimentation masses under a significant anthropogenic bondage is complicated. This reason and usage of insufficient density lineaments maps obscure the fact that small earthquakes is associated with fault zones or small scale fractures.

The common scene is more clear in case data from the most comprehensive seismic catalog such as earthquakes catalog generated at the Northern California Seismic Network are used [Waldhauser, 2008]. We use such precisions catalogs to make a 3D-model that shows an image of great number of earthquakes sources compared to the sharp surface. It's a conditional fault surface. The fault lines mapped at the surface seems to be widening due to not-vertical fault surface orientations and due to local destruction areas close to general line and containing small sources is available.

References

- Kocharyan G.G., Kishkina S.B., Ostapchuk A.A. Seismic picture of a fault zone. What can be gained from the analysis of fine patterns of spatial distribution of weak earthquake centers?// *Geodynamics&Tectonophysics*. 2010. Vol. 1. № 4. 419–440
- Waldhauser, F. and D.P. Schaff. Large-scale relocation of two decades of Northern California seismicity using cross-correlation and double-difference methods // *J. Geophys. Res.* – 2008. – Vol. 113, B08311, doi:10.1029/2007JB005479.